STUDIES OF STIMULATED EMISSION OF RADIATION

by

J. B. Atkinson

ABSTRACT

Laser action has been observed on a number of 3p - 3s transitions in the infra-red in neutral atomic Carbon and Nitrogen. Mixtures of Helium or Neon with Carbon Monoxide or Nitrogen were excited with current pulses of up to 90amps and a duration of 2μsec. Depending on the pressure, current, and transition, laser action occurred either during the current pulse risetime or in the afterglow. The laser tube was 2 metres long with a bore of 7mm, and was fitted with internal electrodes and Brewster angle end windows.

The time dependence of the laser output as a function of current and pressure has been investigated, and the interpretation is based on observations of the spontaneous emission from the upper and lower levels of the laser transitions. In addition to the laser transitions, other related transitions in Carbon and Nitrogen and transitions to the metastable and resonance trapped levels of Helium and Neon were studied. Techniques have been developed to measure the populations of these metastable and resonance trapped levels by comparing the light emitted from the side of the laser tube to the light emitted from the end of the tube along the tube axis. Absolute values for the populations of the upper and lower level of the laser transition have also been obtained without the use of a calibrated detector.

The different mechanisms whereby excited states may be populated in a gas discharge are discussed, and cross-sections for the different collision processes estimated. These are used, together with the measured values of populations, to determine the likely dominant processes in the afterglow. Measurements of the rates of decay of the populations of the levels in Helium, Neon, Carbon and Nitrogen show a correlation between the populations of the metastable states of Helium and Neon and the 3p levels of Carbon and Nitrogen. It is therefore proposed that the dominant excitation mechanism for the 3p Carbon and Nitrogen levels is

$$\left.\begin{matrix}\text{He}\\ \text{Ne}\end{matrix}\right\} \text{Metastable} + \left.\begin{matrix}\text{CO}\\ \text{N}_2\end{matrix}\right\} = \left.\begin{matrix}\text{He}\\ \text{Ne}\end{matrix}\right\} + \left.\begin{matrix}\text{C}^*\\ \text{N}^*\end{matrix}\right\} + \left.\begin{matrix}\text{O}\\ \text{N}\end{matrix}\right\}$$

Energy considerations require that, in general, the molecule be in an excited vibrational state produced by excitation during the current pulse. From the measured populations, a cross-section for this reaction is estimated and found to be $7 \times 10^{-16} \text{cm}^2$, with vibrational temperatures in the region of $25,000^{\circ}\text{K}$.

BODLEIAN LIBRARY OXFORD
DEPOSITED
THESIS
16.xi.67

STUDIES OF STIMULATED EMISSION OF RADIATION

A Thesis Submitted for the Degree of

Doctor of Philosophy

in the

University of Oxford

by

J. B. Atkinson, B.A.

Wadham College

Clarendon Laboratory

OXFORD

September 1967

CONTENTS

		Page
CHAPTER 1		
INTRODUCTION		1-1
CHAPTER 2		
LASER THEORY		2-1
CHAPTER 3		
APPARATUS		
3.1	Gas Handling System	3-1
3.2	Laser Tube Excitation	3-3
3.3	Optical Detection System	3-4
3.4	Photomultipliers	3-5
3.5	Laser Mirrors	3-6
3.6	Filters	3-7
3.7	Overall Layout	3-7
CHAPTER 4		
EXCITATION MECHANISMS		
4.1	Electron - Atom collisions	4-1
4.2	Atom - Atom collisions	4-4
4.3	Electron - Molecule collisions	4-5
4.4	Atom - Molecule collisions	4-6
4.5	Electron - Ion collisions	4-6

Page

CHAPTER 5

MEASUREMENTS OF POPULATION

5.1 Absolute Emission 5-1

5.2 Absorption 5-2

5.3 Absolute populations by calibration with a laser 5-8

CHAPTER 6

RESULTS FOR HELIUM - CARBON MONOXIDE

6.1 Term Diagram 6-1

6.2 Laser Lines 6-2

6.3 Excitation Mechanisms 6-8

CHAPTER 7

RESULTS FOR NEON - CARBON MONOXIDE

7.1 Laser Lines 7-1

7.2 Excitation Mechanisms 7-3

CHAPTER 8

RESULTS FOR HELIUM - NITROGEN

8.1 Term diagram 8-1

8.2 Laser Lines 8-3

8.3 Excitation Mechanisms 8-8

CHAPTER 9

RESULTS FOR NEON-NITROGEN, HELIUM-NEON AND CONCLUSIONS

9.1 Laser Lines 9-1

9.2 Excitation Mechanisms 9-2

9.3 Helium - Neon Laser 9-5

9.4 Conclusions 9-6

ACKNOWLEDGEMENTS

TABLES

		Page
3.1	Laser Mirror Details	3-6
4.1	Energy coincidences (He-Ne)	4-4
5.1	F_1', F_2', and $1 + (RF_2'/F_1')$ vs. $k_o l$	5-7
5.2	$k_o l$ from different theories vs. t	5-10
6.1	Carbon transition parameters	6-2
6.2	Carbon laser transitions (Helium)	6-3
7.1	Carbon laser transitions (Neon)	7-1
8.1	Nitrogen transition parameters	8-2
8.2	Nitrogen laser transitions (Helium)	8-3
9.1	Nitrogen laser transitions (Neon)	9-1

FIGURE CAPTIONS

2.1	Hole Burning and Laser output spectrum
3.1	Schematic diagram of gas handling system
3.2	Laser tube dimensions
3.3	Pulser circuit diagram
3.4	Schematic diagram of Optical layout
3.5	Photomultiplier circuit
3.6	General view of apparatus
4.1	Electron-Atom collision cross-sections (Theoretical)
4.2	Excitation rate coefficients (Theoretical)
4.3	Molecular potential curves illustrating the Franck-Condon principle
5.1	Diagram for self-absorption calculation
5.2	F_1', F_2', and $1 + (RF_2 / F_1)$ vs. $k_o l$
5.3	F_1' and S vs. $k_o l$
5.4	Graph for absolute population calculation
6.1	Carbon term diagram (Triplets)
6.2	Carbon term diagram (Singlets)
6.3	Oscilloscope traces (He-CO)
6.4	Oscilloscope traces (He-CO)
6.5	9406Å laser delay vs. current
6.6	9406Å laser peak gain vs. Helium pressure
6.7	9406Å laser delay vs. Helium pressure
6.8	$k_o l$ and laser output vs. time
6.9	3888Å side-light and end-light vs. time
6.10	5876Å side-light and end-light vs. time
6.11	9406Å side-light vs. time
6.12	2479Å side-light and end-light vs. time

7.1 Oscilloscope traces (Ne-CO)

7.2 9406Å laser delay vs. current

7.3 9406Å laser peak gain vs. Neon pressure

7.4 9406Å laser delay vs. Neon pressure

7.5 9406Å side-light vs. time

7.6 2479Å side-light vs. time

7.7 5852Å side-light and end-light vs. time

7.8 2837Å side-light and end-light vs. time

7.9 5882Å side-light vs. time

8.1 Nitrogen term diagram (Quartets)

8.2 Nitrogen term diagram (Doublets)

8.3 Oscilloscope traces (He-N_2)

8.4 Oscilloscope traces (He-N_2)

8.5 9393Å laser delay vs. current

8.6 9393Å laser delay vs. Helium pressure

8.7 9393Å laser peak gain vs. Helium pressure

8.8 9393Å gain and laser output vs. time

8.9 9393Å and 9387Å side-light vs. time

8.10 3888Å side-light and end-light vs. time

8.11 5876Å side-light and end-light vs. time

8.12 5015Å side-light and end-light vs. time

9.1 Oscilloscope traces (Ne-N_2)

9.2 Oscilloscope traces (Ne-N_2)

9.3 9393Å laser delay vs. current

9.4 9393Å laser delay vs. Neon pressure

9.5 9393Å and 9387Å laser peak gain vs. Neon pressure

9.6 5852Å side-light and end-light vs. time

9.7 5882Å side-light and end-light vs. time

9.8 9393Å, 9387Å and 8680Å side-light vs. time

9.9 Oscilloscope traces (He-Ne-N_2)

9.10 11523Å laser delay vs. current

COMMONLY USED SYMBOLS

N_i	Atomic population of level i
g_i	Statistical weight of level i, $= (2J_i + 1)$
τ_i	Lifetime of level i
λ	Wavelength
ν	Frequency
Å	Ångström ($= 10^{-8}$cm.)
A	Einstein A coefficient
f	Absorption Oscillator Strength
$\Delta\nu_D$	Full width at half maximum of Doppler line profile
$\Delta\nu_N$	Full width at half maximum of natural broadened profile
k_ν	Absorption coefficient for frequency ν
k_o	Peak value of k_ν
l	Active length of discharge
c	Velocity of light
h	Planck's constant
e	Electron Charge
m	Electron Mass
i	Peak discharge current
I	Light intensity

CHAPTER 1

Introduction

The concept of stimulated emission of radiation was first put forward by Einstein in 1917. He showed that the equilibrium between atoms and thermal radiation was consistent with statistical theory only if an atom in an excited state can make a radiative transition to a lower state either spontaneously or by interaction with an electromagnetic wave of the appropriate frequency. This latter process, stimulated emission, is the inverse of the more common process of absorption. By means of the Planck black-body radiation formula and statistical agruments, he derived the relative probabilities of the two processes. Under conditions of thermal equilibrium, the rate of absorption outweighs the rate of stimulated emission, giving a net absorption, since there are more atoms in the lower state than the upper state. If there is some means of producing more atoms in the upper level than the lower level, there will then be amplification of the electromagnetic wave.

In 1954, Gordon, Zeiger and Townes succeeded in producing a population inversion in ammonia gas, and observed amplification in the microwave region. This device was called a MASER, the word being an acronym for Microwave Amplification by Stimulated Emission of Radiation. Several other materials were found which would amplify in the microwave region, but it was not until 1960 that Maiman extended the technique to the optical region. The first Laser used a ruby rod for the amplifier and the operational wavelength was 6943Å. This was soon followed by the first gas laser which used a mixture of Helium and Neon, excited by r.f. power from a transmitter, as the amplifying medium. Since then, a great many

lasers have been constructed, operating at wavelengths between 2800Å and 600μ, using a large variety of materials.

One important aspect of laser research is the study of the mechanisms by which atoms are excited, since a knowledge of these enable improvements in performance to be made. The work described in this thesis deals with population inversion between certain levels in atomic Carbon and Nitrogen and the mechanisms by which it is produced. A brief outline of laser theory and the important parameters is given in Chapter 2, while Chapter 3 describes the apparatus used. Chapters 4 and 5 deal with general methods for exciting atomic levels and the measurement of the populations, and discusses the techniques developed by the author. The remaining Chapters give the experimental results together with their interpretation.

CHAPTER 2

Laser Theory

Application of the Einstein Theory of Radiation to a medium containing two energy levels, E_2, E_1, produces the following relationship between the integrated absorption coefficient for the transition between the levels and their respective populations, (Ref. 2.1)

$$\int_0^\infty k_\nu \, d\nu = \frac{A_{21}}{g_1} \frac{\lambda^2}{8\pi} (g_2 N_1 - g_1 N_2) \qquad (2.1)$$

$$= \frac{\pi e^2}{mc} \frac{f}{g_2} (g_2 N_1 - g_1 N_2) \qquad (2.2)$$

If $g_1 N_2 > g_2 N_1$, then the integrated absorption coefficient is negative, and radiation of wavelength λ passing through the medium is amplified. By means of positive feedback, oscillation can then be produced. The feedback is achieved by enclosing the medium in a resonant cavity, which in practice consists of a pair of mirrors facing each other.

Consider a mode of the resonant cavity. In order that it may be sustained, the amplification or gain must compensate for the total losses. These losses are in general made up of absorption and scattering in the medium, diffraction at the mirrors, and absorption, scattering and transmission in the mirrors. For gas lasers, mirror losses dominate.

For a peak gain coefficient k_o, the mathematical expression for this is

$$(1 - L_1)(1 - L_2) \exp(2k_o l) = 1$$

where l is the length of the amplifying medium, and L_1, L_2, are the

fractional energy losses at each end of the medium. In most practical cases, the minimum losses are the same at both ends, each being about 1%.

Thus, typically, $k_o l \geq 0.01$ for oscillation.

The optical resonant cavity, consisting of the two mirrors, differs from the resonant cavities encountered in microwave theory by the absence of sidewalls. This absence severely restricts the number of possible high-Q modes for the optical cavity. The calculation of the possible modes has been considered by many authors (e.g. Ref 2.2), with the conclusions that the modes with the highest Q are those resembling a TEM_{oo} microwave cavity mode. For mirrors spaced a distance l_o apart, these modes are separated in frequency by $c/2l_o$ in the empty cavity. The mode frequency separation is affected by the presence of the oscillating medium, but the change in the separation is small compared to the separation. For a mirror separation of 200cm., the mode frequency separation will therefore be approximately 150MHz.

The relationship between k_ν and ν generally depends on a number of processes and interactions within the medium. Of the five common types of line broadening, only natural broadening and Doppler broadening can be easily calculated, and in the media to be considered, these are the dominant forms.

The lineshape due to Doppler broadening is

$$k_\nu = k_o \exp(-\ln 2 (2(\nu - \nu_o)/\Delta\nu_D)^2)$$

where $k_\nu = k_o$ at $\nu = \nu_o$ and $\Delta\nu_D$, the Doppler width, is the full width at half maximum and is given by

$$\Delta\nu_D = 2\sqrt{2R\ln 2}\ \nu_o \sqrt{T/M}\ /c = 7.16 \times 10^{-7} \nu_o \sqrt{T/M}$$

T being the temperature, and M the molecular weight.

The lineshape due to natural broadening is

$$k_\nu = k_o/(1+(2(\nu - \nu_o)/\Delta\nu_N)^2)$$

where $\Delta\nu_N = \Lambda/2\pi = 1/2\pi\tau = \dfrac{4\pi e^2 g_1 f}{mcg_2 \lambda^2}$

The combination of both types of broadening gives rise to a lineshape known as the Voigt Profile.

As will be shown later, Doppler broadening is the more important in the transitions to be considered, so to first order, only the Doppler lineshape will be considered. Performing the integrals of k_ν over ν and using Equ. 2.2 gives

$$k_o = \frac{2}{\Delta\nu_D}\sqrt{\frac{\ln 2}{\pi}}\ \frac{\pi e^2}{mc}\ N_1 f\left(\frac{N_2 g_1}{N_1 g_2} - 1\right)$$

$$= 1.162 \times 10^{-6}\ \frac{N_1 f}{\sqrt{T/M}}\left(\frac{N_2 g_1}{N_1 g_2} - 1\right)$$

where N_1, N_2, are in cm.$^{-3}$, λ in cm., T in ^oK, M is the Molecular Weight and k_o in cm.$^{-1}$.

Hence from a knowledge of the oscillator strength of the transition, the molecular temperature and the discharge length, the minimum population difference to support laser action can be estimated. Here, and in the thesis, the term, population difference, is used for $g_1N_2 - g_2N_1$.

The laser output spectrum is determined by two main factors, the width and the shape of the gain curve of the amplifying medium. If the line is Doppler broadened and the natural width is much less than the mode spacing of the cavity, the line is known as an inhomogeneously broadened line. For such a line, one can calculate the probability of stimulated emission by means of time-dependent perturbation theory. The result is that the probability is

a Lorentzian function of frequency, the peak occurring at the frequency of the stimulating wave, and the half width being the natural width. Since for steady state conditions, the total loss, including that due to the output, must exactly equal the gain, the gain curve at each mode frequency must equal the threshold value. "Holes" are burned into the gain curve whose half widths are the natural width and a typical gain curve will look like Fig. 2.1. The laser output spectrum will then consist of lines very close to the empty cavity mode frequencies, but the widths will be less than the natural widths, theoretical values being as low as 10^{-3} Hz. This is also illustrated in Fig. 2.1. Use of this theory has been made in Chapter 6 where a reference is given which discusses the whole problem in considerably more detail.

References

2.1 A. C. G. Mitchell & M. W. Zemansky — Resonance Radiation and Excited Atoms p 95 (1961)

2.2 A. G. Fox & T. Li — Proc IEEE 51, 80 (1963)

Fig 2.1

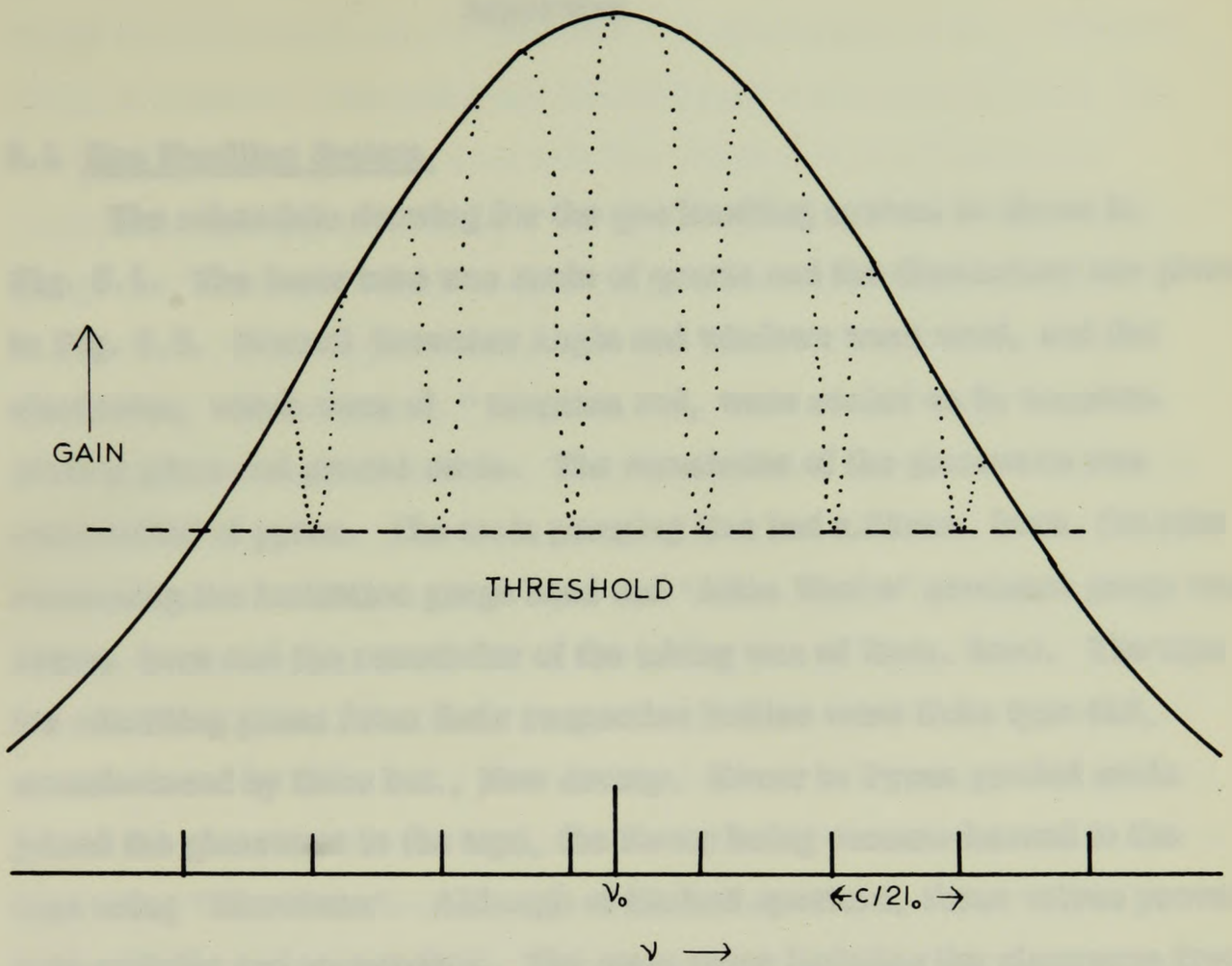

HOLE BURNING IN GAIN CURVE

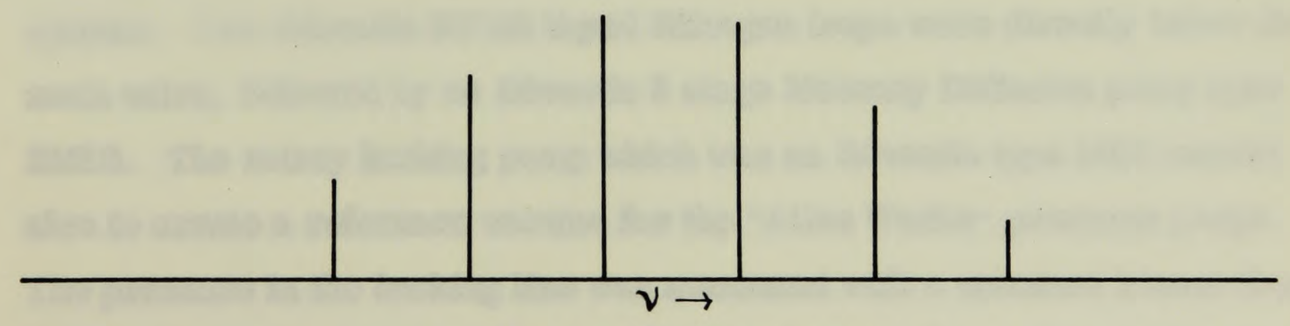

LASER OUTPUT SPECTRUM

CHAPTER 3

Apparatus

3.1 Gas Handling System

The schematic drawing for the gas handling system is shown in Fig. 3.1. The laser tube was made of quartz and the dimensions are given in Fig. 3.2. Normal Brewster Angle end windows were used, and the electrodes, which were of " tungsten rod, were sealed on by tungsten sealing glass and graded seals. The remainder of the glassware was constructed of pyrex. The main pumping line had a 25mm. bore, the tube connecting the ionisation gauge head and "Atlas Werke" pressure gauge was 15mm. bore and the remainder of the tubing was of 7mm. bore. The taps for admitting gases from their respective bottles were Hoke type 413, manufactured by Hoke Inc., New Jersey. Kovar to Pyrex graded seals joined the glassware to the taps, the Kovar being vacuum-brazed to the taps using "Nicrobraz". Although of limited aperture, these valves proved both reliable and economical. The main valve isolating the glassware from the diffusion pump and liquid Nitrogen traps was a Palatine Edwards Model MCV4. This has a pumping area of 1 sq. in. for rapid pumping of the main system. Two Edwards NTM2 liquid Nitrogen traps were directly below the main valve, followed by an Edwards 3 stage Mercury Diffusion pump type 2M3B. The rotary backing pump which was an Edwards type 1350 served also to create a reference vacuum for the "Atlas Werke" pressure gauge. The pressure in the backing line was measured with a standard Pirani Gauge. Three pressure gauges were used on the main apparatus. An Alpert type ionisation gauge was used to measure the ultimate vacuum in the apparatus. The remaining two gauges were for measuring the pressure in the laser tube during operation. The first was a bakeable-type Pirani gauge manufactured

by the firm of LKB, and proved to be stable and reproducible over a range of pressures from 0.1 microns to 1 atmosphere of air. Unfortunately, it required calibrating for different gases and gas mixtures, but nevertheless, it proved to be a valuable monitor of small pressure variations during gas clean-up. The other gauge was the "Atlas Werke" gauge mentioned previously. This gauge operates by measuring the capacitance formed by a fixed plate and a spring-loaded vacuum-tight diaphragm. The diaphragm divides a chamber into two sections. The first of these is evacuated by the rotary pump and serves as a reference vacuum. The other section is connected to the main manifold of the high vacuum system. Pressure changes give rise to linear changes in capacitance, and these are measured by means of a radio-frequency bridge circuit. Since thermal fluctuations can cause considerable errors in this type of gauge due to expansion, the measuring chamber is maintained at 55°C by means of a heating element and a thermostat. The same heating element is used to bake the measuring chamber during the evacuation and baking of the whole system. Both the LKB gauge and the "Atlas Werke" gauge were calibrated against an oil manometer.

The glassware and taps were mounted on a 1" thick asbestos-concrete baseboard. This provided good thermal insulation during baking. An iron U-channel, 2" high by 3" wide was mounted along the centre of the baseboard, and on it were mounted the supports for the laser tube, the heating elements for the oven, and optical benches at each end for the mirror mounts. Three bar elements, each rated at 1kW, were used for baking. The laser supports were made of brass for the purposes of baking, but perspex supports were substituted when the pulser was operating. For baking, an oven was lowered on to the baseboard. The oven was constructed of dural, and the walls were filled with vermiculite. Temperatures of 350°C could be attained, but an

arbitrary upper limit of 300°C was controlled by a thermostat. The upper cold trap was baked at the same time with heating tapes, and also the Atlas Werke gauge. The final pressure achieved was always less than 2×10^{-8} Torr.

The gases used in this work were spectrally pure Helium, Neon, Carbon Monoxide and Nitrogen, supplied by British Oxygen Co. in flasks fitted with a breakseal. After baking, the breakseals were broken with glass-coated iron hammers. Fritted filter tubes were fitted between the breakseals and the taps to prevent glass particles damaging the tap seating.

3.2 Laser Tube Excitation

The circuit diagram for the pulser is shown in Fig. 3.3. A neon-stabilised power supply charges up C2 (or C3 or C4) through VR1 and R1+R2 until the voltage on the anode of the gas-filled thyratron NGT2 is sufficient to fire it. C1 then discharges through the thyratron and R2 to give a pulse whose amplitude is approximately the firing voltage of NGT2 and whose time constant is given by the product of R2 and C1 (0.5μsec.) C2 discharges through the thyratron and the cycle repeats itself. The repetition rate of the pulses is determined by the bias voltage on the grid which determines the firing voltage of the thyratron and the time constant (R1 + R2 + VR1) x C2. The pulse triggers the hydrogen thyratron 3C45. C5 which has charged up to 1kV is then discharged through the 3C45 and R3, the output pulse having an amplitude of approximately the anode voltage and with a time constant given by R3 and C5 (2μsec.). This pulse triggers the hydrogen thyratron 5C22. The delay line is then discharged through the 5C22 and the primary windings of the pulse transformer, the laser tube being connected across the secondary windings. The CV2160 diode provides a short circuit path for any reflected wave from the delay line due to mismatching of impedances. Although the variable D.C. supply voltage has a maximum of

8kV, it is easy to show that the resonant circuit consisting of the delay line acting as a capacitor in series with the charging choke and the diode, charge the delay line to almost double the supply voltage. The maximum pulse current in the discharge tube is limited to 93Amp by the 325Amp rating of the 5C22 and the 3.5 : 1 step up transformer. The peak voltage that can be applied to the 5C22 is 16kV. The pulse current was measured with a current transformer. The earth return line from the tube passed through a toroidal ferrite core, around which 100 turns of 30 gauge wire were wrapped, and a 100 ohm resistor was connected across the coil ends. This transformer was calibrated against the voltage developed across a 1 ohm resistor in series with the discharge tube.

During initial work, the laser tube was connected to the gas system at the tube centre, and trouble was experienced with the discharge passing down the pumping line to earth at one of the taps. Despite changing the pumping connection to one electrode and earthing that electrode, a discharge still passed down to the main tap. Using a current transformer in each lead, it was found that the currents were, within experimental error, identical so that the effects of this discharge on the measurement were discounted.

3.3 Optical Detection System

The general plan for the optical detection system is shown in Fig. 3.4. Wavelength measurements were made with a 3.4 metre Ebert-mounting spectrograph and the appropriate photographic plates. The plane diffraction grating has 288 grooves/mm. and is blazed in 1st order at 2.1μ. The aluminised concave mirrors have a focal length of 3.4m. and this gives a dispersion of 2.5Å/mm. in 4th order. For measurements of intensity as a function of time, the plateholder was replaced by a photomultiplier and mount. There were two main disadvantages of this spectrograph. First, its weight and size made it a fixture, and secondly, its low light gathering

power (f/23) made it unsuitable for viewing light from the side of the discharge tube. For these reasons, a small Czerny-Turner type spectrograph was also used. This instrument has a focal length of 60cm. and has a light gathering power of f/6. The plane diffraction grating had 600 grooves/mm. and is blazed for 1.6μ. The dispersion in 3rd order at the blaze angle is 9Å/mm. As with the Ebert spectrograph, the Czerny-Turner could be used either with photographic film or a photomultiplier. A plane aluminized mirror reflected the light from the end of the laser tube onto the entrance slit, while for viewing the light from the side of the discharge, two quartz right angle prisms set at 90° produced a vertical image of the horizontal discharge tube. Quartz lenses were used to image the discharge tube onto the spectrograph slit.

3.4 Photomultipliers

Three types of photomultiplier were used. A RCA 7102 with a S-1 photocathode was used in the infra-red. An EMI 9558 with a S-20 photocathode was used for the near infra-red region. For measurements in the ultra-violet and visible regions, an EMI 9656QB with a S-13 photocathode was used, and its response stretched from 1900Å to the red region of the spectrum. The diagram of the photomultiplier circuitry is shown in Fig. 3.5. Values for the dynode resistors were 39k for R1-R8 and 82k for R9-R11 with C1-C3 being 0.01μF. These capacitors on the final three dynodes were to prevent increases in gain caused by the change in the dynode voltages when large photocurrents were being drawn. The RCA 7102 had different component values, R1 being 220k and the remaining resistors 100k. The EMI 9558 has 11 dynodes, but only the last three dynodes had larger resistors and de-coupling capacitors. Various anode load resistors ranging from 1M to 100 ohm could be used by means of the 6-way switch. The

signal was displayed on one beam of a Tektronix type 551 double-beam oscilloscope. This oscilloscope, together with the type L plug-in preamplifiers had a risetime of 0.02μsec. The other beam usually displayed the current pulse. A compromise had to be reached between the increased signal with the larger load resistors and the increased time constant which is determined mainly by the anode resistor and the capacitance of the coaxial cable linking the photomultiplier to the oscilloscope and the input capacitance of the oscilloscope pre-amplifier. The latter was 47pF and the cable capacitance 70pF. With the 1k load resistor used with the EMI photomultipliers, the time constant is 0.1μsec. The load resistor with the infra-red photomultiplier was 10k in order to obtain adequate signal, and this increased the time constant to 1μsec. The H.T. for the photomultipliers was supplied by an Isotope Developments Ltd. type 532D EHT unit. This unit provides a stable voltage, variable up to 3kV with a maximum current of 3.5mA, but this can be increased to 5mA for voltages less than 1.5kV. The voltages used in this work were in the range 1.0 -1.45kV.

3.5 Laser Mirrors

Five sets of dielectric coated mirrors were available in addition to the silvered and aluminised mirrors. The details are shown in Table 3.1.

Table 3.1

Diameter	Radius of Curvature	Peak Reflectivity	Wavelength Range (99% Reflectivity)
2"	2.25m.	99.5%	8600-11200Å
1"	2m.	99.5%	6370-8060Å
1"	2m.	99.5%	5900-6900Å
1"	2m.	99.6%	5000-6000Å
1"	2m.	99.5%	3800-4600Å

3.6 Filters

A variety of Chance Glass Filters were used, both for eliminating the problem of overlapping orders in the spectrographs, and as calibrated loss elements in the laser cavity. Their transmission at the laser wavelengths was determined on a Unicam double beam spectrophotometer. The smallest calibrated loss element was equivalent to a k_o of 0.059/metre. Values of k_o between two calibrated values could be estimated by varying the angle of the Filter between Brewsters angle and the normal to the tube axis, and by measuring the intensity of the laser output with the filter(s) in the cavity.

3.7 Overall Layout

Fig. 3.6 is a photograph of the apparatus showing the general layout. The various parts of the apparatus are labelled.

Fig 3.1

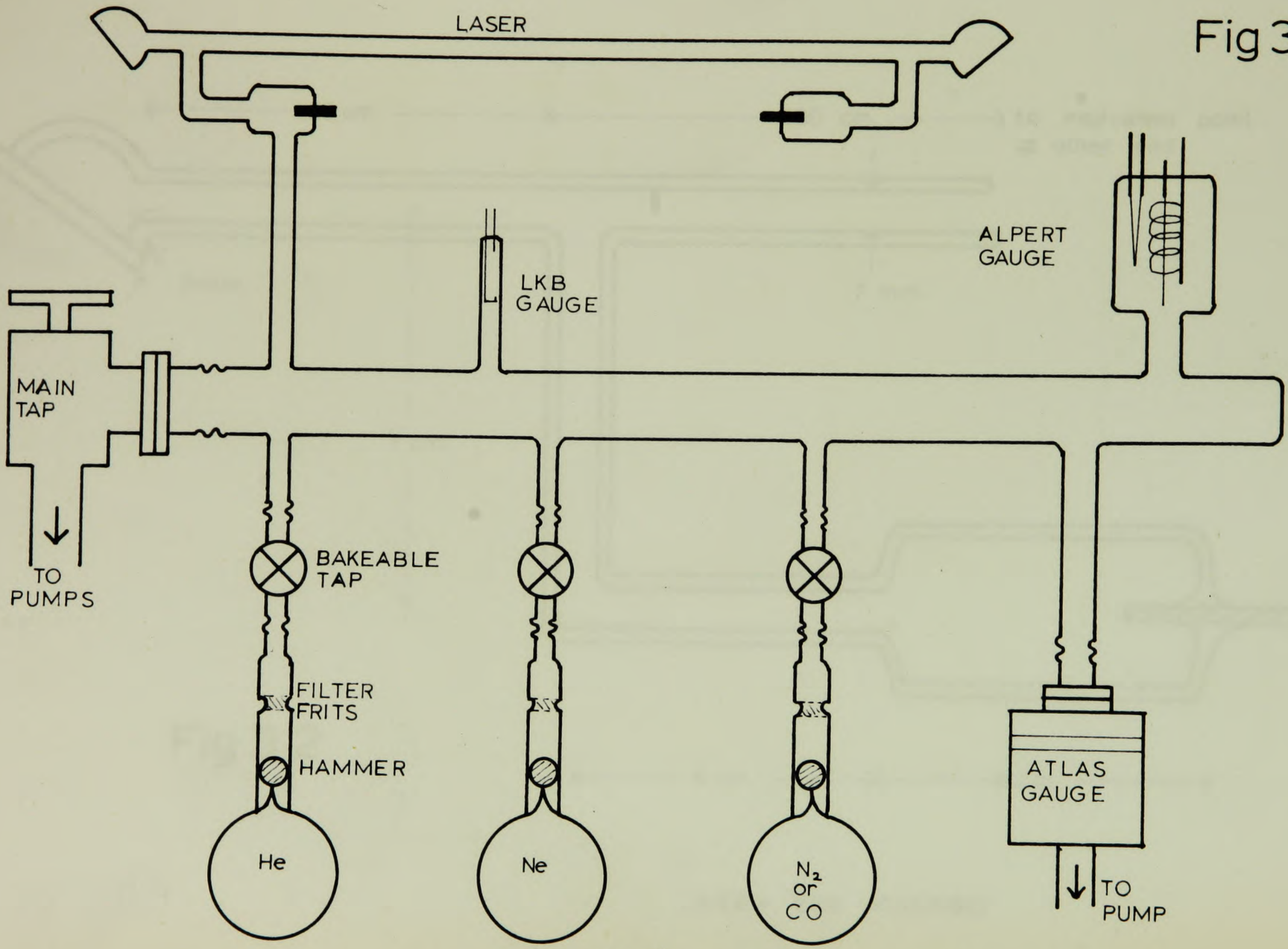

GAS HANDLING APPARATUS (Schematic)

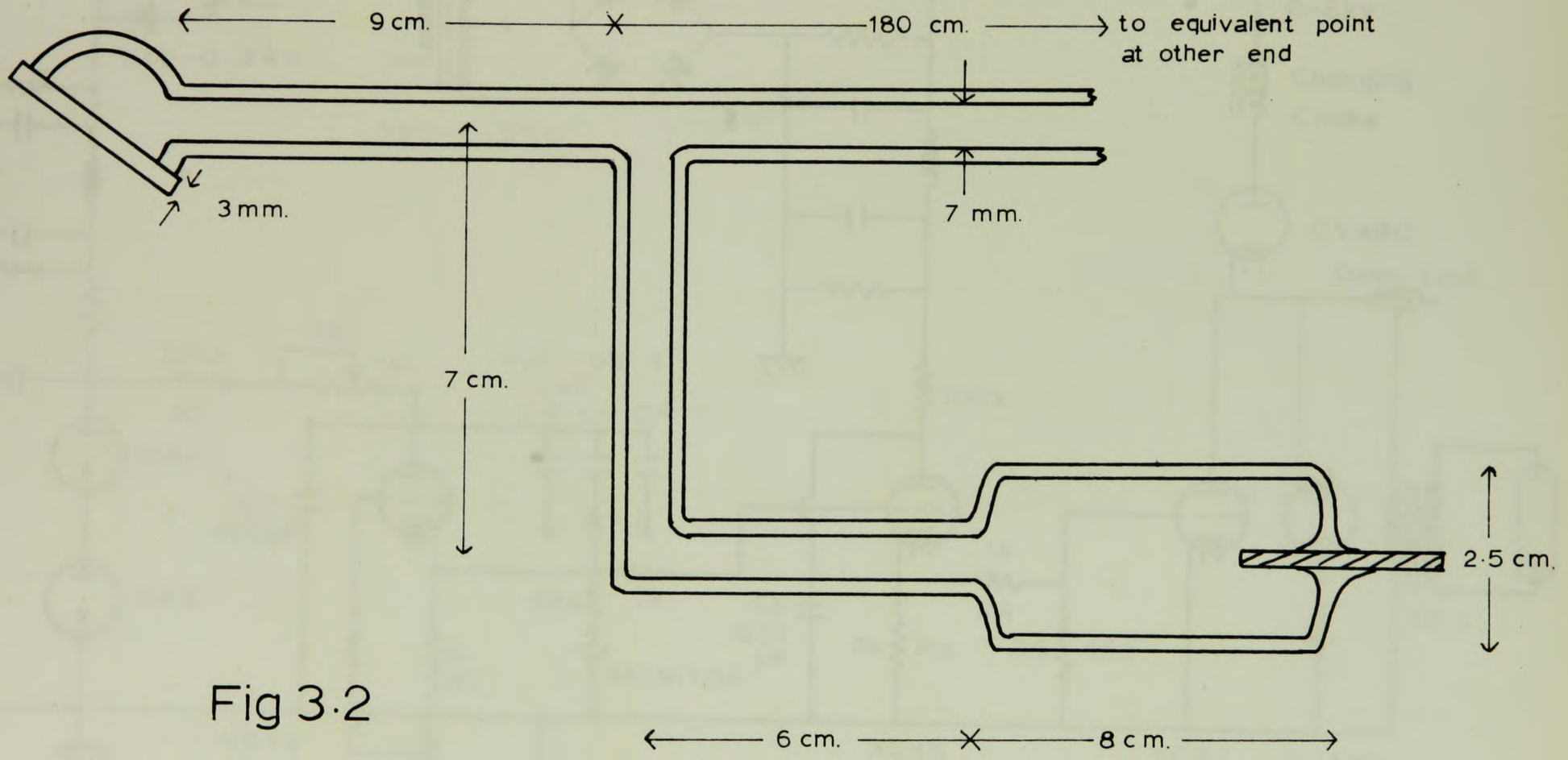

Fig 3·2

LASER END ASSEMBLY

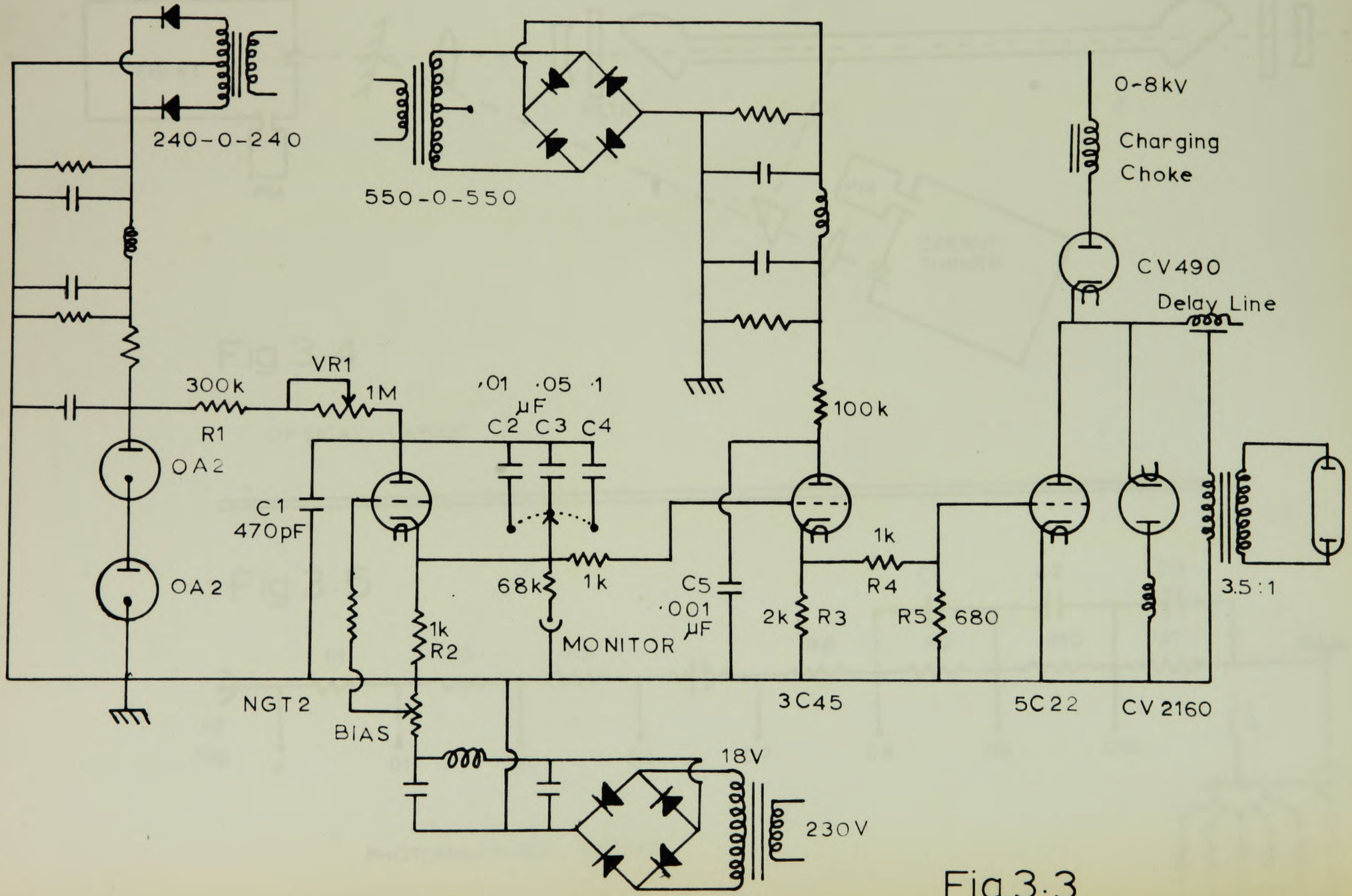
240-0-240
550-0-550
0-8kV
Charging
Choke
CV490
Delay Line
VR1
300k
1M
R1
OA2
OA2
C1
470pF
·01 ·05 ·1
µF
C2 C3 C4
100k
1k
R4
68k
1k
C5
·001
µF
2k R3
R5 680
3.5:1
1k
R2
MONITOR
NGT2
BIAS
3C45
5C22
CV2160
18V
230V

Fig 3.3

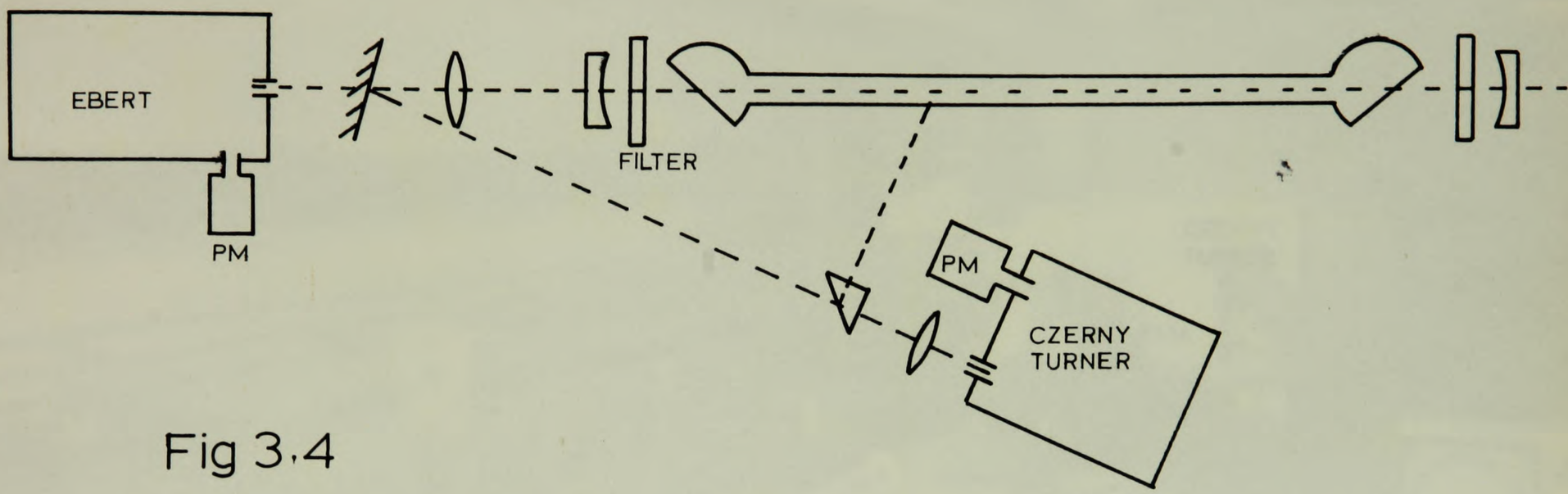

Fig 3.4

OPTICAL LAYOUT

Fig 3.5

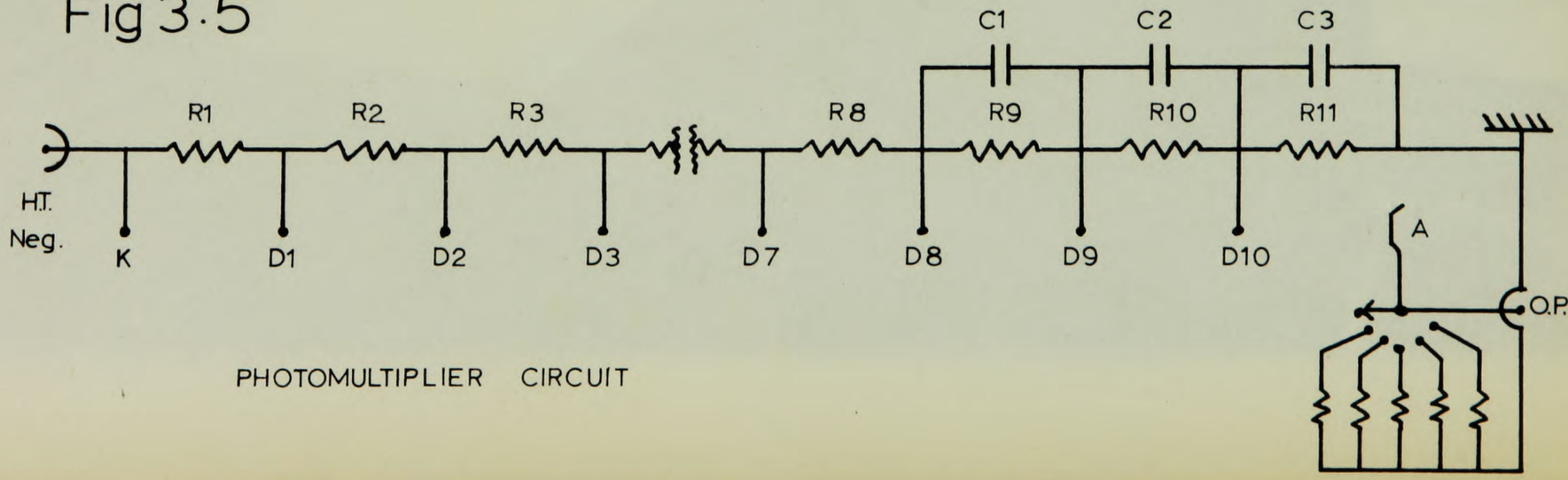

PHOTOMULTIPLIER CIRCUIT

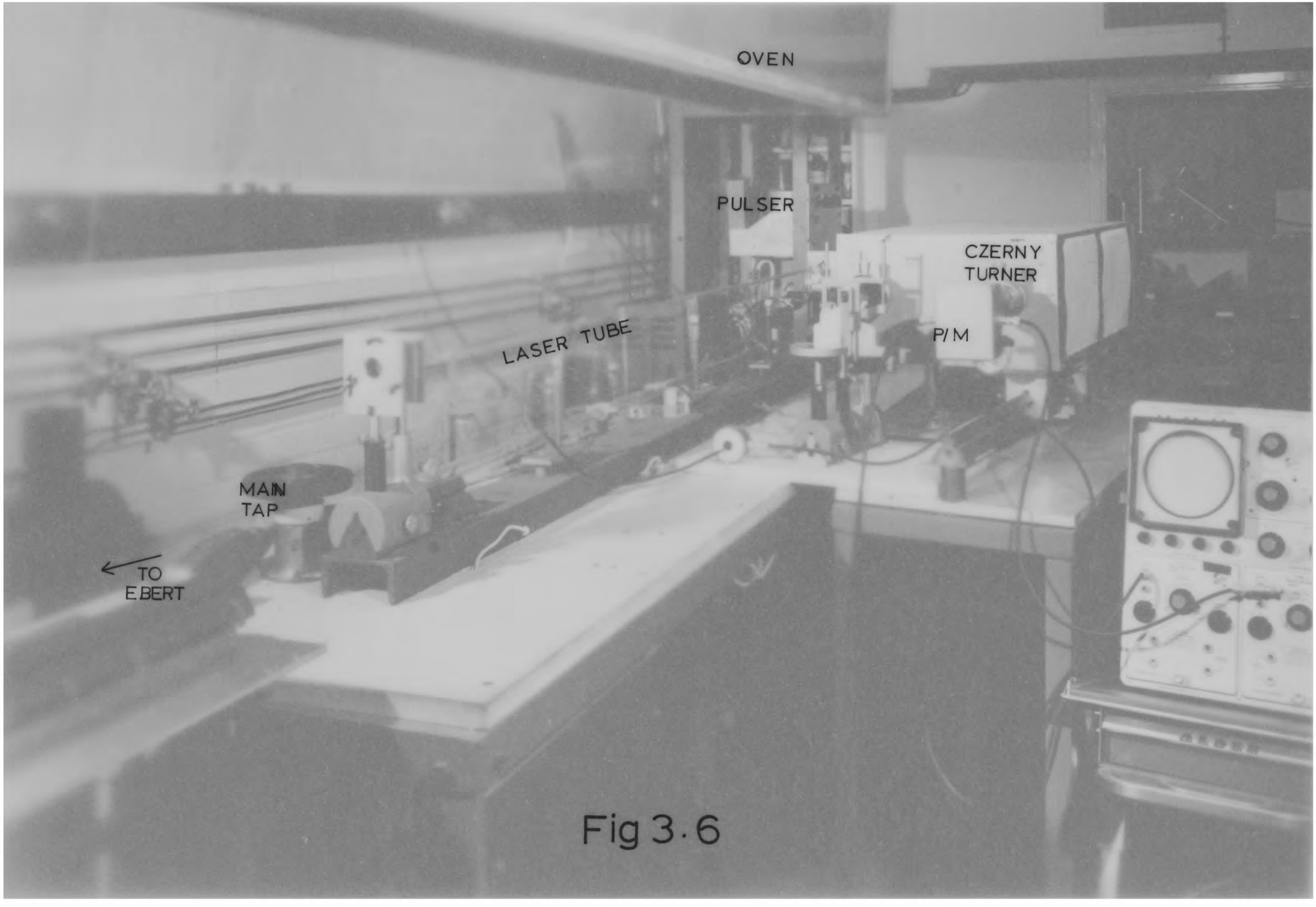

Fig 3.6

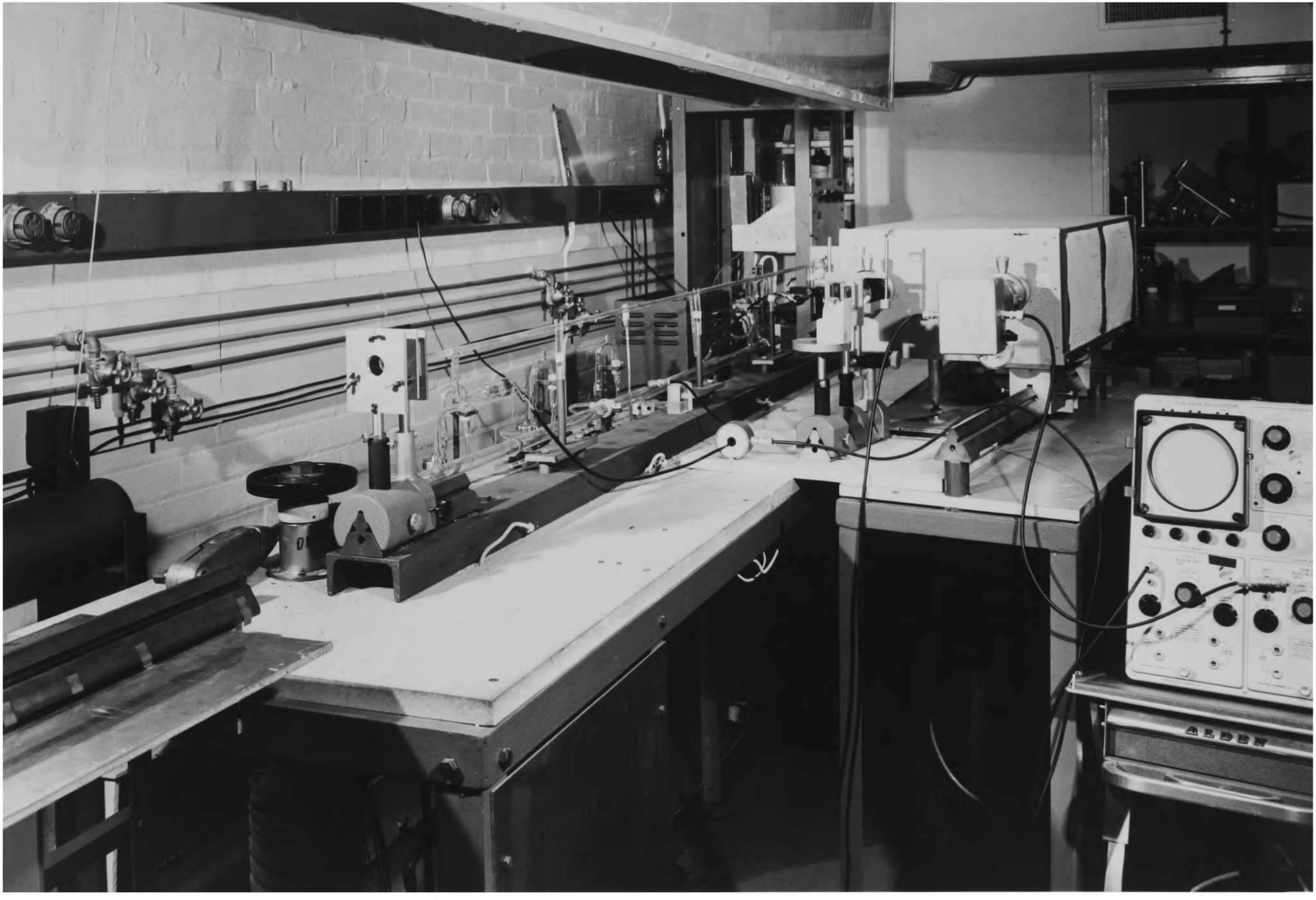
AEDEN

CHAPTER 4

Excitation Mechanisms

There are in general several processes which can excite a particular level of an atom, molecule or ion. In this Chapter, these processes will be briefly discussed and attempts made to estimate their relative importance in specific instances. The concept of cross-section in such processes is important, and the cross section is defined in the following way. Consider a particle with velocity v injected into a gas. The probability, dP, that a particular type of collision process will occur is given by

$$dP = N\sigma(v)\,dx$$

where N is the number of particles per unit volume in the gas, dx is the distance travelled in the gas and $\sigma(v)$ is defined as the cross-section for the collision process. If there are ndv particles per unit volume with velocity between v and v+dv, then the rate of production of an excited state is given by

$$\frac{dN^*}{dt} = Nn(v)\sigma(v)\,v\,dv$$

4.1 Electron - Atom Collisions

This is the most common process of excitation in gas discharges. The result of such a collision will of course depend on the energy of the electron, but it can either ionise the atom, excite it to a higher level or leave it in the same state but with a different velocity. It is the first two processes that interest us. The problems of estimating the cross-sections for these processes is discussed in detail by Massey and Burhop (Ref 4.1) and Mott and Massey (Ref 4.2). In general the Born approximation is found to hold very well for electron energies much greater than the threshold energy for the process. The Born approximation gives for the cross-section for

excitation to level m

$$\sigma_{om} \propto \left| \int \exp(i\underline{K}\cdot\underline{r})\ \psi_m^* \psi_o\ d\tau \right|^2$$

where ψ_m, ψ_o are the wave functions for the atom in state m and the ground state, and $\underline{K}$ is the change in propagation vector for the electron. By expanding the exponential function, we see that the first non-vanishing term is

$$\sigma_{om} \propto \left| \int \psi_m^*\, r\, \psi_o \quad d\tau \right|^2 \propto A_{mo}$$

A_{mo} being the Einstein A coefficient. Hence the largest cross-sections for electron impact are to those states which are optically connected to the ground state. The excitation may occur from an already excited state and all the above arguments still hold, but since the rate of excitation is proportional to the density of atoms in the lower state, there are not in general sufficient atoms in an excited state for this to be an important process. An important exception is metastable states.

Mott and Massey give for σ_{om}

$$\sigma_{om} = \frac{3m\alpha c}{16\pi^2} \quad \frac{g_m A_{mo} \lambda_{mo}^3}{E} \quad \log_e \frac{4E}{W}$$

where α is the fine structive constant, g_m is the statistical weight of level m, A_{mo} the Einstein A coefficient for transition from state m to the ground state, λ_{mo} the wavelength of that transition, W the excitation energy for level m, and E the electron energy. Numerically

$$\sigma = 2.36 \times 10^{-33} \left(\frac{\lambda^3 g_2 A}{E} \log_e \frac{4E}{W} \right) \text{cm}^2.$$

with λ in Å, A in sec^{-1}, and E, W, in eV.

Seaton (Ref: 4.3) gives

$$\sigma = 2.37 \times 10^{-13} (f/EW)\ \text{b} \quad \text{cm}^2.$$

where f is the oscillator strength, E, W, are as before and b is a function of E/W rising from 0 at E/W = 1 to 1.33 at E/W = 100.

Green (Ref. 4.4) considers a number of theories and experimental results and comes to the conclusion that one can use the following phenomenological equation,

$$\sigma(E) = (q_o f / W^2) g(\epsilon)$$

where $q_o = \pi a_o^2$, $(2R_e) = 6.51 \times 10^{-14}$ cm^2 eV^2, f is the oscillator strength, E the electron energy in eV, W the energy level in eV, a_o the first Bohr radius, R_e the Rydberg constant and $\epsilon = E/W$. $g(\epsilon)$ has the form

$$g(\epsilon) = c_o (1-1/\epsilon)^{\nu} (1/\epsilon)^{1-\omega} \quad , \quad 1 < \epsilon < 100$$

For allowed transitions, the values that give the best fit are $c_o = 1$, $\nu = 1/2$, $\omega = 1/4$. If transitions which break the selection rule $\Delta S = 0$ are considered, the best fit is given by $c_o = 1$, $\nu = 1/2$, $\omega = -2$ and for the oscillator strength, one takes the similar allowed transition oscillator strength. Fig. 4.1 compares the different cross-sections from these equations. By taking a Maxwell-Boltzmann energy distribution for the electron energy, the integral over velocity can be performed. The result is

$$\frac{dN_2}{dt} = \frac{4nNq_o f}{(2\pi m(kTe)^3)^{1/2}} g(W/kTe) \qquad \text{cm}^{-3}\ \text{sec}^{-1}$$

$$= 4.35 \times 10^{-6} \frac{Nnf}{(kTe)^{3/2}} g(W/kTe) \text{cm}^{-3}\ \text{sec}^{-1}$$

where T_e is the electron temperature, kTe is in eV, and $g(W/kT_e)$ is an integral which is shown as a function of W/kT_e in Fig. 4.2. The integral was performed numerically on the KDF9 computer. Although the absolute accuracy of the excitation rate is not likely to be high, it does enable order of magnitude estimates to be made.

4.2 Atom - Atom Collisions

The analysis of this reaction when both atoms are in their ground states is similar to that for electron - atom collisions. However, because of the mass of the incident particle is of the same order as the target particle, the threshold energy is about twice the electron - atom collision threshold. Furthermore, the peak cross-section for the reaction occurs when the time during which the two particles are approximately an atomic radius apart is the same as the time for the atomic transition. The velocity of the indident atom at the peak cross-section is thus about 10^7 cm./sec. For an atom, this corresponds to an energy of the order of 10^3 eV and hence is most unlikely in a gas discharge. Of far greater importance is the case when one of the atoms is in an excited state. The probability that this excitation energy will be transferred from one atom to the other has been studied extensively, and such a collision is one example of a collision of the second kind. The cross section for these reactions is sharply peaked at the excitation energy for the initially ground state atom, and is only significant over an energy range of a few kT around this excitation energy. The most well known example of such a collision process occurs in the Helium-Neon laser. The relevant levels are noted in Table 4.1.

Table 4.1

Donor	Acceptor	E (cm^{-1})	
He 2^3S	Ne $2s_2$	-314	
He 2^3S	Ne $2s_3$	-469	kT(300 K)
He 2^3S	Ne $2s_4$	-1053	
He 2^3S	Ne $2s_5$	-1247	= 208 cm^{-1}
He 2^1S	Ne $3s_2$	+387	

Here, a positive value for ΔE means that the energy of the donor is less than the excited level of the acceptor. The peak values for these cross-sections can be greater than 10^{-16} cm.^{2} when $\Delta E \leqslant kT$. While any excited atom can act as donor, only those with a lifetime considerably longer than the acceptor will be effective because of the reversibility of the reaction. Thus metastable atoms are efficient donors to levels with allowed transitions. Both the Helium levels in Table 4.1 are metastable, and the allowed transitions from the neon levels are laser transitions. In addition to excitation, ionisation can occur in collisions between an excited atom and a ground state atom of a different species. These reactions are known as Penning reactions. In mixtures of neon and a trace of argon, the probability of ionisation of the argon by neon metastables is almost unity since the neon metastables have an energy in excess of the ionisation energy of argon by 0.8eV. Collisions between two metastables in rare gases can produce an ion and a fast electron together with a ground state atom. This process will be mentioned further in Chapter 6.

4.3 Electron - Molecule Collisions

In addition to ionisation and excitation, the molecule may be dissociated by collision with electrons. It has been found experimentally that the Franck-Condon hypothesis is obeyed in considering excitation to higher states. Fig. 4.3 shows a typical set of potential energy vs. atomic separation curves for a diatomic molecule. Assuming that the molecule is in its ground state, the transition will occur at a constant value of r as indicated by the vertical shaded area, the range of r being determined by the lowest vibrational level of the ground electronic state. If the electron energy was such as to excite the molecule to curve a, the molecule will finish up in an excited vibrational and electronic state. If the electron energy is such as to excite the molecule

to curves b or c, the two atoms will fly apart because of the repulsive potential with a final kinetic energy equal to E(excitation) - E(dissociation). E(dissociation) is the thermal dissociation energy, and corresponds to the case when vibrational and rotational quanta are absorbed on heating of the gas until the energy of the molecule is greater than the binding energy, and the two atoms separate. It can be easily seen that the threshold for electron impact dissociation may be greater than the thermal dissociation energy because of the shape of the repulsive potential curve. The cross-sections for these reactions have peak values of the order of 10^{-16} cm.^{2}, the same order of magnitude as for allowed transitions in atoms.

4.4 Atom - Molecule Collisions

Similar arguments to those used in sections 4.2 and 4.3 apply here. The important difference between section 4.2 and this section lies in the fact that an exact resonance in energy levels between donor and acceptor is no longer required. This is due to two facts. First, there is a range of energies on each potential curve for the range of r allowed by the Franck-Condon principle, shown in Fig. 4.3 by shading. Secondly, there are likely to be a number of repulsive potential curves which terminate on the same dissociation products. These two factors make this mechanism an extremely promising one for selective excitation of certain energy levels. The difficulty of predicting the importance or likelihood of these reactions is considerable, since the repulsive potential curves are only known in a few cases.

4.5 Electron - Ion Collisions

Collisions between ions and fast electrons can lead to further ionisation or excitation. The discussion in section 4.1 applies equally well to these collisions. In addition to these, the electron may recombine with the ion to

form an excited atom. The recombination may be either the simple one or a three body recombination, the third party being an electron or a ground state atom. Recombination with a molecular ion may also give rise to dissociation of the molecule. These processes are mentioned further in Chapter 6 with specific examples.

References

4.1 H.S.W. Massey & E.H.S. Burhop — Electronic and Ionic Impact Phenomena (1952)

4.2 N.F. Mott & H.S.W. Massey — The Theory of Atomic Collisions 3rd Edition (1965)

4.3 M.J. Seaton — Atomic and Molecular Processes (Ed. D.R. Bates) Ch. 11 (1962) see also Astrophysical Quantities (Ed. C.W. Allen) p42 (1962)

4.4 A.E.S. Green — American Institute for Aeronautics & Astronautics Journal 4, 769 (1966)

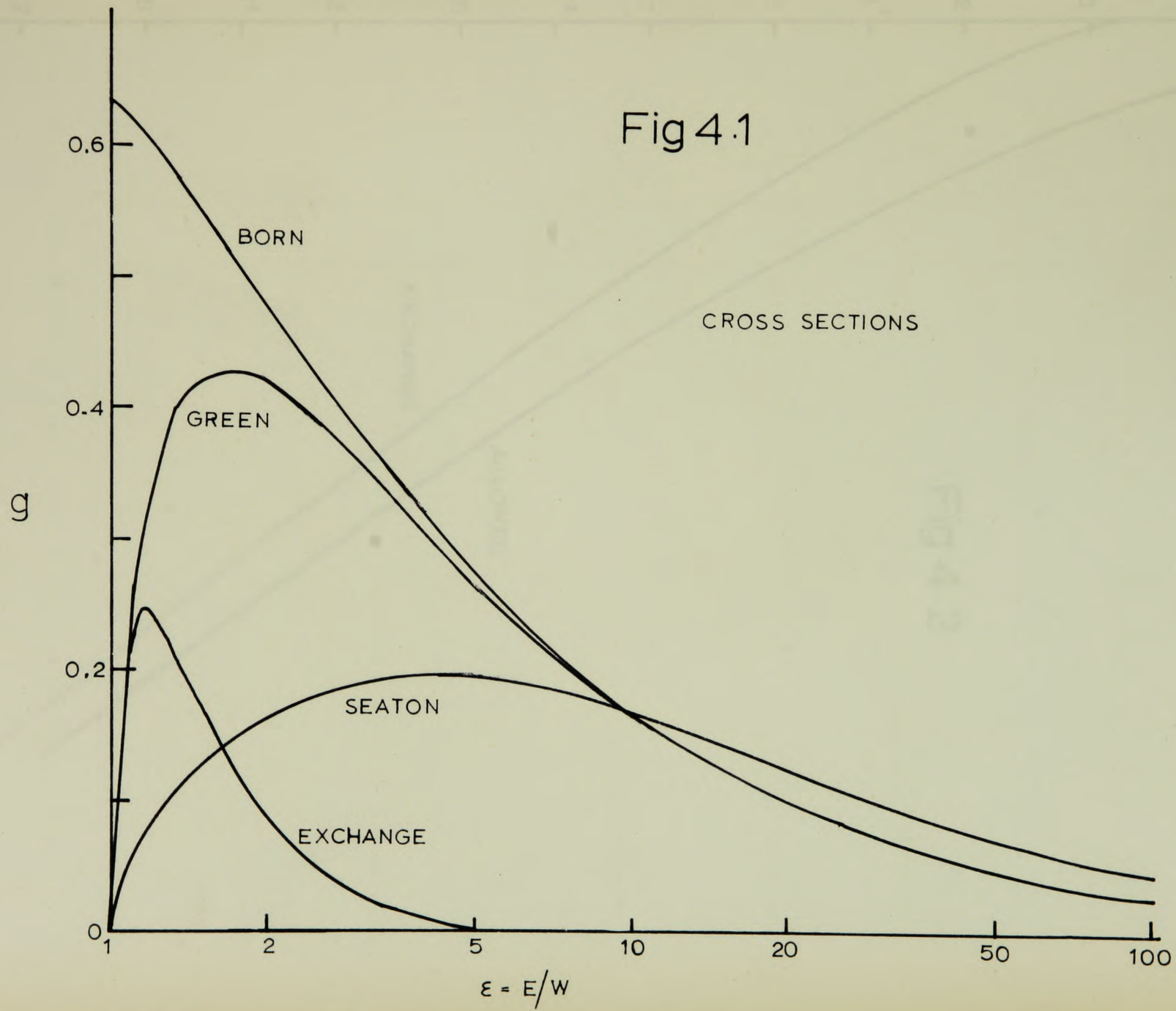
Fig 4.1
CROSS SECTIONS
BORN
GREEN
SEATON
EXCHANGE
g
0.6
0.4
0.2
0
1
2
5
10
20
50
100
ε = E/W

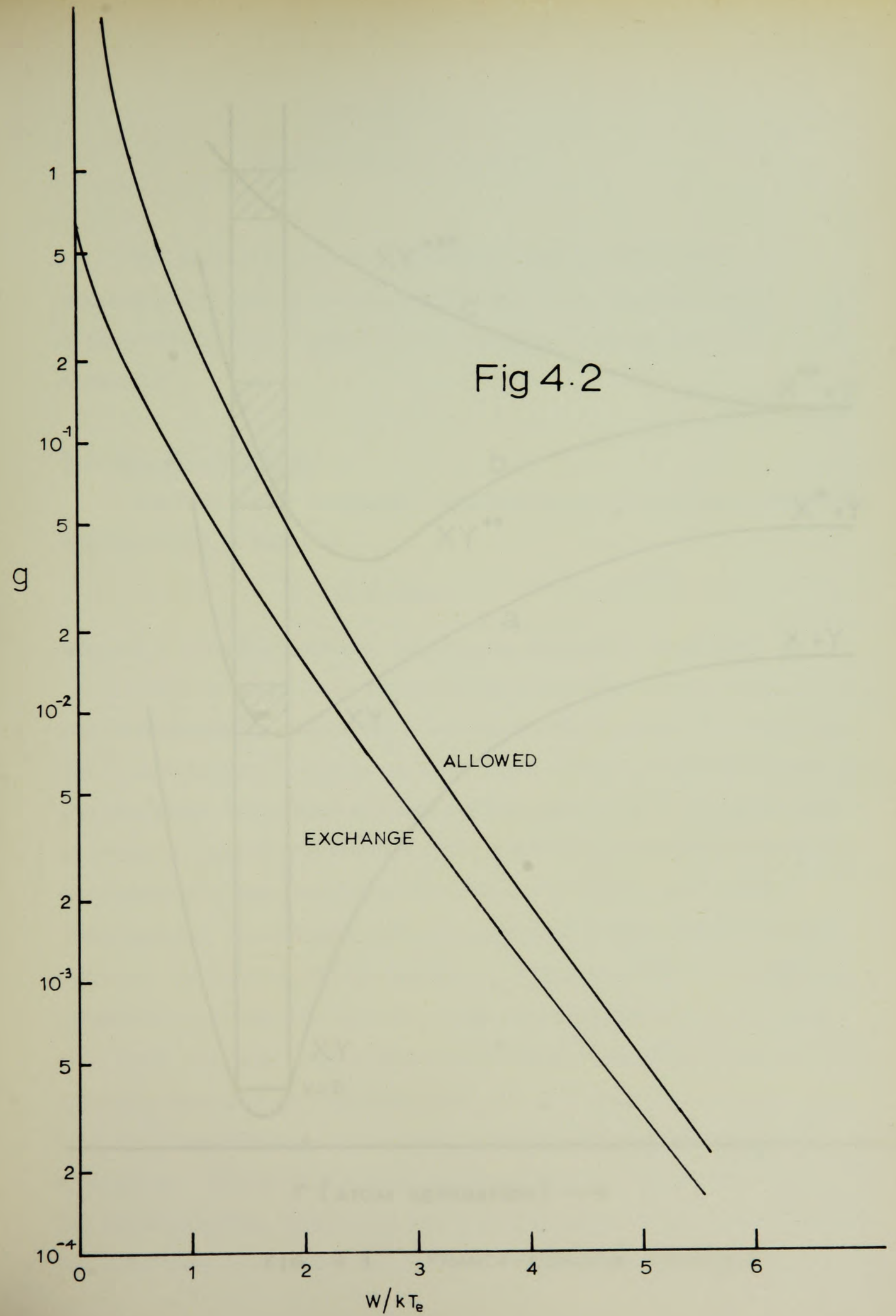

Fig 4.2

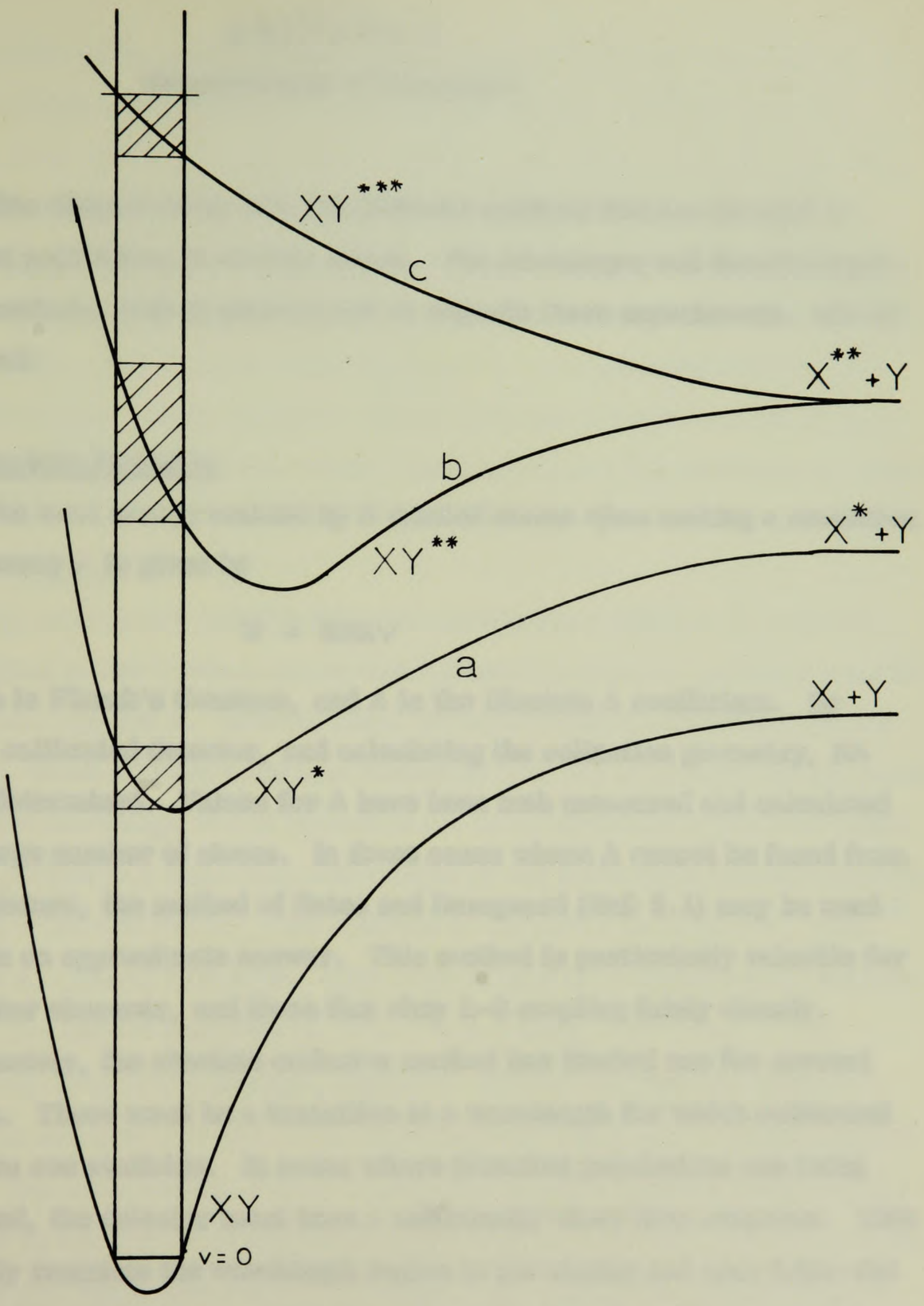

FIG 4.3 FRANCK-CONDON PRINCIPLE

CHAPTER 5

Measurements of Population

This chapter deals with the different methods that can be used to measure populations in excited states. The advantages and disadvantages of the methods, both in general and as regards these experiments, will be discussed.

5.1 Absolute Emission

The total energy emitted by N excited atoms when making a transition of frequency ν is given by

$$W = NAh\nu$$

where h is Planck's Constant, and A is the Einstein A coefficient. By using a calibrated detector, and calculating the collection geometry, NA can be determined. Values for A have been both measured and calculated for a large number of atoms. In those cases where A cannot be found from the literature, the method of Bates and Damgaard (Ref. 5.1) may be used to obtain an approximate answer. This method is particularly valuable for the lighter elements, and those that obey L-S coupling fairly closely. Unfortunately, the absolute emission method has limited use for several reasons. There must be a transition at a wavelength for which calibrated detectors are available. In cases where transient populations are being measured, the detector must have a sufficiently short time response. This generally restricts the wavelength region to the visible and near infra-red where photomultipliers can be used. There is also the problem of self-absorption. Unless the source is optically thin, a correction has to be made for self absorption, requiring a separate absorption measurement. Except for a few lines in Hydrogen and Helium, A values are not known to accuracies

greater than 20%, which further limits the experimental accuracy. In addition there are metastable levels and ion ground states from which there are no radiative transitions. Where there are a number of spectral line being studied, some form of monochromation is needed. Narrow band filters which are the most convenient are usually at least 100Å wide in their pass band, so that a prism or grating monochromator must be used. Not only does this complicate the calculation of the geometry factor, but also calibration may be difficult. Since there are a large number of lines in the spectra studied in this thesis, this method was not seriously considered.

5.2 Absorption

The expression relating the peak absorption coefficient k_o with the populations of two levels between which there is a allowed radiative transition is given in Chapter 2. Leaving aside the experimental difficulties for the moment, there are two problems connected with the theoretical result quoted. First, the knowledge of f is limited to the same extent as is the knowledge of A in section 5.1 since they are related by the wavelength and the statistical weights of the two levels. The equation in Chapter 2 is based on a pure Doppler broadened lineshape. This is generally an extremely good approximation for lighter elements at room temperatures. However, many transitions have fine structure, hyperfine structure or isotope shifts in which the separation of the components is of the same order as the Doppler width. The relationship between k_o and the populations must therefore be obtained by numerical or graphical integration over the particular lineshape. Mitchell and Zemansky (Ref: 5.2) discuss fully the effects of lineshape on absorption measurements. They derive relationships between the line absorption A_L, defined as the fraction of incident light that is absorbed, and k_o. This depends not only on the lineshape of the absorbing medium,

but also on the lineshape of the source lamp. Graphical or numerical integration again has to be used for partially resolved fine structure, hyperfine structure or isotope shifts. The general experimental procedure is to use a chopped light source and to detect the absorption with a phase sensitive detector. Calibrated attenuators serve as reference measurements of absorption. Pulsed discharges create two problems which are linked. First, ω , the chopping frequency, must now be increased so that $1/\omega$ is much less than the time constant of the transient populations. For time constants of a few microseconds, this means a chopping frequency of a few MHz. While this can be achieved in the visible part of the spectrum by Kerr cells or other electro-optic modulators, the second difficulty of phase sensitive detection at such frequencies is at present impractical. Direct measurement of absorption by observing the difference between the sum of the separate light signals from source and absorber, and the light signal from both together, suffers from the fact that the pulsed discharges in which absorption is to be measured often emit more light than the source lamp, since the latter has to be quasi-cw to avoid problems of synchronisation. This problem would of course not arise if phase sensitive detection were possible. One method that has been used on pulsed discharges is to gate the photomultiplier or other detector on for a time short compared to the time constant of the varying population. This improves the signal to noise ratio but does not overcome the problem of emission by the absorbing discharge. It has been used successfully by Phelps and his coworkers (Ref: 5.3) to measure the metastable populations in the afterglow of a spark discharge in rare gases, under conditions where the emission was small relative to the source lamp. One method which was originally used by Ladenburg and Reiche (see Ref: 5.1) is to make the source tube and absorption tube identical. Although the sensitivity of this method is high,

it suffers from the practical difficulty of providing identical source and absorption tubes. This in turn calls for exact synchronism in the case of pulsed discharges, and the errors in calibration are likely to be large. One simplification which removes the last two objections is to use the absorption tube as its own source lamp by placing a plane mirror at the opposite end of the tube to the detector. The accuracy of the method for dimensions typical of a pulsed laser tube will now be estimated. Examining Fig. 5.1, the light flux incident on the detector when the mirror is removed is first calculated.

Let there be $N_\nu d\nu$ atoms/cc. which can radiate in the frequency interval ν to $\nu + d\nu$, and let k_ν be the absorption coefficient in the same frequency interval. The total light flux incident on the detector of area Q from the length element dx is given by

$$I_{nm}(\nu, x)\, d\nu\, dx = \frac{N_\nu d\nu A h\nu}{4\pi} \frac{Q}{(p+x)^2} \exp(-k_\nu x)\, P dx$$

where P is the cross sectional area of the tube.

$$\text{Hence } I_{nm} = \frac{AhQP}{4\pi} \int_{-\infty}^{\infty} N_\nu \nu \, d\nu \int_0^1 \frac{\exp(-k_\nu x)}{(p+x)^2} \, dx$$

With a plane mirror of reflectivity R, accurately aligned on the axis of the tube, the light flux incident on Q becomes

$$I_m = I_{nm} + \frac{AhQPR}{4\pi} \int_{-\infty}^{\infty} N_\nu \nu \, d\nu \int_0^1 \frac{\exp(-k_\nu (l+x))}{(p+l+2q+x)^2} \, dx$$

Hence the ratio of these light fluxes is

$$\frac{I_m}{I_{nm}} = 1 + \frac{R \int_{-\infty}^{\infty} N_\nu \, d\nu \int_0^1 \frac{\exp(-k_\nu (l+x))}{(p+l+2q+x)^2} \, dx}{\int_{-\infty}^{\infty} N_\nu \, d\nu \int_0^1 \frac{\exp(-k_\nu x)}{(p+x)^2} \, dx}$$

This can be simplified further for the simple case of a single Doppler broadened line since

$$N_\nu = N_o \exp\left(-\left(2\sqrt{\ln 2} \; (\nu - \nu_o) / \Delta\nu_D\right)^2\right)$$

$$k_\nu = k_o \exp\left(-\left(2\sqrt{\ln 2} \; (\nu - \nu_o) / \Delta\nu_D\right)^2\right)$$

where N_o, k_o, are the peak values of N and k at frequency ν_o, and $\Delta\nu_D$ is the Doppler width.

Putting $y = 2\sqrt{\ln 2} \; (\nu - \nu_o) / \Delta\nu_D$

and noting that

$$\frac{I_m}{I_{nm}} = 1 + \frac{R \int_{-\infty}^{\infty} e^{-y^2} dy \int_0^1 \frac{\exp(-k_o (l+x) e^{-y^2})}{(p+2q+l+x)^2} \, dx}{\int_{-\infty}^{\infty} e^{-y^2} dy \int_0^1 \frac{\exp(-k_o x e^{-y^2})}{(p+x)^2} \, dx}$$

Calling the double integral in the numerator of the above expression F_2 and the integral in the denominator F_1, $I_m / I_{nm} = 1 + (RF_2/F_1)$

F_1 and F_2 may be obtained in the following manner.

Since $\exp(x) = \sum_{n=0}^{\infty} x^n / n!$

then F_2 can be written in the form

$$F_2 = \int_{-\infty}^{\infty} \int_0^1 \sum_{n=0}^{\infty} e^{-y^2} \frac{(-k_o (l+x))^n}{n!} \, e^{-ny^2} \frac{1}{(p+l+2q+x)^2} \, dy \, dx$$

by expanding $\exp(-k_o(l+x) \exp(-y^2))$.

Integrating over y,

$$F_2 = \sqrt{\pi}\int_0^1 \sum_{n=0}^{\infty} \frac{(-k_o(1+x))^n}{n!\sqrt{n+1}} \quad \frac{1}{(p+2q+1+x)^2} \; dx$$

Expanding the term $(p+2q+1+x)^{-2}$ by the Binomial Theorem and integrating over x we get finally,

$$F_2 = \frac{\sqrt{\pi}}{p+2q} \sum_{n=0}^{\infty} \frac{(-k_o l)^n}{n!\sqrt{n+1}} \sum_{m=1}^{\infty} (-1)^{m-1} \frac{m}{n+m} \left(\frac{l}{p+2q}\right)^m (2^{n+m} - 1)$$

for $p+2q > 2l$ and $p > l$

Similarly, we obtain

$$F_1 = \frac{\sqrt{\pi}}{p} \sum_{n=0}^{\infty} \frac{(-k_o l)^n}{n!\sqrt{n+1}} \sum_{m=1}^{\infty} (-1)^{m-1} \frac{m}{n+m} \left(\frac{l}{p}\right)^m$$

Putting $F_1' = \frac{n(p+l)}{l} F_1$, $F_2' = \frac{(p+l+2q)(p+2l+2q)}{l} F_2$

then $F_1' = F_2' = 1$ for $k_o l = 0$

For the laser tube used, l = 180 cm., p = 335 cm., q = 20 cm., and R = 0.9. Table 5.1 gives values for F_1', F_2' and $1 + (RE_2/F_1)$ as a function of $k_o l$.

In it, positive values of $k_o l$ indicate absorption, and negative values indicate gain.

Table 5.1

$k_o l$	F_1'	F_2'	$1+(RF_2/F_1)$
-2	2.100	11.46	3.07
-1	1.399	3.092	1.84
0	1.000	1.000	1.38
1	0.760	0.399	1.201
2	0.607	0.196	1.123
3	0.504	0.116	1.087
4	0.430	0.078	1.069
5	0.376	0.058	1.059
6	0.335		
8	0.275		
10	0.235		
12	0.204		
15	0.173		
18	0.150		
20	0.138		
25	0.115		
30	0.099		
50	0.065		
80	0.043		
100	0.036		
150	0.025		

Fig. 5.2 shows these values graphically. It is immediately obvious that $1+(RF_2/F_1)$ is somewhat insensitive to $k_o l$ and becomes more so as $k_o l$ increases. This method is therefore not very useful for large absorption, but increases in accuracy as the gain increases. However, F_1' can be measured quite easily by comparing the light emitted from the side of the tube to the light emitted from the end of the tube. Since the tube bore is only 7mm., those lines for which $k_o l \leqslant 60$ are almost unaffected by self-absorption in side light emission since $k_o R \leqslant 0.2$. Calibration is effected by choosing a line for which $k_o l$ is zero, and taking the ratios of the signals from the end of the tube and the side of the tube. The theory

developed so far does not take into account the effect of reflections from the side walls of the tube. Because of these, the elements of volume at the end of the tube farthest from the detector see a larger solid angle subtended by the detector. Even on the assumptions of a perfect cylindrical bore for the tube, the calculation of the correction can only be done by complicated numerical integration. The problem can be approximated crudely in the following way. The effective volume of plasma which is emitting is increased to eliminate the solid angle term $(p+x)^{-2}$ in F_1. We now have for this corrected value F_1'', normalised to unity, at $k_o l = 0$,

$$F_1'' = \frac{1}{\sqrt{\pi}\, k_o l} \int_{-\infty}^{\infty} (1 - \exp(-k_o l \exp(-y^2)))\, dy = \sum_{n=0}^{\infty} \frac{(k_o l)^n}{(n+1)!\sqrt{n+1}}$$

This is the same as the function S as defined in Mitchell and Zemansky (Ref: 5.1). Fig. 5.3 shows F_1' and S plotted against $k_o l$ for comparison. F_1', F_2' and S were all computed on the English Electric KDF9 computer. The values obtained by numerical integration were checked by means of the summation formula. In a later section, it will be shown that the function F_1' is in fact a better approximation, and this has been used extensively as a measure of populations. It is not sensitive enough to indicate a small gain for which oscillation can be obtained, and the most obvious approach to all spectral lines where gain is suspected is to align a confocal Fabry-Perot cavity, and look for oscillation.

5.3 Absolute populations by calibration with a laser

The method described above, while giving population differences, does not give the populations of the individual levels. In the case of a laser transition, the exact populations at any moment may be determined in the

following way, assuming that there is a spontaneous transition from the lower levels that can be detected.

Let the value of $k_o l$ at times t_1, t_2, be x_1, x_2.

Let the intensity of spontaneous emission from the upper level (2) at times t_1, t_2, be I_2, I_2'.

Let the intensity of spontaneous emission from the lower level (1) at times t_1, t_2, be I_1, I_1'.

Now $I_2 = N_2(t_1) A_{21} h \nu_{21}$

and $I_1 = N_1(t_1) A_{10} h \nu_{10}$

Also $x_1 = \gamma (g_1 N_2(t_1) - g_2 N_1(t_1))$

where $\gamma = 2l / \Delta\nu_D \sqrt{\frac{\ln 2}{\pi}} \frac{\pi e^2}{mc} f_{12}/g_2$

and $x_2 = \gamma (g_1 N_2(t_2) - g_2 N_1(t_2))$

Putting $I_2' = aI_2$ and $I_1' = bI_1$ gives

$$x_2 = \gamma (g_1 a N_2(t_1) - g_2 b N_1(t_1))$$

Solving the equations for x_1, x_2 gives for $N_2(t_1)$ and $N_1(t_1)$.

$$N_2(t_1) = \frac{x_2 - bx_1}{\gamma g_1 (a - b)}$$

$$N_1(t_1) = \frac{x_2 - ax_1}{\gamma g_2 (a - b)}$$

The method of calibration is as follows. The time at which laser oscillation commences is noted for no loss in the cavity and on insertion of a known loss in the cavity. Spontaneous emission measurements are made under exactly the same conditions. From these, b, a, x_1, x_2 are

determined, and, given the value for γ, the N's are determined. The advantage of this method over the absolute spontaneous emission method is that only one f value is required instead of two. An example will now be calculated to show the sort of accuracy that can be obtained.

Fig. 5.4 shows the intensities of the lines 9406Å and 2479Å as a function of time.

$$x_1 = 0.01 \qquad x_2 = 0.106$$

$$a = 0.707 \qquad b = 0.658$$

$$\gamma = 3.98 \times 10^{-10} \text{ for } 9406\text{Å}$$

giving $N_2(t_1) = 1.71 \times 10^9$ cm.$^{-3}$

$N_1(t_1) = 1.01 \times 10^9$ cm.$^{-3}$

compared with $g_1 N_2(t_1) - g_2 N_1(t_1) = 8 \times 10^7$ cm.$^{-3}$

In this case, a - b is small, so that the main source of error is likely to be in measuring b and a. This calculation has also assumed that the line is Doppler broadened at 300°K.

The values of N_1 and N_2 at earlier times were then calculated and values for $k_o l$ at these times evaluated. At the same time, values of $k_o l$ were calculated by comparing the tube sidelight to the light emitted from the end as discussed in 5.2 using both F_1' and S. These values are shown in Table 5.2.

Table 5.2

t(usecs)	$k_o l$ (S)	$k_o l$ (F_1')	$k_o l$ (N_2 and N_1)
16	0	0	-0.01
10	0.54 ± 0.12	0.65 ± 0.14	0.65
5	2.82 ± 0.29	3.55 ± 0.40	3.71

It would therefore seem that the theory using F_1' will give the most accurate values for $k_o 1$ in absolute terms. As far as relative values of $k_o 1$ are concerned, the ratios of $k_o 1$ at the two times are the same in both theories to within 5%.

References

5.1 D. R. Bates & A. Damgaard — Proc. Roy. Soc. 242 A 101 (1957)

5.2 A. C. G. Mitchell & M. W. Zemansky — Resonance Radiation and Excited Atoms (1961)

5.3 A. V. Phelps — Phys. Rev. 99, 1307 (1955)

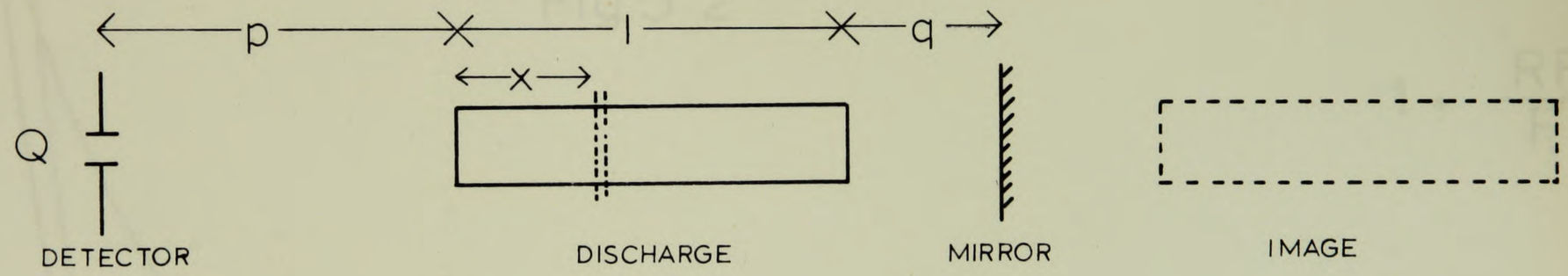

Fig 5.1

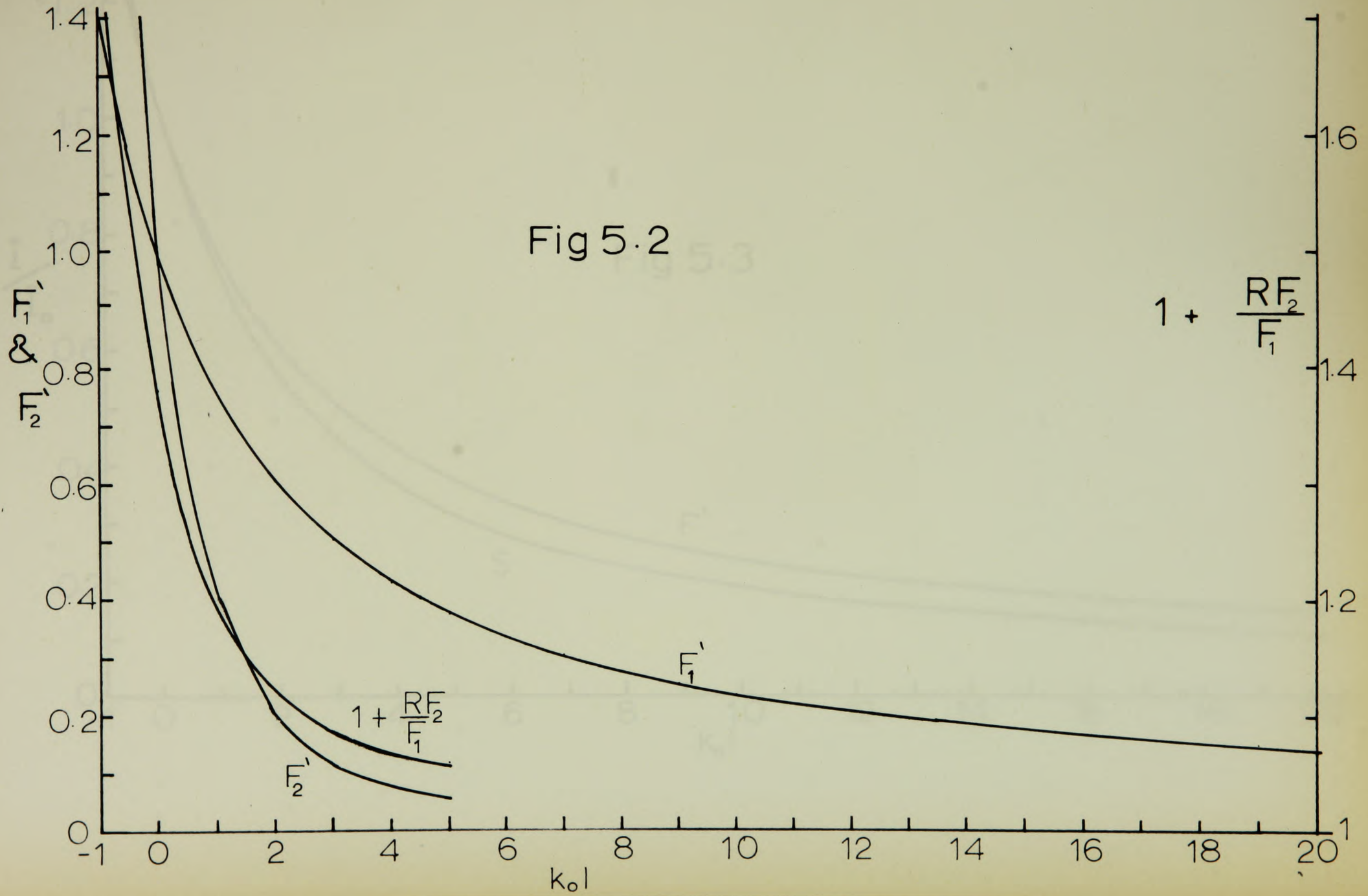
Fig 5.2
F_1' & F_2'
$1 + \frac{RF_2}{F_1}$
F_1'
$1 + \frac{RF_2}{F_1}$
F_2'
$k_o l$
1.4
1.2
1.0
0.8
0.6
0.4
0.2
0
1.6
1.4
1.2
1
-1
0
2
4
6
8
10
12
14
16
18
20

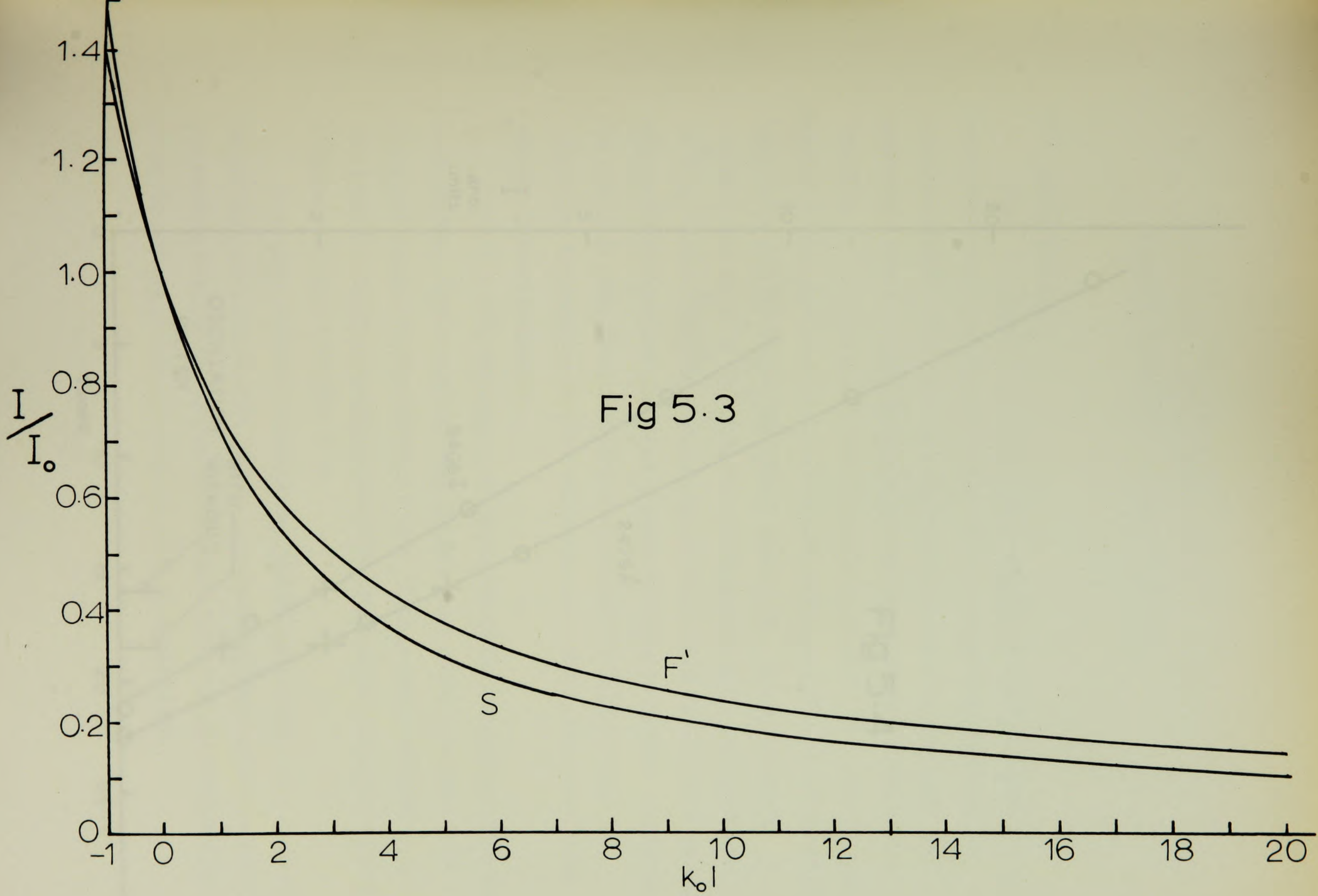

Fig 5.3

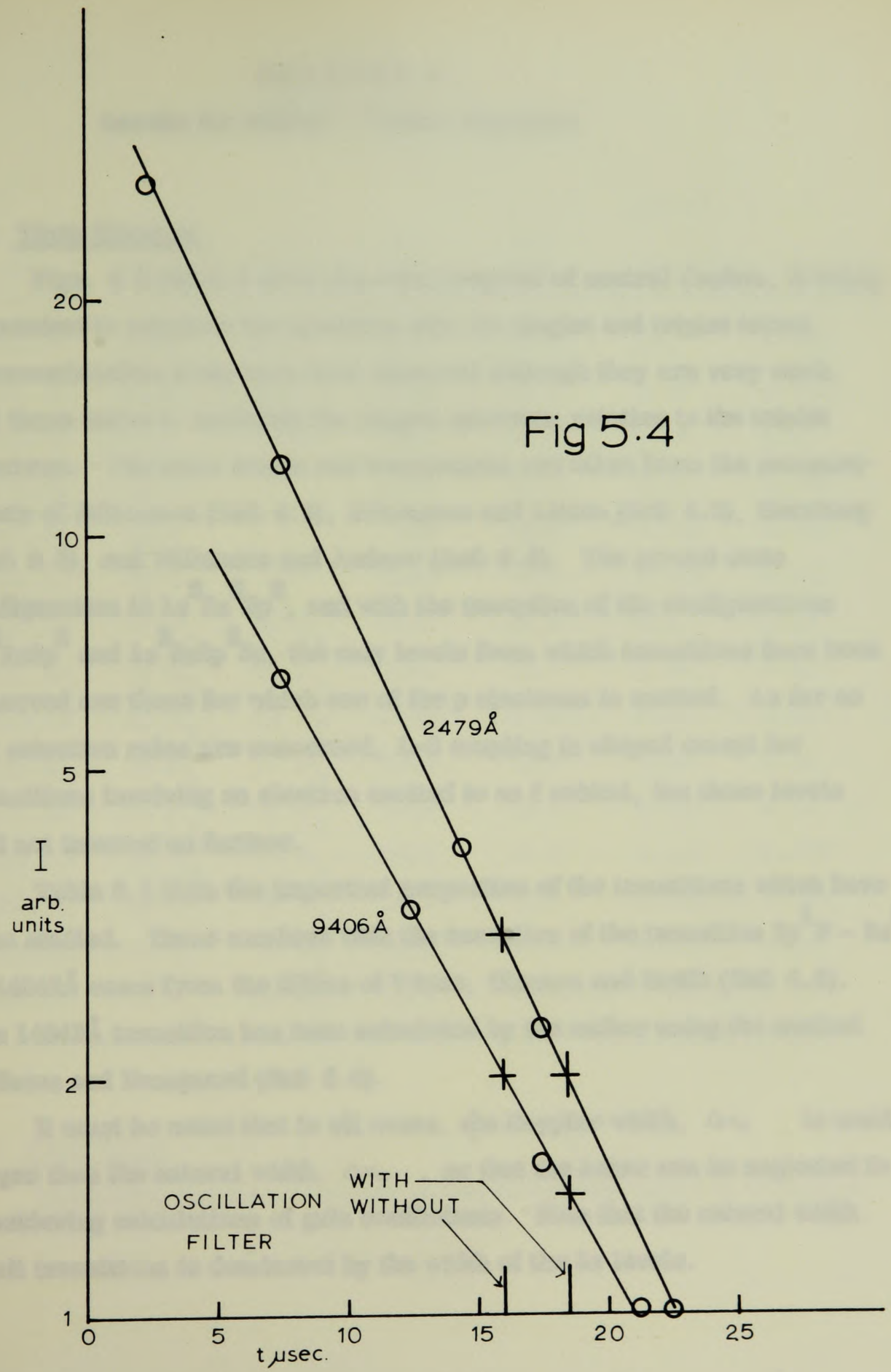
20
10
5
2
1
I
arb.
units
2479Å
9406Å
OSCILLATION
FILTER
WITH
WITHOUT
0
5
10
15
20
25
t μsec.

Fig 5.4

CHAPTER 6

Results for Helium - Carbon Monoxide

6.1 Term Diagram

Figs. 6.1 and 6.2 show the term diagram of neutral Carbon, it being convenient to separate the spectrum into the singlet and triplet terms. Intercombination lines have been observed although they are very weak, and these serve to establish the singlet spectrum relative to the triplet spectrum. The term values and wavelengths are taken from the measurements of Johansson (Ref: 6.1), Johansson and Litzen (Ref: 6.2), Herzberg (Ref: 6.3), and Wilkinson and Andrew (Ref: 6.4). The ground state configuration is $1s^2 2s^2 2p^2$, and with the exception of the configurations $1s^2 2s2p^3$ and $1s^2 2s2p^2 3s$, the only levels from which transitions have been observed are those for which one of the p electrons is excited. As far as the selection rules are concerned, L-S coupling is obeyed except for transitions involving an electron excited to an f orbital, but these levels will not interest us further.

Table 6.1 lists the important properties of the transitions which have been studied. These numbers with the exception of the transition $3p\,^1P - 3s\,^1P$ at 14542Å come from the tables of Wiese, Glennon and Smith (Ref: 6.5). The 14542Å transition has been calculated by the author using the method of Bates and Damgaard (Ref: 6.6).

It must be noted that in all cases, the Doppler width, $\Delta\nu_D$, is much larger than the natural width, $\Delta\nu_N$, so that the latter can be neglected in considering calculations of gain coefficients. Note that the natural width of all transitions is dominated by the width of the 3s levels.

Table 6.1

λ Å	Upper Level	Lower Level	$\Delta\nu_D$ MHz	$\Delta\nu_N$ MHz	$A \times 10^8$ $sec.^{-1}$	f
1930.93	$3s\,^1P$	$2p\,^1D$	5560	43.5	2.4	0.082
2478.56	$3s\,^1P$	$2p\,^1S$	4330	43.5	0.34	0.094
8335.19	$3p\,^1S$	$3s\,^1P$	1290	48.6	0.32	0.11
9405.73	$3p\,^1D$	"	1140	47.2	0.23	0.506
14542.50	$3p\,^1P$	"	740	44.5	0.066	0.208
5052.12	$4p\,^1D$	"	2120	43.8	0.017	0.011
1657.00	$3s\,^3P_2$	$2p\,^3P_2$	6480	68.8	3.1	0.13
10691.25	$3p\,^3D_3$	$3s\,^3P_2$	1000	71.7	0.18	0.43
10683.08	$3p\,^3D_2$	$3s\,^3P_1$	1000	71.6	0.13	0.38
10685.34	$3p\,^3D_1$	$3s\,^3P_0$	1000	71.6	0.10	0.51
10707.33	$3p\,^3D_1$	$3s\,^3P_1$	1000	71.6	0.072	0.12
10729.53	$3p\,^3D_2$	$3s\,^3P_2$	1000	71.6	0.043	0.074
10753.98	$3p\,^3D_1$	$3s\,^3P_2$	1000	71.6	0.005	0.005
9658.49	$3p\,^3S_1$	$3s\,^3P_2$	1120	72.3	0.12	0.10
9094.89	$3p\,^3P_2$	$3s\,^3P_2$	1180	72.9	0.19	0.23

6.2 Laser Lines

Oscillation has been observed on the transitions listed in Table 6.2.

Table 6.2

λ Å	Upper Level	Lower Level	Comments
14542.5	$3p\,^1P$	$3s\,^1P$	Strong
9405.7	$3p\,^1D$	$3s\,^1P$	Strong
10691.2	$3p\,^3D_3$	$3s\,^3P_2$	Strong
10683.1	$3p\,^3D_2$	$3s\,^3P_1$	Strong
10685.3	$3p\,^3D_1$	$3s\,^3P_0$	Weak

C.W. oscillation at 14542Å and 10691Å was reported by Patel, McFarlane, and Faust (Refs 6.7 and 6.8) and pulsed oscillation at these wavelengths by Boote and Clunie (Ref 6.9). C.W. oscillation at 9406Å and at 9095Å ($3p\,^3P_2 - 3s\,^3P_2$) were reported by Shimazu and Suzaki (Ref: 6.10).

The experiments were performed in a mixture of Helium and Carbon Monoxide. The CO pressure varied from about 1mtorr to 0.5torr, with Helium at pressures up to 20torr. Unfortunately, measurement of the CO partial pressure was extremely difficult, as the CO was driven both into and out of the walls, depending on the Helium pressure. For example, the 9406Å laser line would oscillate after as many as 10 flushings with 10torr of Helium. Despite this difficulty, the general behaviour of the laser lines as a function of pressure could be observed quite clearly.

Before discussing in detail the results that were obtained, a few comparisons can be made between the results for the different transitions. The transition at 9406Å was observed only in the afterglow of the current pulse. At low pressures of CO, the three lines of the 10691Å multiplet also oscillated in the afterglow, but as the CO pressure was increased,

the afterglow oscillation ceased, and oscillation was observed on the two stronger lines of the multiplet during the risetime of the current pulse. The line at 14542Å was the only line which would oscillate both in the afterglow and during the current pulse risetime under the same excitation conditions. However, the afterglow oscillation peak power was at least twenty times larger than the current pulse oscillation peak power.

Fig. 6.3(a) shows a typical oscilloscope trace of the 9406Å laser pulse and the current pulse for different values of current. On this, and all other oscilloscope photos in this thesis, the current pulse is shown on the upper trace, and the zero light signal trace is also shown. As the current increases, the start of the laser pulse is delayed further, and the peak output power decreases. Fig. 6.5 is a plot of the delay of the laser pulse relative to the termination of the current pulse against the peak discharge current for different values of Helium and Carbon Monoxide pressures. Fig. 6.6 shows the peak gain of the 9406Å laser pulse as a function of Helium pressure with 0.11torr of CO. Figs. 6.3(b) and (c) show typical oscilloscope photos of the spontaneous emission of the 9406Å and 2479Å Carbon atomic lines and Figs. 6.3(d), (e), and 6.4(a) and (b) show the 3888Å and 5876Å Helium atomic lines. In the latter cases, the spontaneous emission from both the side and the end of the discharge tube are shown, the effects of the time-varying self-absorption discussed in Chapter 5 being clearly seen. The end-light appears to decay more slowly and the peak afterglow intensity is much less than that of the side-light, although the ratio of end-light to side-light for an unabsorbed line was unity. The relative intensity scales for side-light and end-light are shown for each line.

The behaviour of the 9406Å laser output as a function of current and pressure can be explained by examining the behaviour of the spontaneous

emission of the 9406Å and 2479Å lines. The 9406Å line decays more slowly than both the 2479Å line and the Helium lines. Furthermore, the intensity of the 9406Å line for times greater than 5μsec. in the afterglow is almost independent of current for currents in excess of 20amps, the approximate threshold for afterglow emission. The intensity of the 2479Å line and the Helium lines increases approximately linearly with current. Since the spontaneous emission is a direct measure of the upper and lower level populations, the variation of gain with time and current can be determined from the spontaneous emission. The decay of both the upper and lower levels is approximately exponential, as will be seen later, so that the expression for the populations is

$$N_1 (i,t) = N_1 (i_o, 0) (i/i_o) \exp (-t/\tau_1)$$

$$N_2 (i,t) = N_2 (i_o, 0) \exp (-t/\tau_2)$$

N_1 is the lower level population with a time constant of decay of τ_1, and N_2, τ_2, refer to the upper level. i_o is an arbitrary value of current. These equations can now be used to determine the variation of the delay of the laser output with current.

Let times, T_a, T_b, be defined so that

Laser Delay = $T_a + T_b(i)$

where $T_b = 0$ when $i = i_o$

The gain at the threshold of oscillation when $i = i_o$ is proportional to

$$g_1 N_2 (i_o, T_a) - g_2 N_1 (i_o, T_a)$$

When the current is i, the gain at the threshold for oscillation must be proportional to

$$g_1 N_2 (i, T_a + T_b) - g_2 N_1 (i, T_a + T_b)$$

Calling this constant quantity N*, and substituting the equations for the populations as a function of current and time, the value of N* can be rewritten in the form,

$$N^* = \frac{(\exp(-T_b/\tau_2) - (i/i_o)\exp(-T_b/\tau_1))\, g_1 N_2 (i_o, T_a)}{(1 - (i/i_o)\exp(-T_b/\tau_1))}$$

If $N^* \ll g_1 N_2 (i_o, T_a)$, this can be further simplified to

$$T_b = \frac{\tau_1 \tau_2}{\tau_2 - \tau_1} \log_e (i/i_o)$$

The dotted curve on Fig. 6.5 shows this dependence with the curve fitted at i = 20amps and 80amps. Taking $\tau_2 = 7.8\mu$sec., the expression predicts $\tau_1 = 4.5\mu$sec., which agrees with the measured value of 4.6μsecs. This is a good indication that under these conditions, $N^* \ll g_1 N_2 (i_o, T_a)$. It can be seen that at higher Helium pressures, this functional behaviour is no longer obeyed. This is probably due to the discharge no longer being homogeneous at higher currents. The appearance of the discharge was that of three approximately equal sections. The centre section of the discharge was blue-grey, characteristic of the CO spectrum, whereas the two end sections were the pink colour of the Helium discharge.

Fig. 6.7 shows the delay of the laser pulse as a function of Helium pressure for different values of peak current. It demonstrates the systematic behaviour of the delay, and is shown mainly for a comparison with the results in the later Chapters.

Since both the upper and lower levels have a decay which is exponential with time, the gain as a function of time can also be calculated, and compared with the power output as a function of time. The expression for the gain is

$$k_o 1(t) = g_1 N_2 (t=0) \exp(-t/\tau_2) - g_1 N_2 (t=0) \exp(-t/\tau_1)$$

where $g_1 N_2 (t=0) = g_2 N_1 (t=0)$, and t is thus effectively measured from the start of oscillation. Taking $\tau_1 = 4.6\mu sec$, and $\tau_2 = 7.8\mu sec.$, which are typical observed values, the resulting value of $k_0 l$ is shown plotted against t in Fig. 6.8, together with the measured laser output. One would only expect the laser output to follow the gain under certain circumstances. As has been mentioned previously, the 9406Å line can be treated as an inhomogeneously broadened line. The power in a longitudinal mode is given by an expression of the form

$$P \propto (k_\nu l - f) \Delta\nu_N (1 + 1/A_1 \; A_2 \left| \frac{eE_0 (Z)_{21}}{\hbar} \right|^2)^{1/2} \quad \text{(Ref. 6.11)}$$

Here $k_\nu l$ is the gain at frequency ν, f is the threshold gain for oscillation, $\Delta\nu_N$ the natural width, A_2, A_1 the decay rates of the upper and lower levels, E_0 the electric field strength in the mode, and $(Z)_{21}$ a matrix element related to A_{21} the Einstein A coefficient. Provided that $k_0 l (\nu) \gtrsim 3f$, and assuming that the term containing E_0 is small compared to 1, one can see that

$$P \propto k_0 l (\nu).$$

Fig. 6.8 demonstrates that the general form of power output as a function of time can be predicted. Apart from the error introduced by the approximations in the expression for P, the theoretical curve is drawn on the assumption that the increased rate of deexcitation of the upper level and the extra population of the lower level due to stimulated emission is small. The effects of stimulated emission would be to decrease gain at a particular time and to cause the gain to decrease more rapidly with time. However, the rate of decay of the laser pulse appears to be independent of current. On the basis of the variation of N_2 and N_1 with current and time discussed previously, this would only be true if this deexcitation of N_2 due to stimulated emission were small compared to other deexcitation processes.

The fact that no change in the spontaneous sidelight from both the upper and lower levels could be detected when lasing was prevented indicates either that the above is true or that the population difference is small compared to the absolute populations. The difference between gain and power outputs as a function of time will be discussed again in Chapter 8.

As has been mentioned previously, the difficulties of accurately measuring the low CO pressures used make the interpretation of the laser output and the upper and lower level populations as a function of the CO pressure difficult. Both the upper and lower level populations increase with CO pressure over the range of pressures used. No attempts to get reliable data on populations as a function of CO pressure were therefore made.

6.3 Excitation Mechanisms

Having discussed some of the observations of laser action at 9406Å, and interpreted them by observations on upper and lower levels, the possible mechanisms for excitation must now be discussed. From the different decay rates of the two levels and the variation of peak populations with current, it seems likely that different mechanisms are responsible. The general behaviour of the 2479Å line in the afterglow is similar to the Helium lines. This similarity points to a general mechanism such as electron impact being responsible for the lower laser level population. Electron impact on the molecule can dissociate it and excite one of the atoms, the excitation energy required being the sum of the molecular dissociation energy and the atomic excitation energy. After the current pulse, a large number of ground state atoms are likely to remain, and electron excitation of the atoms will also contribute to the lower level population. As can be seen from the energy level diagram, the lower level is directly connected to the two metastable states of the ground state configuration, so that the cross section for excitation can be quite large, as discussed in Chapter 4.

The rate equation for the $3s\,^1P$ level population can be written as

$$\frac{dN_1}{dt} = R(t) - N_1 A_1 + \sum_k N_k A_k$$

Here, $R(t)$ is the rate of excitation by all collision processes, $N_k A_k$ is due to cascading into the level by spontaneous emission from all higher levels and $N_1 A_1$ is due to spontaneous emission from the level. Experimentally N_1 decays exponentially with time so that

$$\frac{dN_1}{dt} = -N_1/\tau_1$$

where τ_1 is the measured time constant of decay.

For $\tau_1 = 4 \times 10^{-6}$ sec.,

$$\frac{dN_1}{dt} = -2.5 \times 10^5 N_1 = R(t) + \sum_k N_k A_k - N_1 A_1$$

$A = 2.7 \times 10^8 \text{ sec}^{-1}$, and the most important cascading transitions are the $3p\,^1D, {}^1P, {}^1S - 3s\,^1P$ transitions which include the lasing transitions. The lasing transitions have $N_k \approx N_1$, $A_k \approx 0.1A_1$ so that the dominant positive term in the rate equation is $R(t) \approx N_1 A_1 \gg N_1/\tau_1$. This confirms that the decay rate is determined by the decay rate of $R(t)$ and implies that $R(t)$ decays exponentially with a time constant τ_1. Since $N_1 \approx 10^9/\text{cm}^3$, $R(t) \approx 10^{17}/\text{cm}^3$ sec.. It must be noted that all the Helium levels decay at the same rate, so that if electron impact is the excitation mechanism, the electron temperature must be effectively constant, and the electron density decaying at the same rate as $R(t)$. To consider this possibility, the mechanisms for production of fast electrons will now be examined. Since the ionisation potential of CO is only 14eV, the following reaction can take place,

$$He(2^3S) + CO(X^1\Sigma^+) = He(1^1S) + CO^+ + e + 5.8eV$$

The electron, being the lightest particle, will effectively take all the excess energy in the form of kinetic energy. The collision may also occur with excitation of the CO^+, the electron taking correspondingly less energy. The total cross section for the ionising collision has been measured by Sholette and Muschlitz (Ref: 6.12) and found to be 7×10^{-16} cm.^{2}.

A second reaction is

$$He(2^3S) + He(2^3S) = He(1^1S) + He^+ + e + 15.06eV$$

The first excited state of He^+ is at 40.7eV, so no excitation of He^+ is possible, and the electron will take all the excess energy. Cross-sections of 10^{-14}cm.^{2} have been measured by Biondi (Ref: 6.13).

Later in this Chapter, it will be shown that the $He(2^3S)$ population is independent of current, and that a typical value for it is 10^{11}cm.$^{-3}$. Since the $CO(X^1\Sigma^+)$ population is typically 10^{15}cm.$^{-3}$, the rate of production of fast electrons can be estimated. Using the formula in Chapter 4, the rate for the first process is

$\frac{dn}{dt} = 10^{15}$cm^{-3} sec.$^{-1}$ where v has been taken as the mean velocity of the Helium metastable at T = 300°K. Since the afterglow populations build up in the order of 1μsec., the electron density due to this process will be 10^9cm.$^{-3}$. It is also clear that the contribution due to the second process is smaller by a factor 10^2. Taking the electron density above, with an electron temperature of 6eV and a Carbon ground state population of 10^{14}cm.$^{-3}$, the excitation rate to the lower laser level can now be estimated. Using the equations for electron impact excitation developed in Chapter 4, the rate becomes

$$R = 10^{15}\text{cm.}^{-3}\text{sec.}^{-1}$$

This is two orders of magnitude down on the value estimated earlier and almost definitely rules out this form of excitation. In addition, since the He(2^3S) population is independent of current, the resulting electron impact excitation should also be independent, if the processes mentioned above are the ones producing the electrons.

Before discussing further the possible excitation mechanism for the lower laser level in Carbon, it will be useful to consider the afterglow in pure Helium. Numerous authors have attempted to explain the afterglow and three mechanisms have been put forward which involve recombination. These are

$$He^+ + e = He^* = He + h\nu$$

$$He^+ + e + e = He^* + e = He + e + h\nu$$

$$He_2^+ + e = He_2^* = He^* + He + \text{kinetic energy}.$$

Gerber, Sauter and Oskam (Ref. 6.14) in experiments with pulsed r.f. discharges in pure Helium have shown that for preasures less than 20torr, the dominant processes are the first two, and that the decay of He^+ is exponential. Their experiment involved measurements of atomic and molecular Helium ion densities with a mass-spectrometer and of the spontaneous emission from excited atomic and molecular energy levels. Although no excited He^+ has been observed spectroscopically in our discharge, it was not possible to determine whether ground state He^+ was present. Excited C^+ has been observed both during the current pulse and very early in the afterglow. It was also noted that the C^+ spontaneous emission varied quadratically with current, implying that a two stage process is involved, the intermediate state being the C^+ ground state. Further discussion of the C^+ spectra will be made in Chapter 7.

A further experiment on the Helium afterglow was performed by Hinnov and Hirschberg (Ref: 6.15). Their measurements were made on the quiescent afterglow in a magnetically confined Helium plasma.

Working with pressures of the order of 10^{-3} torr, they observed a similar light output as a function of time to that shown by the Helium lines in this experiment. However, their time scale was of the order of 500 microseconds compared with the 5 microseconds observed here. The reason for this will become clearer after the theory of the afterglow behaviour has been explained. First, they found that the populations of the excited states of the n^3D series follows a Maxwell-Boltzmann distribution law with a time varying characteristic temperature of the order of 1eV or less. It would therefore appear that these levels are in equilibrium with the electrons. By means of the Saha equation, the calculated electron density agreed well with the electron density, measured with a microwave interferometer. The implication of the thermal equilibrium with the electrons is that the levels are populated by the reaction

$$He^+ + e + e \rightleftarrows He^* + e$$

since this reaction is also reversible. By detailed balancing, it is clear that the probability that the resulting excited state has a principal quantum number n is an increasing function of n. The populations of the lower levels are too large for radiative cascading to be the populating mechanism, unless both the electron density and temperature are small. The major populating mechanism is due to superelastic and inelastic collisions of higher bound states with electrons. The general approach to solving the problems of the decay times of populations is as follows.

An excited atom, formed by the three body recombination process, can be reionised by electron impact or make a transition to another

bound state by inelastic collisions with an electron or by a radiative transition. If the ionisation rate from a given level is greater than the total downward transition rate, the level will be in thermal equilibrium with the electrons, and this happens for levels with a high value of n. At a particular level, which depends on electron density and temperature, the ionisation rate and downward transition rate are the same but for the levels lower than this, the downward transition rate is the dominant one. In principle, by writing out the rate equations for all the levels, the complete problem can be solved. Unfortunately, this requires a knowledge of collisional transition probabilities which are not known. By making a number of approximations and simplifications, Himnov and Hirschberg show that the rate of loss of electrons is given by

$$-\frac{dNe}{dt} = a(kT_e)^{-3/4} N_e^{\,2} + b(kT_e)^{-9/2} N_e^{\,3}$$

where a and b are constants depending on pressure of the gas. For constant kT_e, this does not give rise to an exponential decay for N_e, but as kT_e decreases, so $\frac{dNe}{dt}$ increases for fixed N_e. Thus a particular rate of decay of electron energy will give rise to an exponential decay of electron density and consequently an exponential decay of light intensity. Since this process is governed by collision rates, it is obvious that an increase of pressure will increase the decay rate of electrons, thus explaining the difference between Himnov's results and the results quoted here. Similar results were obtained with Argon, so that Neon would also be expected to show the same behaviour. Neon levels, observed under the same conditions of excitation as the Helium levels, did in fact show the same behaviour, as will be seen in Chapter 7.

It would therefore seem probable that the populations of $3s\,^1P$ level in Carbon, and also the $3s\,^3P$ levels, are due to the same mechanism

of recombination of the electrons with C^+. Any difference in time dependence between the Helium spontaneous emission and the 2479Å emission will then be due to the difference in the recombination coefficients for the Helium ions and the Carbon ions.

Fig. 6.9 is a graph of the intensity of the spontaneous emission from the 3888Å ($3^3P - 2^3S$) line of Helium. The side-light, end-light and the resulting value of $k_o l$ are plotted on a logarithmic scale, so that an exponential decay is a straight line on the graph. Fig. 6.10 is a similar graph of the side-light, end-light and resulting $k_o l$ for the 5876Å ($3^3D - 2^3P$) Helium line. Both these Helium lines are not single lines, so that the calculation of the lower level populations from the ratio of side-light to end-light requires a knowledge of the line shape. On the basis of Doppler broadening of the components of each line, and that the intensities of the components are given by L-S coupling, the relationship between the intensity ratio and the lower level population was calculated. This was then compared with the value obtained by treating the complex line as a single line, and using the mean f value for the transition. It was found that this latter value was smaller than the true value by a constant factor of the order of 1.5. The values of $k_o l$ shown on the graph are the single line values, and are therefore too small by the above factor. This does not alter the decay rates for $k_o l$ and the lower level populations.

The 2^3P population is found to decay with almost the same rate as the other Helium levels. Absorption on the $3^1P - 2^1S$ 5015Å Helium transition is negligible, except for about 5usec. at the start of the afterglow.

Fig. 6.11 is the graph of the side-light of the 9406Å Carbon line Fig. 6.12 shows the side-light, end-light and resulting value of $k_o l$ for the 2479Å Carbon line. The latter is a single line so that the population of the

lower level (2^1S) can be directly calculated using the equation of Chapter 2 and the values in Table 6.1. The resulting population for this metastable level is 7×10^{10} cm.$^{-3}$.

It can be seen that there is good agreement between the decay rates for the Helium 2^3S metastable population and the 9406Å emission. This is therefore strong evidence that the $3p^1D$ Carbon population is due to a collision process involving the Helium 2^3S metastable. Referring back to the energy level diagrams for Carbon, the energy of the 2^3S metastable has been shown, after subtracting the known dissociation energy of the CO molecule which is 11.11eV (89,613cm.$^{-1}$) (Ref 6.16). It can be seen that this 2^3S level is lower than the $3p^1D$ Carbon level by 2380cm.$^{-1}$. Since $kT \approx 200$cm.$^{-1}$ at room temperature, the number of Helium 2^3S metastables with the extra energy of 2380cm.$^{-1}$ in the form of kinetic energy is small. However, the first excited vibrational level of the $X^1\Sigma^+$ ground state of CO is 2143cm.$^{-1}$ above the lowest vibrational level (Ref 6.17), so that the energy discrepancy is now only 157cm.$^{-1}$. This and the higher vibrational levels of the $X^1\Sigma^+$ state are appreciably populated during the current pulse, and in pure CO the lifetimes range from 33×10^{-3} sec. for v = 1 to 4.3×10^{-3} sec. for v = 9 (Ref 6.17). The collisional deactivation of these levels by Helium ground state atoms is small (Ref 6.18), so that the populations of the excited vibrational levels are constant during the afterglow. As mentioned previously, the 2^3S metastable population is almost independent of current as is the 9406Å line. The behaviour of the 4p - 3s singlet transitions and the 5p - 3s singlet transitions in Carbon is similar to that of the 9406Å line. On energy considerations, the collision process must be between CO vibrational levels with $v \geq 2$ and the Helium 2^3S metastable.

The Helium 2^1S metastable and the 2^3P radiating level have also been shown in Figs. 6.1 and 6.2 with the CO dissociation energy subtracted.

It must be noted that both these levels have more than sufficient energy to dissociate the CO molecule in its lowest vibrational state and produce an excited 3p Carbon atom. For the Helium 2^1S metastable, there is an excess energy of approximately $4000cm^{-1}$ if a $3p^1D$ Carbon atom is produced. This will be in the form of kinetic energy of the Helium, Carbon and Oxygen atoms. By considering the volume of phase space available, it can be shown that the energy distribution for a particle with mass M_1 in a three body disintegration is

$$N(W_1)dW_1 \propto (W_1)^{1/2} \left(E - \frac{M_1 + M_2 + M_3}{M_2 + M_3} W_1\right)^{1/2} dW_1 \quad \text{(Ref 6.19)}$$

where E is the excess energy to be distributed, W_1 the final energy of particle 1, and M_2, M_3, are the masses of the other two particles. The resulting velocity distribution is therefore

$$N(V_z)\,dV_z = \frac{16N\beta}{15\pi E^3} (E - \beta V_z^2)^{3/2} (2E + 3\beta V_z^2)\, dV_z$$

where $$\beta = \frac{M_1}{2} \frac{(M_1 + M_2 + M_3)}{(M_2 + M_3)}$$

For the particles He, C, O, the full width at half maximum of the velocity distribution for the C atom is 3400m./sec., compared with the width due to thermal motion at 300^0K of 1060m./sec. . Since both the He 2^3S metastable and CO molecule have thermal velocities before collision, a thermal distribution should be "folded" in with the three body distribution, resulting in an even broader distribution. Provided the thermalisation time of the excited Carbon atoms is long compared to the radiative lifetime of the Carbon $3p^1D$ state, the spectral distribution of the light from the $3p^1D$ level will not be the usual Gaussian distribution, and will also be

wider than the Doppler width at 300°K. Extension of a method due to Gravath (Ref. 6.20) indicates that the thermalisation time is indeed long compared with the $3p^1D$ lifetime. Efforts were therefore made to measure the line-width of the spontaneous emission at 9406Å with a Fabry-Perot etalon. Because of lack of sensitivity of photographic plates at this wavelength, this direct experiment proved impossible. The indirect experiment of measuring the spectral range of the lasing cavity modes was therefore attempted. It has been previously shown in Chapter 2 that under certain conditions, the laser output will be similar to the gain curve, if the modes are not resolved. The gain at which the line width was measured was 10%, compared to an estimated threshold gain of 1%. Furthermore, the thermal Doppler width at 300°K is 1140MH_z compared to a longitudinal mode spacing of 72MH_z, so that many modes will be oscillating. The measured width was found to be equal to the Doppler width at 300°K to within 50%.

The above result, coupled with the similar decay rates for the 2^3S metastable with the 9406Å line show that it is the metastable colliding with the vibrationally excited CO molecule that is responsible for excitation of the $3p^1D$ level.

Although the dielectric coated mirrors have a reflectivity of only 26% at 14542Å, and the sensitivity of the RCA 7102 photomultiplier is so small that it is not shown on the published sensitivity curves, oscillation at this wavelength was detected with the photomultiplier. The behaviour was similar to that of the 9406Å line but the delay before oscillation was 8μsec. less. The line was studied further by means of a InSb Photo-conductive Cell, the Mullard RPY 36. This detector, which operates at liquid Nitrogen temperatures, has a measured time constant of less than 0.5μsec. At peak gain, the transition at 14542Å would oscillate with a 26% reflectivity curved mirror and a plane quartz flat as the other mirror.

This corresponds to a value of $k_o l$ of 2.28. A plane mirror was aligned at one end of the discharge tube and the output at the other end observed. The intensity in the afterglow in this double-pass arrangment was about two or three times greater than the corresponding single-pass intensity, but was not really large enough to call the line superradiant. Before proceeding with a detailed experimental study of the line, a calculation was made of the population in the upper level in comparison with the upper level of the 9406Å line and of the population of their mutual lower level at a fixed time. The results of this, using the method described in Chapter 5 are

$3p^1P_1$ population = 11.00×10^9 cm.$^{-3}$

$3p^1D_2$ population = 10.15×10^9 cm.$^{-3}$

$3s^1P_1^o$ population = 9.85×10^9 cm.$^{-3}$

With all the populations being approximately the same, it is the statistical weight factors of the levels that determine the relative magnitude of the gain for the 9406Å and 14542Å lines, since the f value for the 9406Å transition is almost double that for the 14542Å transition. Assuming that the cross-section for excitation of this $3p^1P$ level by dissociative excitation is the same as that for the $3p^1D$ level, the ratios of the populations divided by the statistical weight should tell us the distribution of CO molecules on the two vibrational levels, and thus the effective vibrational temperature. This temperature is calculated to be about 3600°K, a not unreasonable value when it is remembered that the distribution is unlikely to have changed much since its formation during the current pulse. The explanation of the observation of a laser pulse at 14542Å during the current pulse risetime will be deferred until after the discussion of the laser action at 10691Å.

At very low pressures of CO, the transitions at 10691Å, 10683Å and 10685Å behaved in a similar way as did the 9406Å transition. The latter

transition was very weak and only oscillated at peak conditions for the other two lines. The main interest of these lines lay in the fact that generally, the 10683Å line oscillated earlier and had greater gain, even though the 10691Å line is the strongest line of the multiplet in spontaneous emission. Possible explanations for this are that either the upper or lower levels are not populated according to the statistical weights, or that the decay rates for the $3s^3P_2$ and $3s^3P_1$ Carbon levels are different. Unfortunately, the lower levels are in the vacuum ultraviolet, so that the relative intensities and hence the statistical weights were not determined. The sensitivity of the photomultiplier at 10691Å is 1/6th of that at 9406Å so that measurements on the 10691Å multiplet require that the spectrograph slits be fully open. Since the resolution of the spectrograph (Czerny-Turner) is only 13Å/mm. the multiplet lines are unresolved. Measurements taken with the Ebert spectrograph, although somewhat unreliable because of self-absorption, indicate that the ratio of intensity of the two strongest lines is nearer unity than the theoretical ratio of 1.8. This is probably the cause of the weaker spontaneous line oscillating more strongly. As the pressure decreased further, the stronger line in spontaneous emission gradually oscillated more strongly than the other. The 10685Å line, which is the third strongest line in spontaneous emission, lased fairly weakly at a pressure such that the 10683Å line was lasing at its strongest in the afterglow.

Under typical operating pressures of 7Torr Helium and 0.05 Torr CO, the 10691Å and 10683Å lines oscillated only during the current rise-time. When these lines were observed in spontaneous emission, no significant emission could be seen at the time of laser output. Unlike the behaviour in the afterglow, the 10691Å line is always the stronger.

The general behaviour of the lines as a function of current is as follows :-

The current as which the 10691Å gain has its peak value is lower than the current at which the 9406Å gain has its peak value at the same pressure. The gain is a sharply peaked function of current, the current usually being of the order of 15Amps for peak gain. The actual magnitude of the gain is greater than 18% /metre. The behaviour as a function of Helium pressure is that the 10691Å line starts oscillating at about 3Torr and increases to a maximum output at about 13Torr. At higher pressures, the gain slowly decreases and at 20Torr is down to 2/3rds of the value at 13Torr. The laser pulse lasts for 0.4μsec. and Fig. 6 4(c) shows the oscilloscope trace of the laser pulse with a time scale of 0.5μsec /div. It was noticed that the spontaneous output of the Helium lines differed considerably from that of all the Carbon lines during the current pulse. The latter lines followed the current pulse both with respect to time and magnitude. The Helium lines all increased very rapidly with time to a maximum while the current was still rising and had decayed to approximately half intensity by the time the current had reached its maximum. This can be seen in figs. 6.4(d) - (f). Due to electrical pick up in the detection circuitry, accurate self absorption measurements were not attempted. However, since all the Helium lines behave similarly, it seems most likely that the metastable populations will at least show this rapid rise, even if their decay is much slower. The populations of the $3p\,^1P$ and $3p\,^3D$ Carbon levels will then be due to two mechanisms. First there is electron impact which has an overall dominant effect as shown by the similarity between the light output and the current pulse. This will populate both the upper and lower laser levels, but the populations will tend to be distributed according

to the electron energy distribution and the lower level will have the greater population.

The second mechanism, which is the important one as far as laser action in concerned, is the one discussed earlier, namely dissociation and excitation by collision of the CO molecule with the Helium 2^3S metastable. Although this is comparatively small and cannot be detected in the spontaneous emission of the upper laser level, it dominates at this early time because it occurs much earlier than that due to electron impact, and assuming that the lower level has not been populated at all, a population of only $1.5 \times 10^7 cm.^{-3}$ is all that is required for a gain of 2%. This is three orders of magnitude smaller than the populations seen at the current pulse peak, and it also explains the laser behaviour with current. As the current increases from zero, the metastable population also increases, increasing the population of the upper level, the population of the lower level still being small at this time. However, as the current increases beyond that for peak output, the lower level has a larger population due to electron impact, and the small increased population of the upper level has less influence, finally disappearing altogether. The reason why the 10691Å, 10683Å and 14542Å lines lase during the current pulse and not the 9406Å line is fairly obvious on reexamining the term diagram. The $3p^3D$ and $3p^1P$ levels lie below the Helium 2^3S metastable, whereas all the other 3p levels are above the metastable. Since vibrationally excited CO is needed to excite these levels, and there is not sufficient time for this to occur during the current pulse risetime, the levels will not be excited, and thus the 9406Å line will not oscillate in the current risetime.

If the population of the $3s^3P$ levels are zero at the time when the prompt laser action commences, the gain of the 10691Å and 10683Å are

proportional to fN_2g_1/g_2. Even if the $3p^3D_3$ and $3p^3D_2$ populations are equal and not in the ratio 7:5 given by the statistical weights, the gain of the 10691Å line will be greater than the gain of the 10683Å line in the ratio of their Einstein A coefficients. With the populations in the ratio of the statistical weights, the ratio of the gain of the 10691Å line to the gain of the 10683Å line will be even larger.

From the data on the populations of the laser upper level and the Helium 2^3S metastable level, an estimate can be made of the cross-section for the dissociation and excitation process. The equation of Chapter 4 is

$$R = N(CO)\,N(He\ 2^3S)\,\sigma\,v$$

For a temperature of 300°K, $v(He) \approx 2 \times 10^5 cm.\,sec.^{-1}$ and $v(C)) \approx 4 \times 10^4 cm.\,sec.^{-1}$.

For a typical CO pressure of 0.05torr, $N(CO) \approx 10^{15} cm.^{-3}$.

From the absorption experiments, $N(He) \approx 3 \times 10^{11} cm.^{-3}$.

Finally, $R = N_2A_{21} \approx 5 \times 10^{16} cm.^{-3} sec.^{-1}$.

Hence $\sigma \approx 7 \times 10^{-16} cm.^2$.

From the values noted in Chapter 4, this value is of the expected order of magnitude, and is further confirmation that the populating process is the collisional dissociation one.

References

6.1 L. Johansson — Arkiv för Fysik 31, 201 (1966)

6.2 L. Johansson & U. Litzen — Arkiv för Fysik 29, 175 (1965)

6.3 G. Herzberg — Proc. Roy. Soc. A248, 309 (1958)

6.4 P.G. Wilkinson & K. L. Andrew — J. Opt. Soc. Am. 53, 710 (1963)

6.5 W. L. Wiese, M. W. Smith & B. M. Glennon — Atomic Transition Probabilities Vol. 1 NSRDS-NBS4 (1966)

6.6 D. R. Bates & A. Damgaard — Proc. Roy. Soc. A242, 101 (1957)

6.7 C.K.N. Patel, R. A. McFarlane & W. L. Faust — Quant. Electronics III, 561 (1964)

6.8 C.K.N. Patel, R. A. McFarlane & W. L. Faust — Phys. Rev. 133, A1244 (1964)

6.9 H.A.H. Boote & D. M. Clunie — Nature 197, 173 (1963)

6.10 M. Shimazu & Y. Suzaki — Jap. J. Appl. Phys. 3, 561 (1964)

6.11 W. R. Bennett Jr. — Phys. Rev. 126, 580 (1962)

6.12 W. P. Sholette & E. E. Muschlitz Jr. — J. Chem. Phys. 36, 3368 (1962)

6.13 M. A. Biondi — Atomic Collision Processes (ed. M. R. C. McDowell) p491 (1964)

6.14 R. A. Gerber, G. F. Sauter & H. J. Oskam — Physica 32, 2173 (1966)

6.15 E. Hinnov & J. G. Hirschberg — Phys. Rev. 125, 795 (1962)

6.16 T. L. Cottrell — The Strengths of Chemical Bonds (1958)

6.17 C.K.N. Patel — Phys. Rev. 141, 71 (1966)

6.18 R. C. Millikan — J. Chem. Phys. 40, 2594 (1964)

6.19 Cao Xuan Chuan — J. de Physique 23, 78 (1962)

6.20 A. H. Gravath — Phys. Rev. 36, 248 (1930)

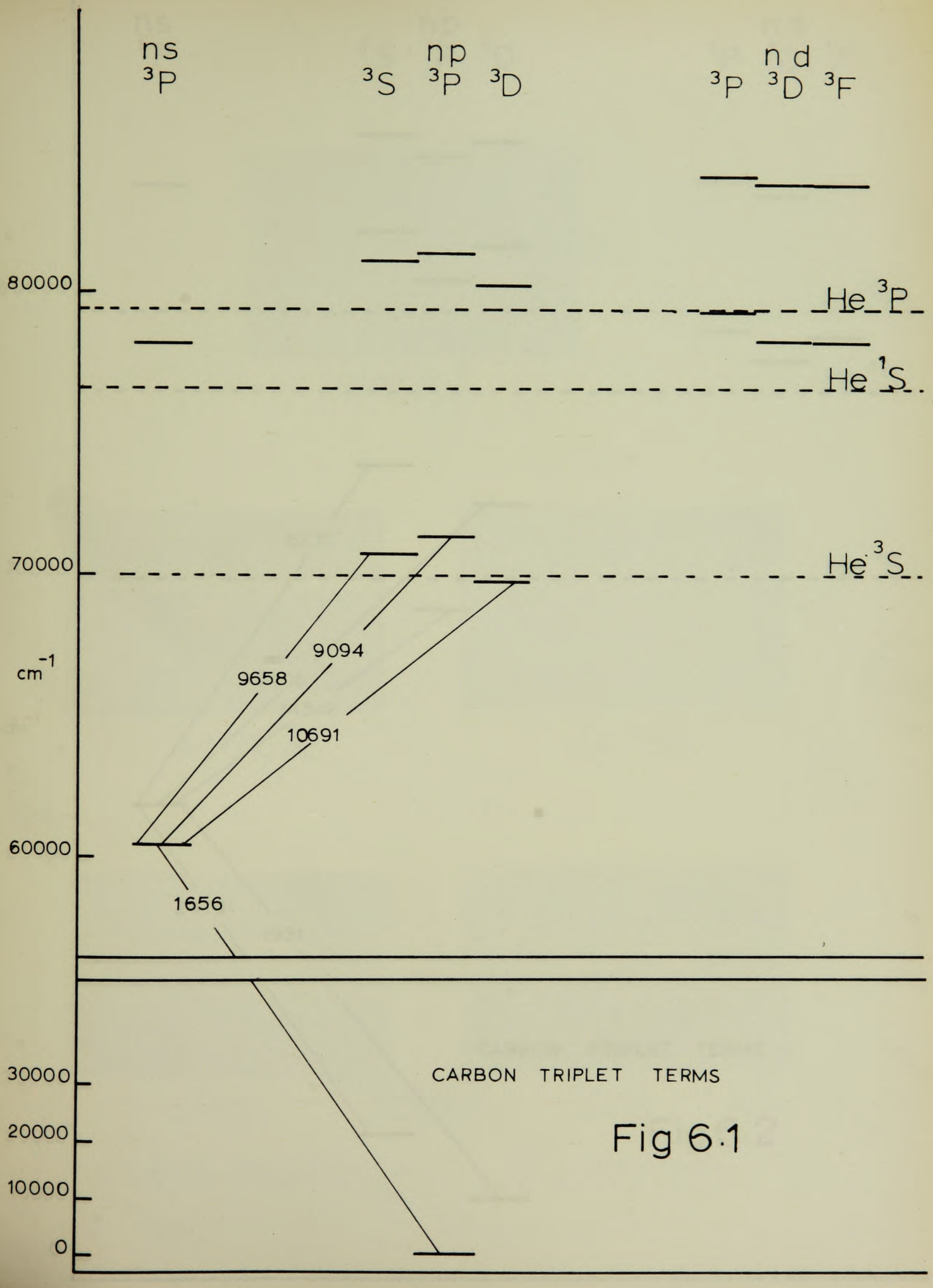
ns
^3P
np
^3S ^3P ^3D
n d
^3P ^3D ^3F
80000
He ^3P
He ^1S
70000
He ^3S
cm^{-1}
9094
9658
10691
60000
1656
30000
20000
10000
0
CARBON TRIPLET TERMS

Fig 6.1

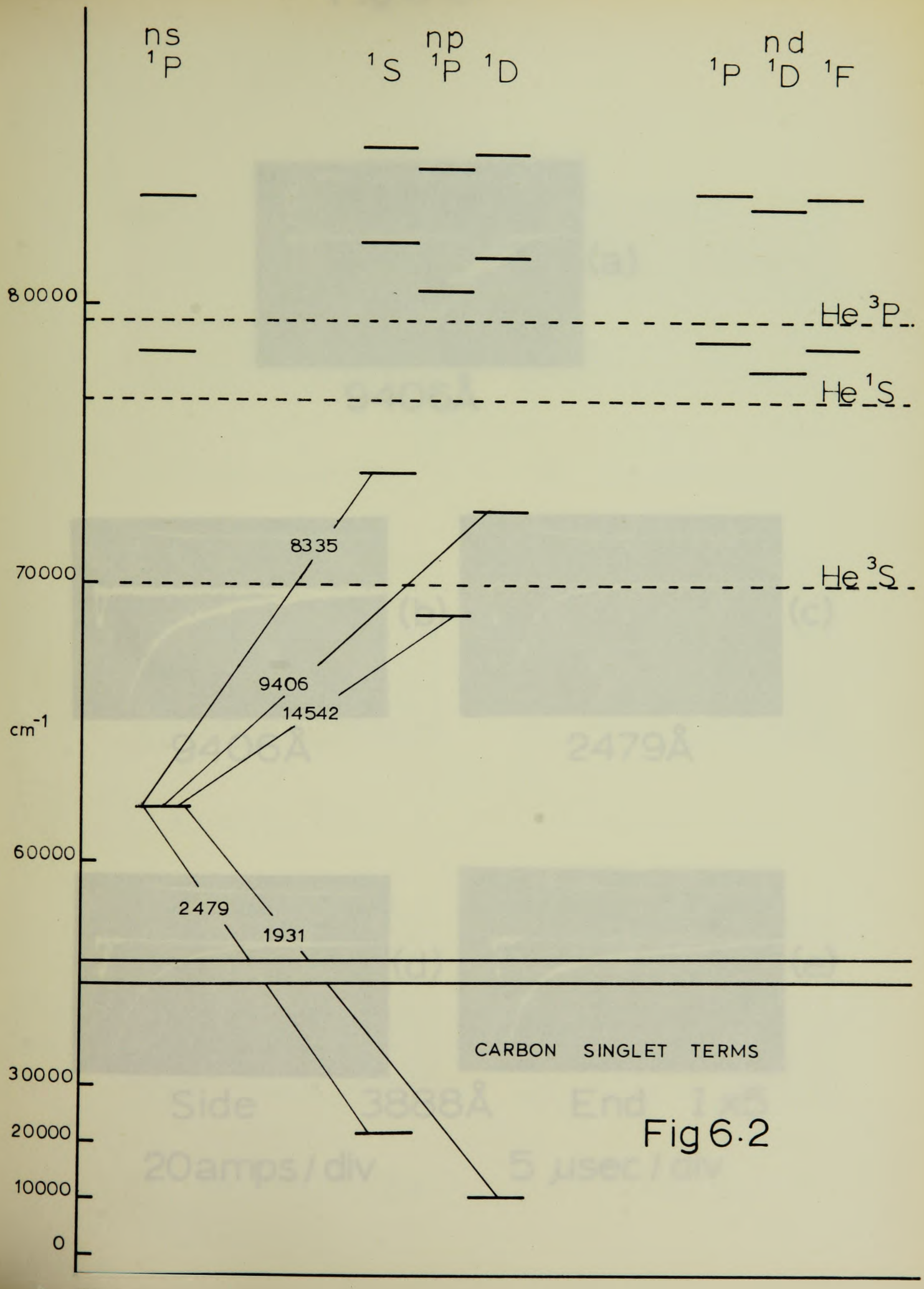
ns
^1P
np
^1S ^1P ^1D
nd
^1P ^1D ^1F
80000
He ^3P
He ^1S
70000
He ^3S
8335
9406
14542
cm^{-1}
60000
2479
1931
CARBON SINGLET TERMS
30000
20000
10000
0

Fig 6.2

Fig 6.3

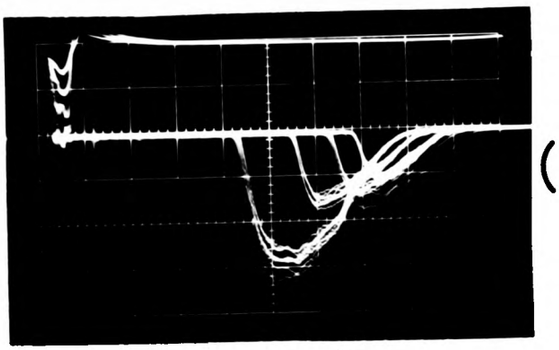

(a)

9406Å

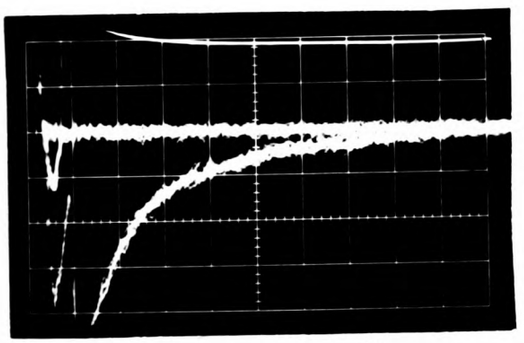

(b)

9406Å

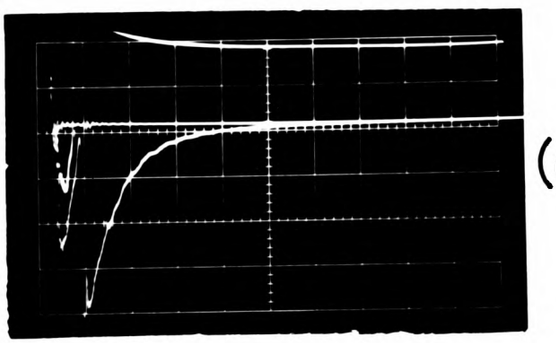

(c)

2479Å

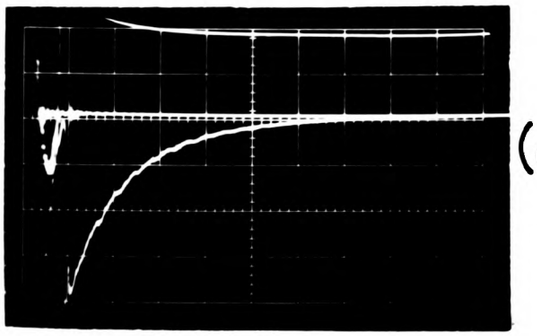

(d)

Side

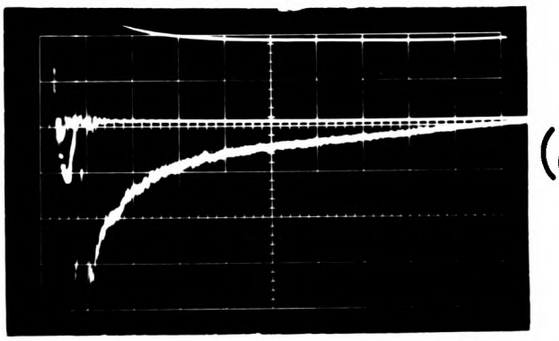

(e)

3888Å End I x5

20amps / div

5 μsec / div

Fig 6.4

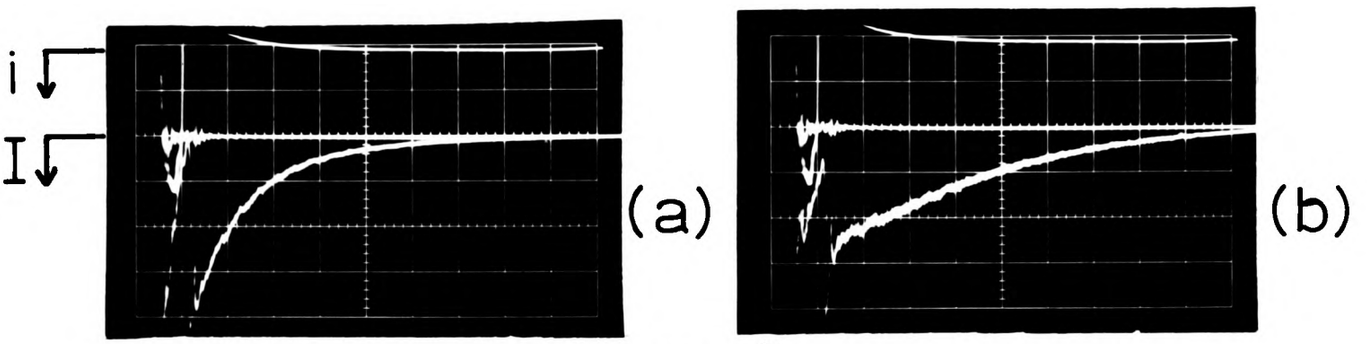

Side 5876Å End I x4

20amps/div 5 μsec/div

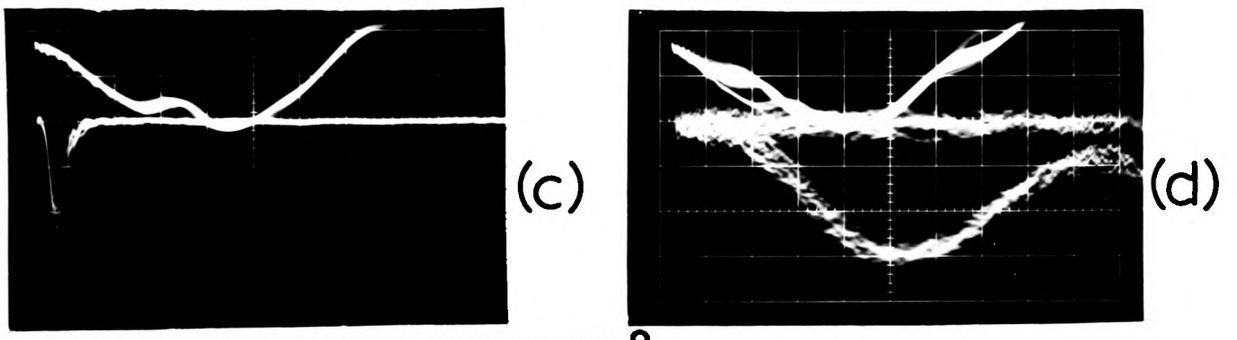

Laser 10691Å

10 amps/div 0.5 μsec/div

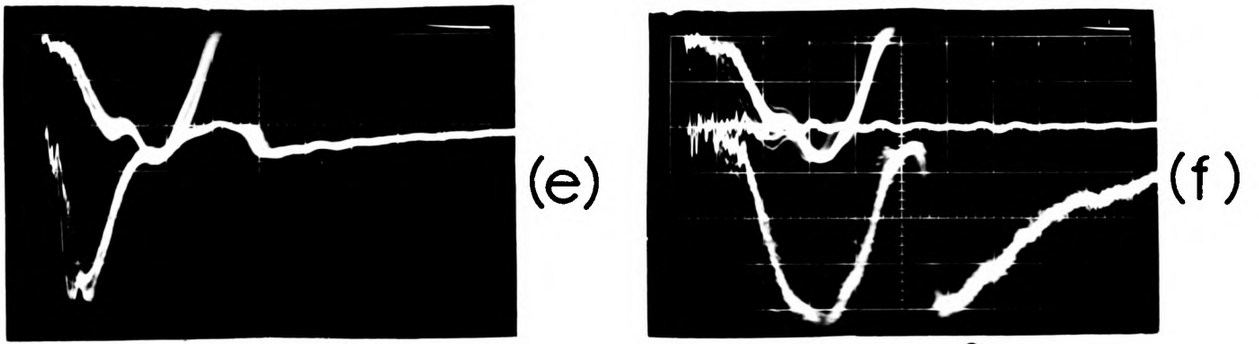

3888Å 2479Å

10amps/div 1 μsec/div

Fig 6.5

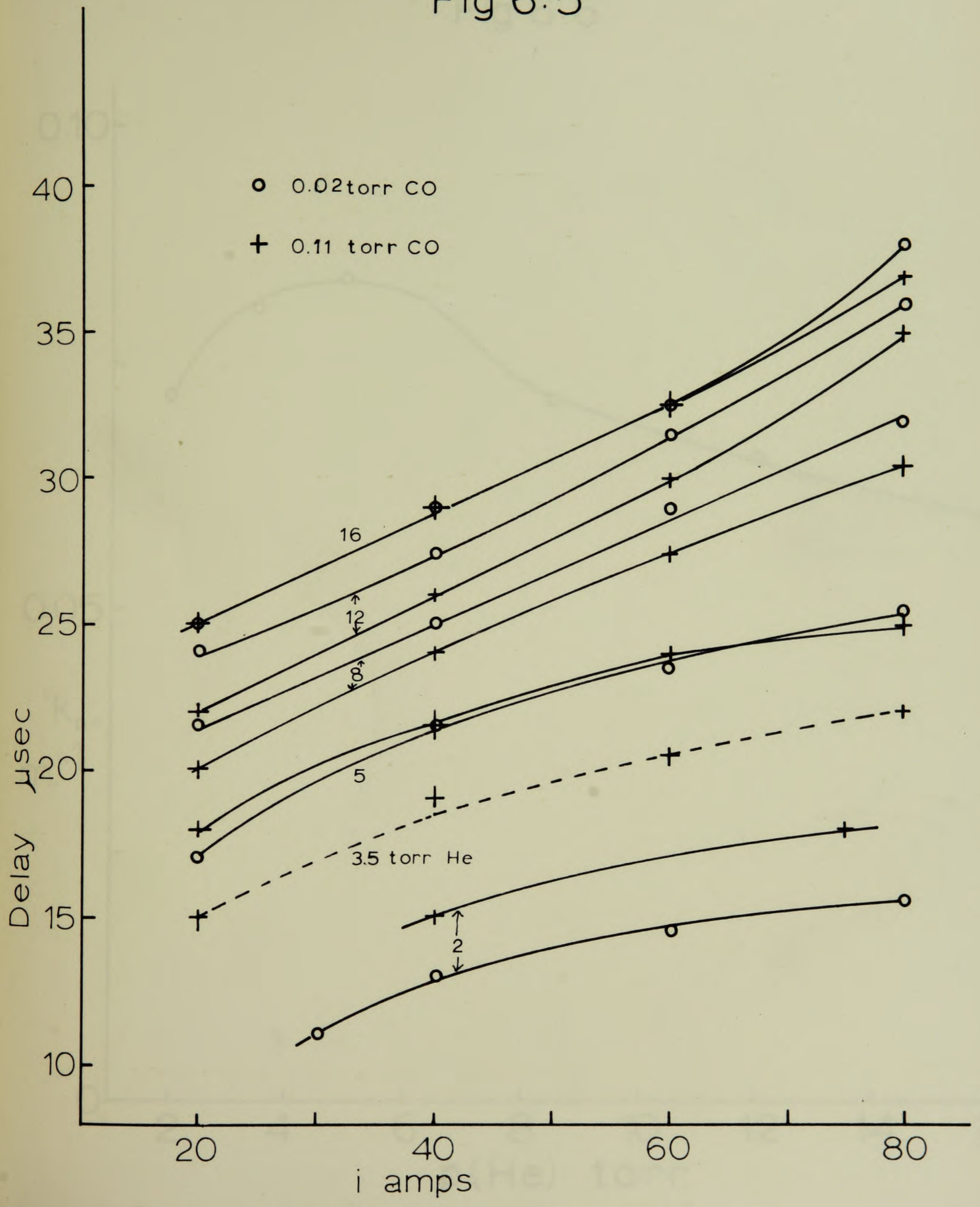
o 0.02torr CO
+ 0.11 torr CO
16
12
8
5
3.5 torr He
2
Delay μsec
i amps
10
15
20
25
30
35
40
20
40
60
80

Fig 6.6

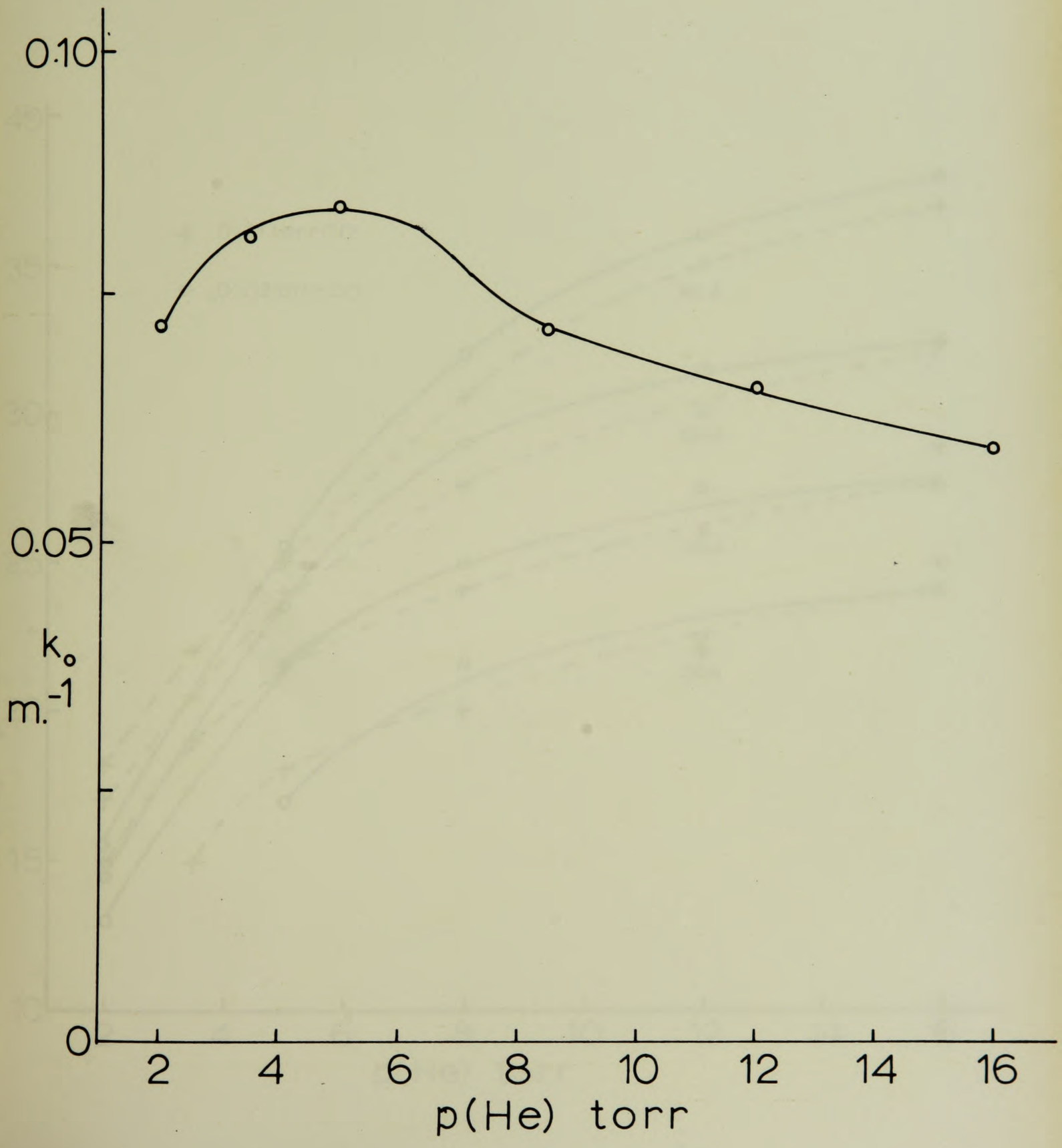

Fig 6.7

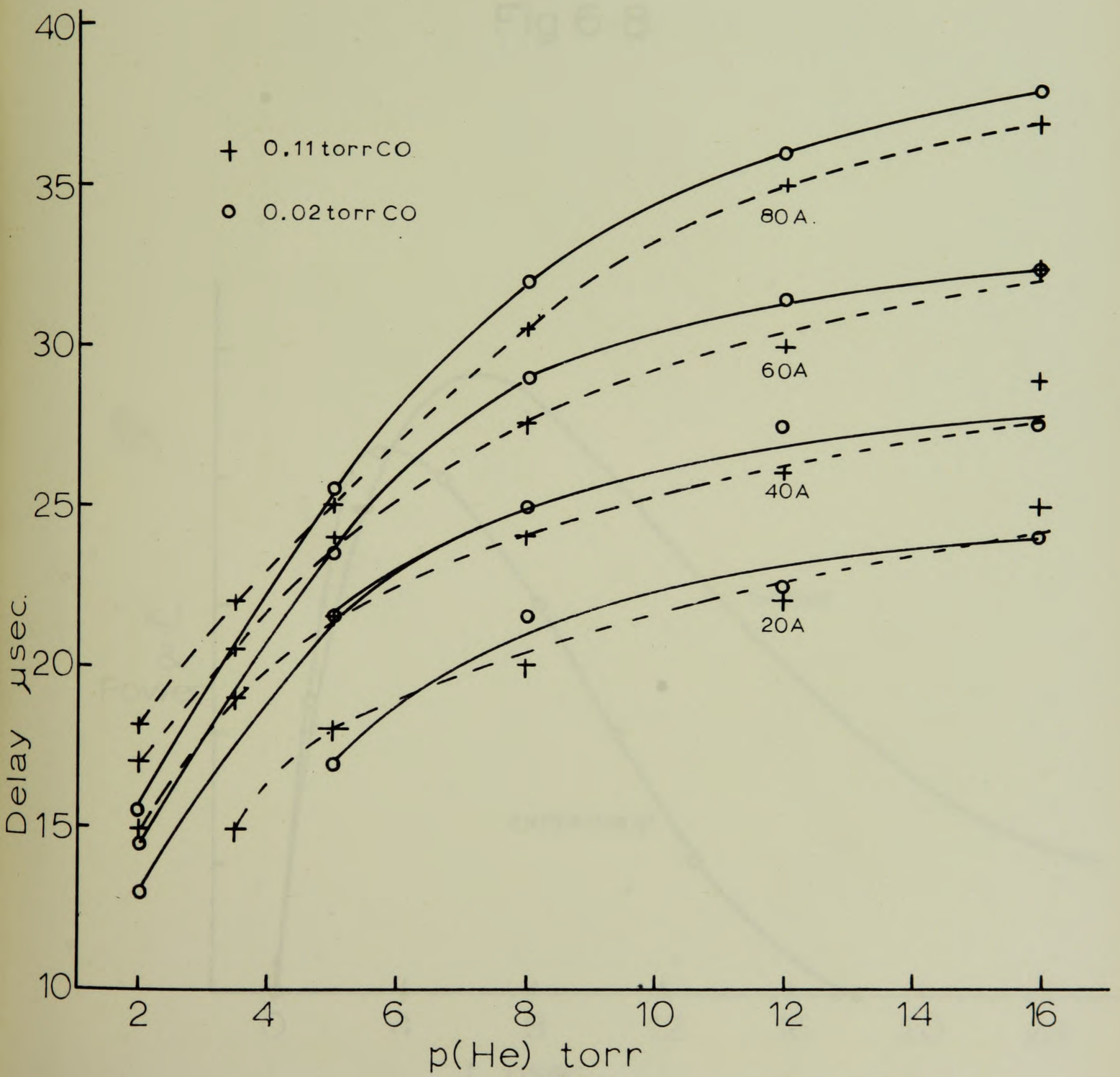
40
35
30
25
20
15
10
Delay μsec.
+ 0.11 torr CO
o 0.02 torr CO
80A.
60A
40A
20A
2
4
6
8
10
12
14
16
p(He) torr

Fig 6.8

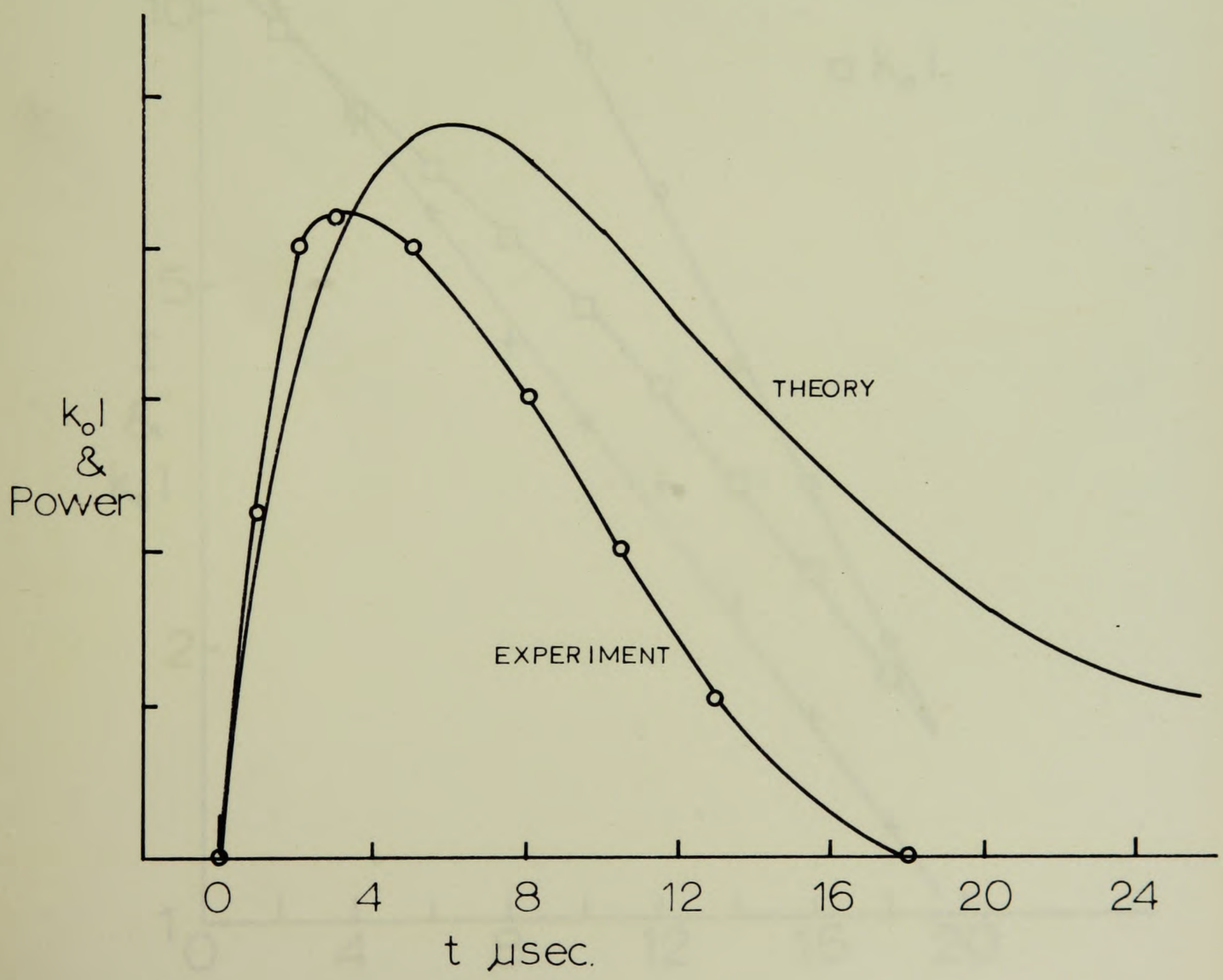

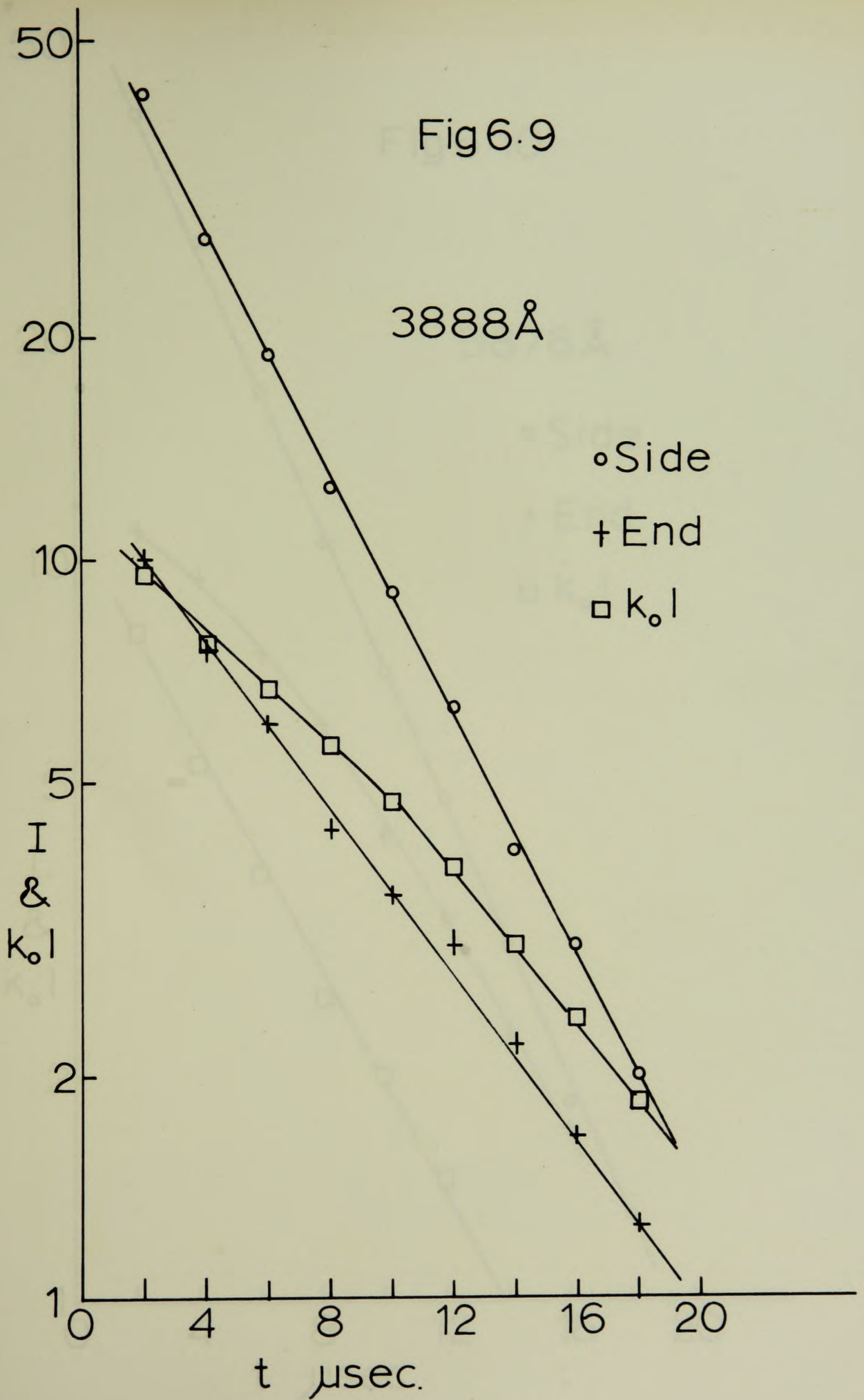
Fig 6.9
3888Å
Side
End
$k_o l$
50
20
10
5
2
1
I & $k_o l$
0
4
8
12
16
20
t μsec.

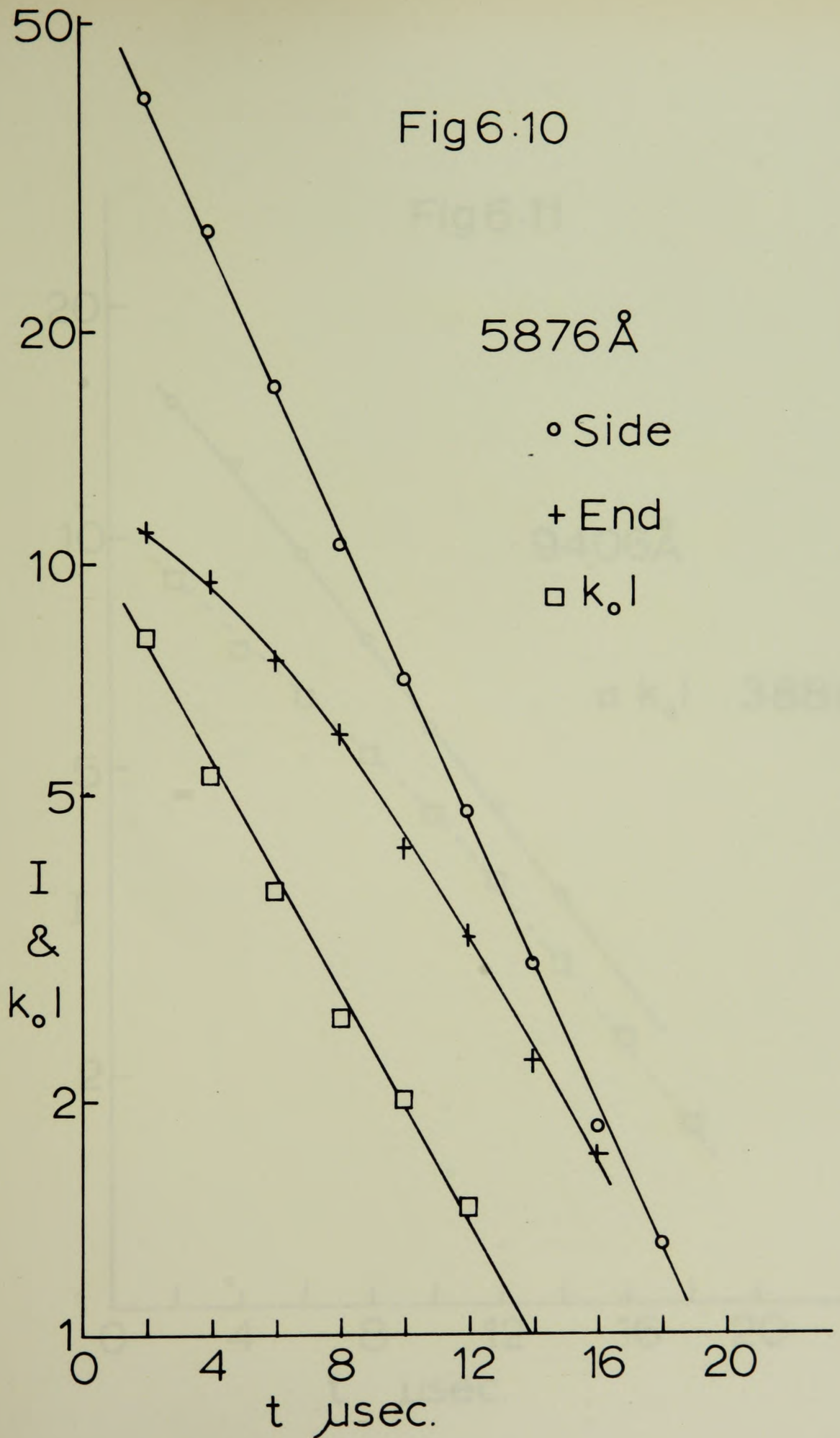
Fig 6.10
5876 Å
o Side
+ End
□ $k_o l$
50
20
10
5
2
1
I & $k_o l$
0
4
8
12
16
20
t μsec.

Fig 6.11

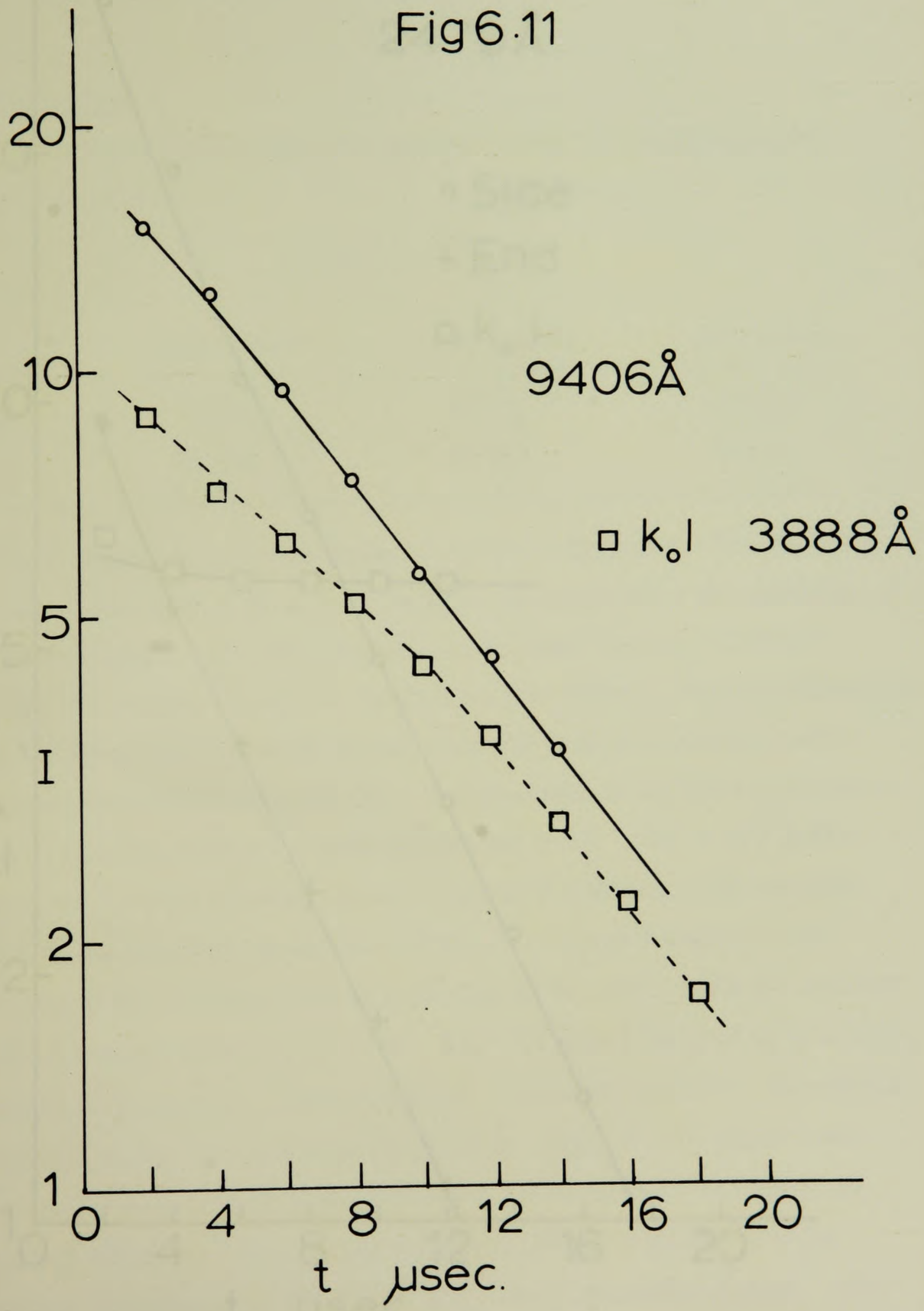

Fig 6.12

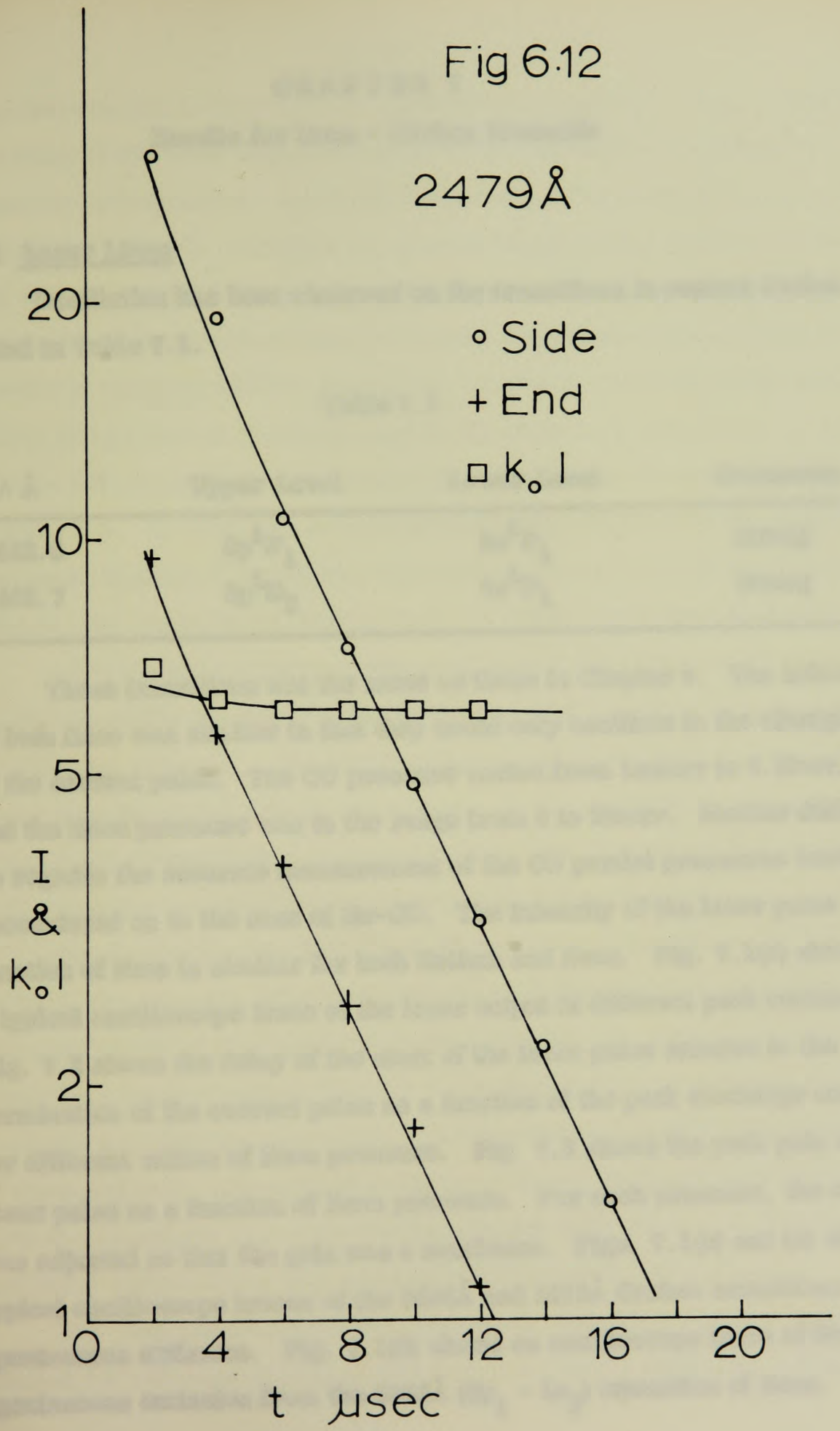

CHAPTER 7

Results for Neon - Carbon Monoxide

7.1 Laser Lines

Oscillation has been observed on the transitions in neutral Carbon listed in Table 7.1.

Table 7.1

λ Å	Upper Level	Lower Level	Comments
14542.5	$3p^1P_1$	$3s^1P_1$	Strong
9405.7	$3p^1D_2$	$3s^1P_1$	Strong

These transitions are the same as those in Chapter 6. The behaviour of both lines was similar in that they would only oscillate in the afterglow of the current pulse. The CO pressure varied from 1mtorr to 0.5torr, and the Neon pressure was in the range from 0 to 20torr. Similar difficulties as regards the accurate measurement of the CO partial pressures were encountered as in the case of He-CO. The intensity of the laser pulse as a function of time is similar for both Helium and Neon. Fig. 7.1(a) shows a typical oscilloscope trace of the laser output at different peak currents. Fig. 7.2 shows the delay of the start of the laser pulse relative to the termination of the current pulse as a function of the peak discharge current for different values of Neon pressure. Fig. 7.3 shows the peak gain of the laser pulse as a function of Neon pressure. For each pressure, the current was adjusted so that the gain was a maximum. Figs. 7.1(b) and (c) show typical oscilloscope traces of the 9406Å and 2479Å Carbon transitions in spontaneous emission. Fig. 7.1(d) shows an oscilloscope trace of the spontaneous emission from the 5852Å ($2p_1$ - $1s_2$) transition of Neon. The

Paschen notation is used for Neon throughout this thesis. Fig. 7.4 shows the delay of the laser output plotted as a function of Neon pressure at different peak currents. All these results are to be compared to those shown in Chapter 6. Although the general trend is very similar, there are several notable differences. With Neon, although the delay always increases with current at higher currents, it decreases with respect to current at currents close to threshold. However, the peak of the laser output always occurs at a later time as the current is increased. A second notable difference between Helium and Neon can be seen clearly in Figs. 7.4 and 6.7. In Neon, the delay decreases with pressure at the higher pressures instead of increasing with pressure as in the case of Helium. Finally, the delays in the case of Neon are much larger than in Helium.

As in the case of Helium, the laser output behaviour can be explained by examining the behaviour of the 9406Å and 2479Å Carbon transitions in spontaneous emission. The 9406Å output has a longer time constant of decay than the 2479Å and the Neon lines. Again, in the late afterglow, the intensity of the 9406Å line is almost independent of current, at currents well above the threshold for the appearance of the afterglow.

The intensity of the 2479Å and the Neon lines does increase with current, the intensity being approximately a linear function of current. The populations of the upper and lower levels can be written down in the same form as they were in Chapter 6, leading to the same expression for the delay as a function of current. The discharge showed visible indications of inhomogeneity, although not to the same extent as in the case of Helium. This is undoubtedly one of the reasons for the delay showing a different functional independence with current to that obtained from theory.

For Neon pressures greater than 8torr, the delay decreases with current for currents just above the threshold for the afterglow. This is

due to the upper level increasing with current over this range of currents, while at higher currents, the upper level population is approximately independent as already mentioned.

The increase in delay as a function of Neon pressure, at constant current for pressures less than 5torr is governed largely by the population of the lower level. In this pressure range, the 2479Å output increases with Neon pressure rapidly, reaching an approximately constant level at a pressure of 8torr. The 9406Å output increases fairly slowly over the whole pressure range, these measurements being taken at a fixed value of current.

The power output of the laser pulse as a function of time can be seen from Fig. 7.1(a) to be similar to that in the Helium-CO mixture. Similar arguments to those of Chapter 6 explain this, although the time constants of the two levels are different.

7.2 Excitation Mechanisms

It is immediately obvious from examination of Figs. 7.1 (b) - (d) that, as in the case of Helium, there are different decay rates for the upper and lower laser levels. Figs. 7.5 and 7.6 show this more clearly and also verify that the decay is approximately exponential. Comparison of these Figures with Figs. 6.11 and 6.12 show that the time scale in the case of Neon is almost twice that in the case of Helium. For the 2479Å spontaneous emission, the time constant of the exponential decay is 6.6μsec. Hence, the rate equation for the $3s^1P$ level in Carbon is

$$\frac{dN_1}{dt} = -1.5 \times 10^5 N_1 = R(t) + \sum_k N_k A_{k1} - N_1 A_1$$

Since the values of N_1 and N_k are approximately the same as for Helium, the conclusions of Chapter 6 are equally valid, and the only important terms are $R(t)$ and $N_1 A_1$. The possibility that $R(t)$ is due electron impact on Carbon ground state or metastable atoms has also been discussed in Chapter 6. The energy of the Neon metastables is 16.65eV, so that the electron energy after the Penning reaction,

$$Ne(1s_5, 1s_3) + CO(X^1\Sigma^+) = Ne(1^1S) + CO^+ + e + 2.65eV$$

is lower than for Helium. If this is the mechanism for producing fast electrons, the electron temperature will be even lower than with Helium. The Carbon atom ground state population is likely to be the same, and the electron density will be about 5 times greater since the metastable density is greater than for Helium by this factor. This is insufficient to compensate for the smaller value of $g(W/kT_e)$ as given in Chapter 4, so that this form of electron impact excitation of the Carbon $3s\,^1P$ level is even more unlikely than it was for Helium.

Although the Neon afterglow has not been studied in such great detail as the Helium afterglow, the dominant afterglow processes have been determined to a fair degree of certainty. Sauter, Gerber, and Oskam (Ref. 7.1) have performed experiments on pulsed r.f. discharges in pure Neon. Using a mass spectrometer and a photomultiplier, the ion densities and the populations of the excited Neon levels were determined as a function of time. The two ions present were Ne^+ and Ne_2^+. The loss of Ne^+ is by electron recombination, ambipolar diffusion to the walls, and by the conversion process

$$Ne^+ + 2Ne \rightarrow Ne_2^+ + Ne$$

The loss of Ne_2^+ is due to ambipolar diffusion to the walls and by

the dissociative recombination process

$$Ne_2^+ + e \rightarrow Ne^* + Ne \rightarrow 2Ne + h\nu$$

They also found that the populations of the 4d levels had a different time dependence from the 3p and 2p levels. From the time correlations, they concluded that the 4d levels were populated by the recombination processes

$$Ne^+ + e \rightarrow Ne^* \rightarrow Ne + h\nu$$

and $$Ne^+ + e + e \rightarrow Ne^* + e \rightarrow Ne + e + h\nu$$

The 3p and 2p levels are populated by the dissociative recombination process written above. This last result confirms measurements made by Connor and Biondi (Ref. 7.2). Their measurements were made on a microwave excited discharge, and they measured the electron density by means of a microwave interferometer instead of the ion densities. In addition, they measured the spectral line broadening on a line from a 2p level. The dissociation energy will be distributed between the two Neon atoms in the form of kinetic energy, giving rise to a Doppler broadening which is not only greater than the room temperature Doppler width but is not the usual Gaussian shape. Their measured line shape agreed well with the theoretical one predicted from the known dissociation energy of Ne_2.

These processes will of course still occur when CO is present. However, because certain levels are likely to be depopulated more rapidly due to the various possible collision processes, the decay rate of these levels may be considerably increased.

In Chapter 6 it was concluded that the dominant excitation mechanism of the Carbon $3s\,^1P$ level was recombination of C^+ with an electron. The same process is almost certainly the dominant one in the Ne-CO mixture.

Several excited levels of C^+ were observed during the current pulse, but only the four transitions from the two levels $1s^2 2s^2 3p\ (^2P^o_{3/2,1/2})$ had an observable afterglow. Figs. 7.1(e) and (f) show typical oscilloscope traces of the 2837Å ($3p^2P_{3/2,1/2} - 2s2p^2\ ^2S_{1/2}$) transitions in both Helium - CO and Neon-CO mixtures. As had been mentioned in Chapter 6, the intensity of all the C^+ spectral lines was similar, and the intensity during the current pulse and the afterglow was quadratic with current. During the current pulse, electron impact on C^+ ground state atoms will be one important excitation process to the excited C^+ states. Furthermore, electron impact ionisation to produce C^{++} will also occur. The processes

$$C^{++} + e \rightarrow C^{+*} \rightarrow C^+ + h\nu$$

and $$C^{++} + e + e \rightarrow C^{+*} + e \rightarrow C^+ + e + h\nu$$

will occur both during the current pulse and in the afterglow, and will be the dominant ones in the He-CO afterglow. These of course will give the quadratic dependence of the C^+ lines on current. The afterglow when produced by these mechanisms is short because of the large recombination coefficient for C^+. The observations of Hinnov and Hirschberg (Ref 6.15) verify this, as they found that all impurity ions behaved in this way. The absence of O^+ spectra in the afterglow, and the small output during the current pulse is due to the greater ionisation potential of both O^+ and O^{++}. Excitation rates are fairly sensitive to the ratio of kT_e to the ionisation potential, particularly when this ratio is small, as can be seen from Chapter 4.

With the Neon-CO mixture, the decay of the C^+ $3p^2P_{3/2,1/2}$ levels in the afterglow is exponential as can be seen from Fig. 7.8. The intensity is approximately linear with current. Noting once more that no other levels of C^+ have an observable afterglow, the only possible excitation process must be some form of selective one. The energies of the $3p^2P_{3/2,1/2}$ levels are

131736 and 131725 cm.$^{-1}$. The energies of the Neon metastable levels $1s_5$ and $1s_3$ are 134044 and 134821 cm.$^{-1}$. The energy difference is 2300cm.$^{-1}$ compared to the value for kT of 180cm.$^{-1}$. The nearest C^+ levels to the $3p^2P_{3/2,1/2}$ are the $3s^2S_{1/2}$ at 116537cm.$^{-1}$ and the $2p^3\,4S_{3/2}$ at 142024cm.$^{-1}$, so that the energy difference between them and the Neon metastables is considerably greater. Despite the large energy difference and the discussions of Chapter 4, the most probable process would therefore seem to be

$$Ne\,(1s_5,\ 1s_3) + C^+ \rightarrow C^+\,(3p^2P_{3/2,1/2})) + Ne + 0.3eV$$

If only these C^+ levels were populated in the afterglow, laser action may be possible with these levels as the upper levels. The most favourable transition is the $3p^2P_{3/2} - 3s^2S_{1/2}$ at 6578Å. No self-absorption was observed on this transition by the techniques of Chapter 5, but alignment of dielectric coated mirrors failed to produce oscillation. Since this was not the aim of this thesis, further investigations into this were not made.

Referring once more to Figs. 7.5, 7.7, and 7.9, we see that the calculated $1s_5$ and $1s_2$ Neon populations appear to decay with a longer time constant than the 9406Å Carbon transition. Also, the metastable decay appears to be not exponential, with the decay rate increasing with time, and tending towards the 9406Å decay rate. With high values of $k_o l$, $k_o R$ begins to become significant, R being the tube radius. This will mean that the side light is less than its value for no self-absorption. Hence the calculated values of $k_o l$, using the intensity ratios will be lower than the true values. The true values of $k_o l$ can be calculated in principle by an iterative procedure, but since the collection geometry for the side light is not simple, this is impractical. Nevertheless, it is obvious that the values of $k_o l$ shown on Figs. 7.7 and 7.9 are minimum values, and the

likely error increases with the value of $k_o l$. This has the effect of making the decay rates for the $1s_5$ and $1s_2$ levels larger than is apparent from the Figs. The $1s_2$ level is not metastable, and has a strong UV transition to the ground state. At a pressure of 8torr, $k_o R \approx 3 \times 10^4$ so that it is strongly resonance trapped and behaves like a metastable.

In all the calculations of $k_o l$, it has been assumed that the transitions are Doppler broadened and that there is no structure in the lines. Neon has only two isotopes with significant abundance. Ne_{20} constituting 90.9% and Ne_{22} 8.8%. Neither of these isotopes has a nuclear spin so that there is no hyperfine structure. The isotope shift for all the transitions of the 2p - 1s group have been measured by Odintsov (Ref 7.3). They are in the range 50-80 x 10^{-3}cm.$^{-1}$ and are to be compared with the Doppler width of a line at 5880Å at 300°K which is 47 x 10^{-3}cm.$^{-1}$. The metastable densities calculated by the methods of Chapters 5 and 2 will thus be in error because of the more complicated line shape. However, calculations have shown that the true metastable densities are a constant factor between 1 and 2 larger than those obtained by assuming a single line and using the equations of Chapter 2.

As has been discussed in Chapter 6, the vibrationally excited levels of the ground electronic state of the CO molecule are highly populated in the afterglow. Thus the collision process

$$Ne(1s_{5,4,3,2}) + CO(X^1\Sigma^+)^* = C(3p^1P, 3p^1D) + O + Ne$$

will occur. Since vibrationally excited CO is needed to populate the Carbon 3p levels, laser action during the current pulse risetime is not to be expected. While failure to observe laser action during the risetime does not prove that laser action cannot be obtained, it is nevertheless significant that it was not observed. Furthermore, laser action only occurs at pressures such

that with Helium, the $3p^1D - 3s^1P$ transitions were lasing during the current pulse. The resonance trapping of the Carbon $3s^3P$ levels is too large at these pressures for laser action to occur during the afterglow on the $3p^3D - 3s^3P$ transitions with either Helium or Neon.

It will be noted that the excess energy of the Neon metastables over the CO dissociation energy is less than the energy of the Carbon $3s^{1,3}P$ levels. It is therefore possible by energy considerations for these levels to be excited also by a collision between a Neon metastable and a vibrationally excited CO molecule. However, only np levels in Carbon are observed to have the slower decay rate. Excitation of the molecule to repulsive potential states will only be significant if these states have quantum numbers related to the ground state by the selection rules for electric dipole transitions. The states of the atoms in which these repulsive potential states terminate will be determined by the molecular states, and in particular the electron orbitals. It is therefore not unreasonable to suppose that the repulsive states which are excited should preferentially dissociate into an Oxygen atom and a Carbon atom with an excited p electron.

Additional verification for these conclusions may be obtained by considering the following. The Carbon 3p level is populated by collisions between a Neon metastable and a CO molecule, so that the decay rate of the level is the same as the decay rate for the metastables. The Carbon 3s P level is populated by recombination between a Carbon ground state ion and an electron, so that the decay rate of this level is the same as the decay rate of the ions. The Carbon ion $3p^2P$ levels are populated by collisions between a Carbon ground state ion and a Neon metastable, so that the decay rate for these levels is given by the sum of the decay rates for the ions and the metastables. Thus

$$\frac{1}{\tau_3} = \frac{1}{\tau_1} + \frac{1}{\tau_2}$$

where τ_1 is the time constant of the metastable decay, τ_2 is the time constant of the ion decay and τ_3 is the time constant of the Carbon $3s^2P_{3/2}$ level. From Figs. 7.5, 7.6 and 7.8 we have

τ_1 = 14.1 μsec. (early afterglow)
and 19.5 μsec. (late afterglow)
τ_2 = 6.6 μsec.
τ_3 = 4.5 μsec. (early afterglow)
and 4.9 μsec. (late afterglow)

The values of τ_3 calculated from the equation agree exactly with the measured values.

References

7.1 G. F. Sauter, R. A. Gerber & H. J. Oskam — Physica 32, 1921 (1966)

7.2 T. R. Connor & M. A. Biondi — Phys. Rev. 140, A778 (1965)

7.3 V. I. Odintsov — Optics and Spectroscopy 18, 205 (1965)

Fig 7.1

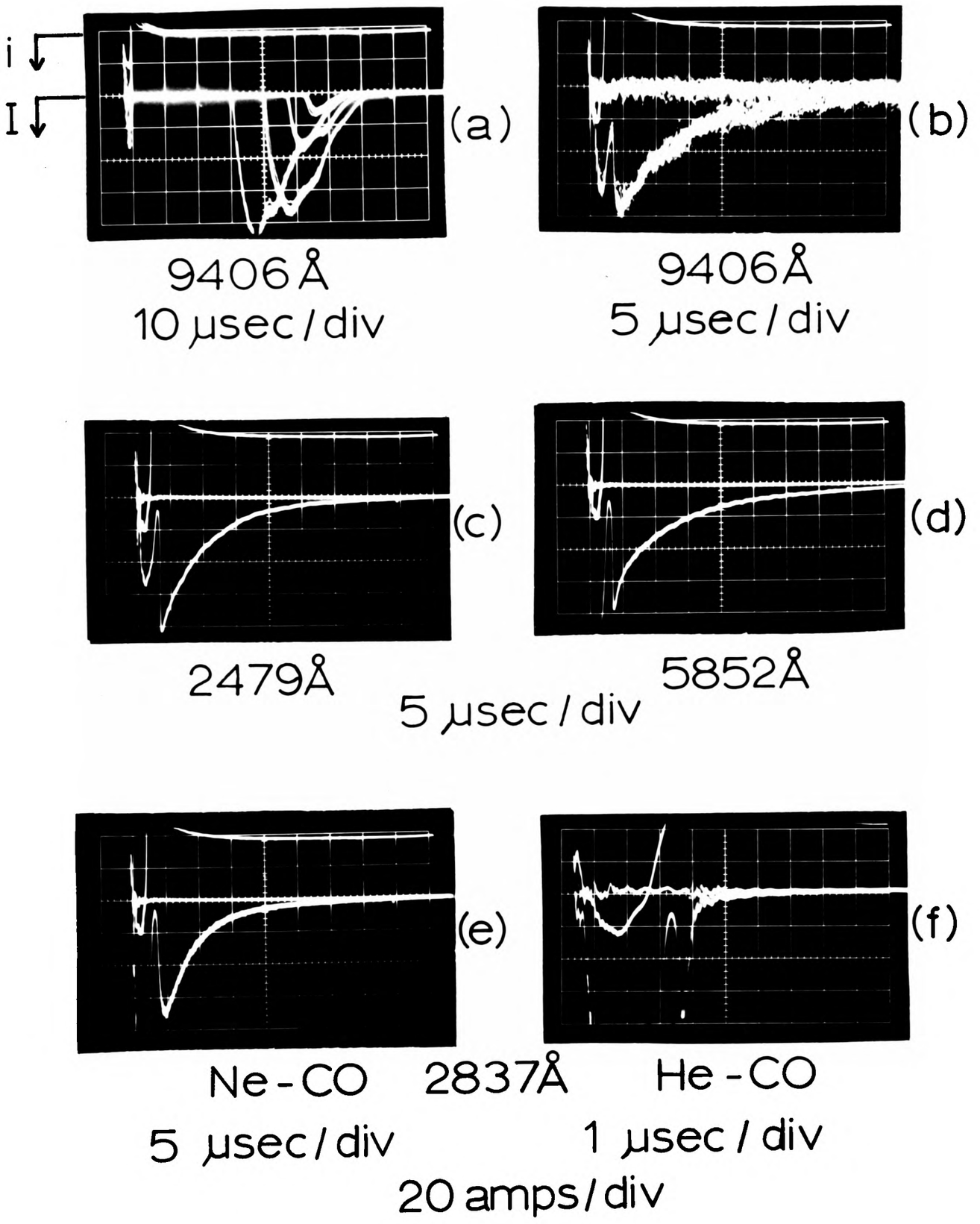
i
I
(a)
(b)
9406 Å
10 μsec / div
9406 Å
5 μsec / div
(c)
(d)
2479Å
5852Å
5 μsec / div
(e)
(f)
Ne - CO
2837Å
He - CO
5 μsec / div
1 μsec / div
20 amps / div

Fig 7·1

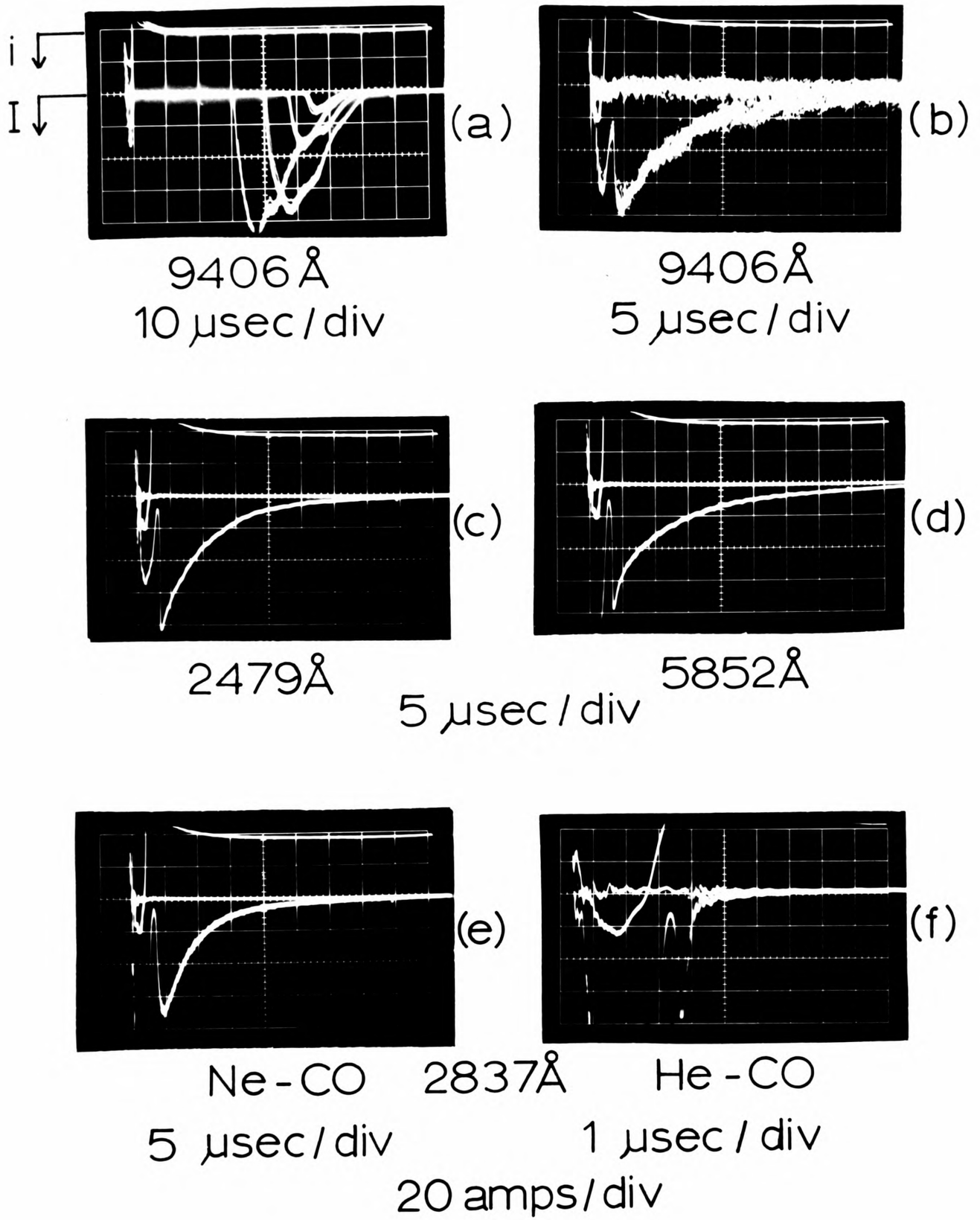
i
I
(a)
9406 Å
10 μsec / div
(b)
9406 Å
5 μsec / div
(c)
2479 Å
(d)
5852 Å
5 μsec / div
(e)
Ne - CO
2837 Å
(f)
He - CO
5 μsec / div
1 μsec / div
20 amps / div

Fig 7.2

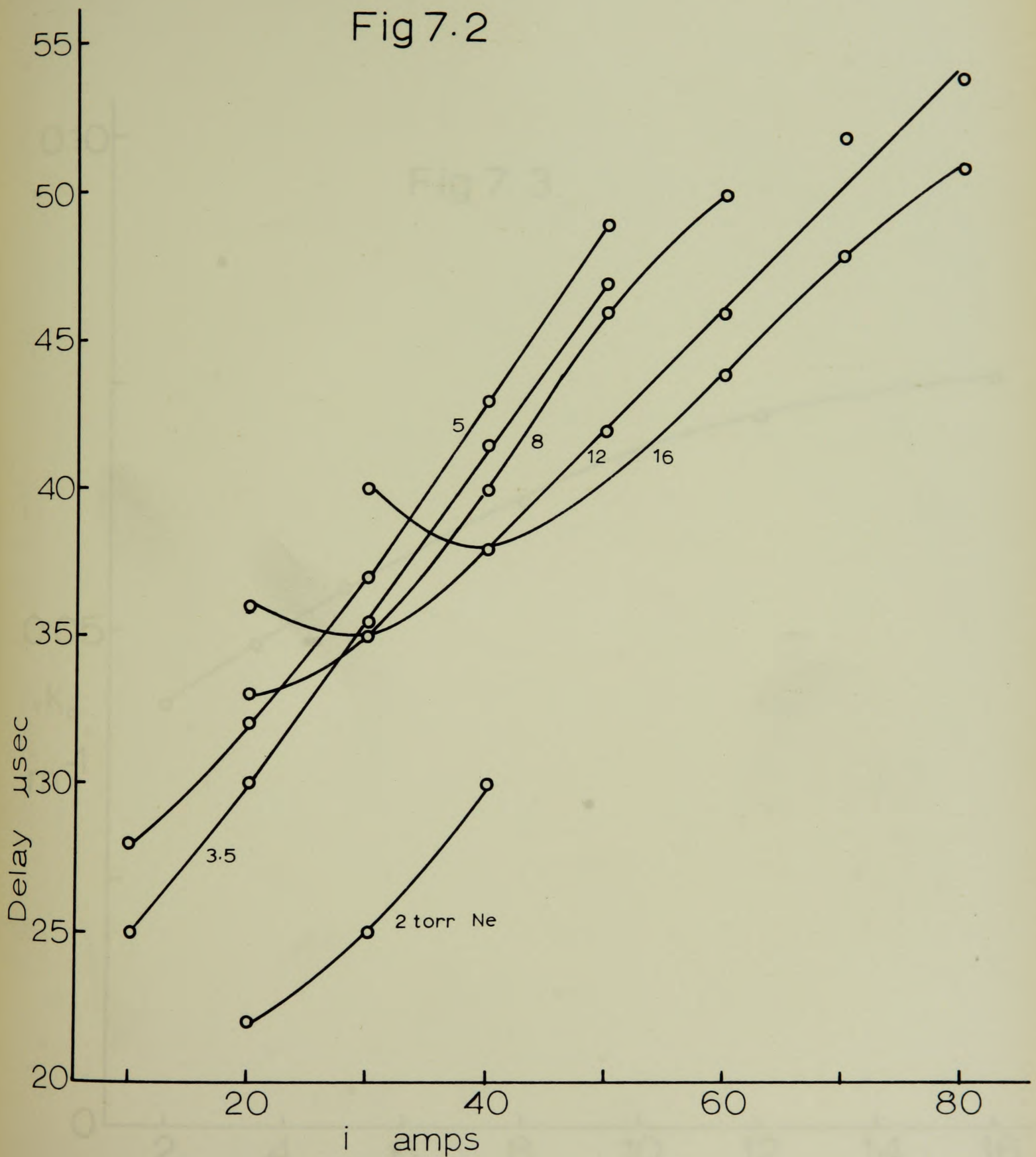
55
50
45
40
35
30
25
20
Delay μsec
20
40
60
80
i amps
5
8
12
16
3.5
2 torr Ne

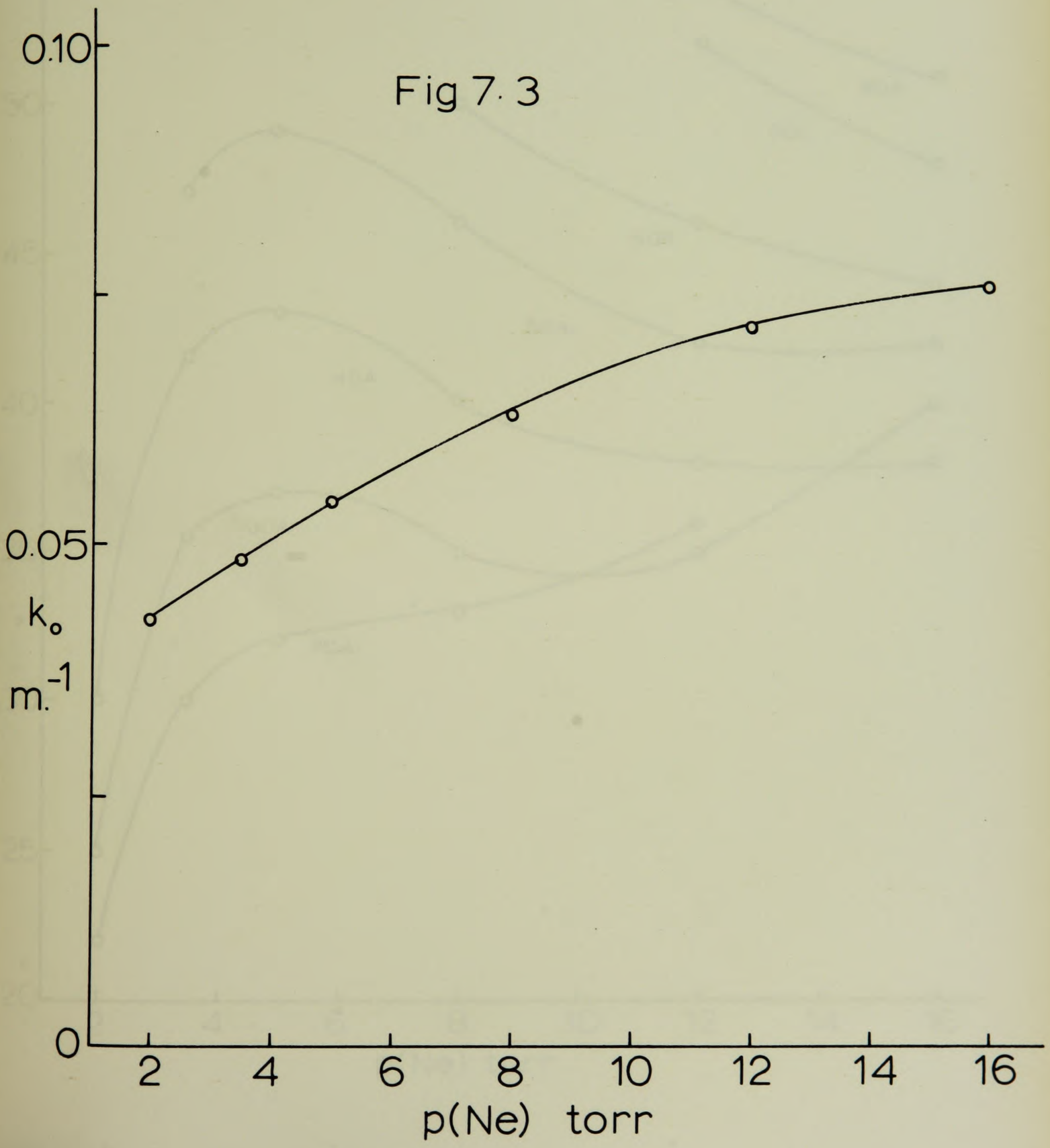

Fig 7.3

Fig 7.4

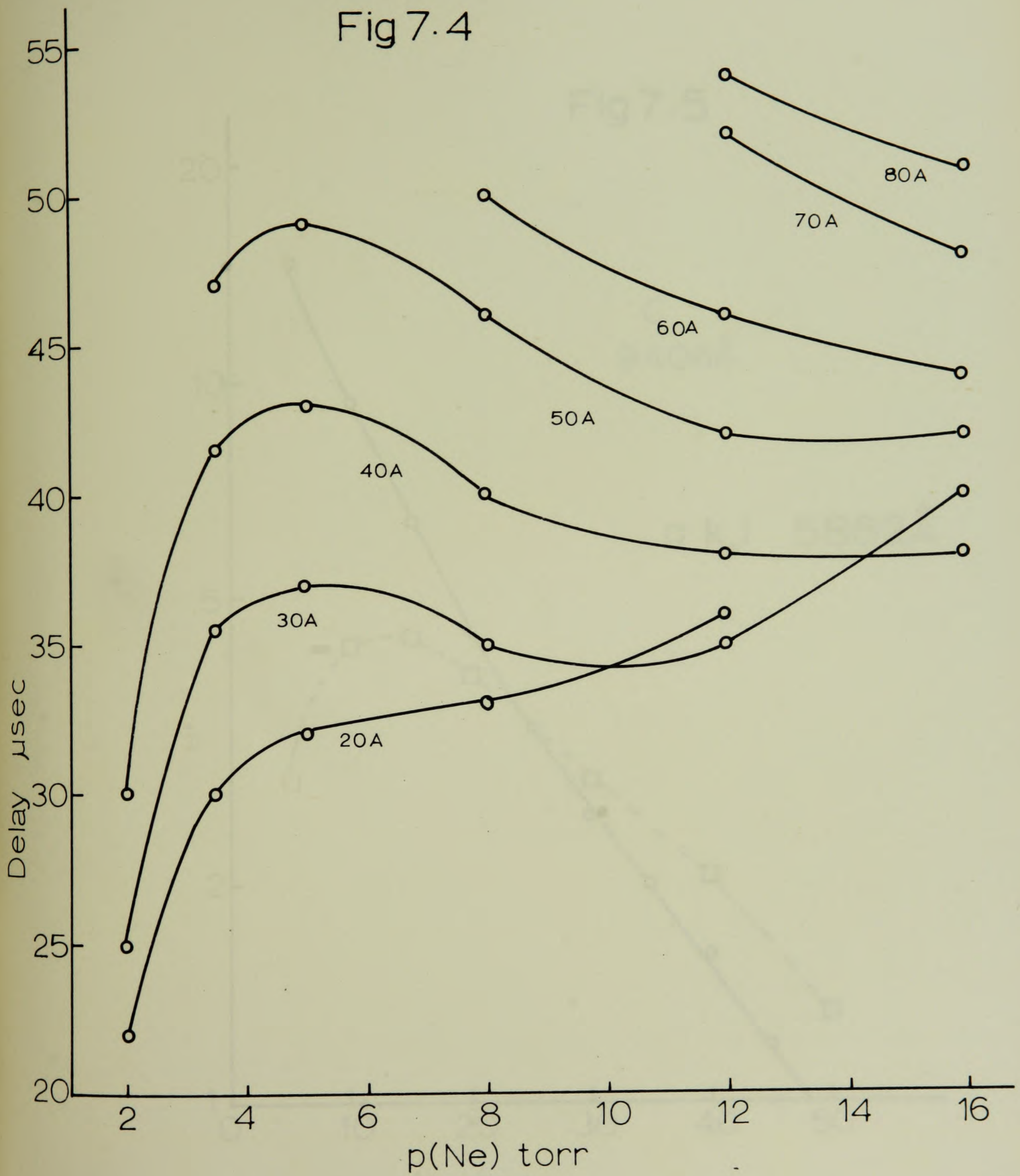
55
50
45
40
35
30
25
20
Delay μsec
2
4
6
8
10
12
14
16
p(Ne) torr
80A
70A
60A
50A
40A
30A
20A

Fig 7.5

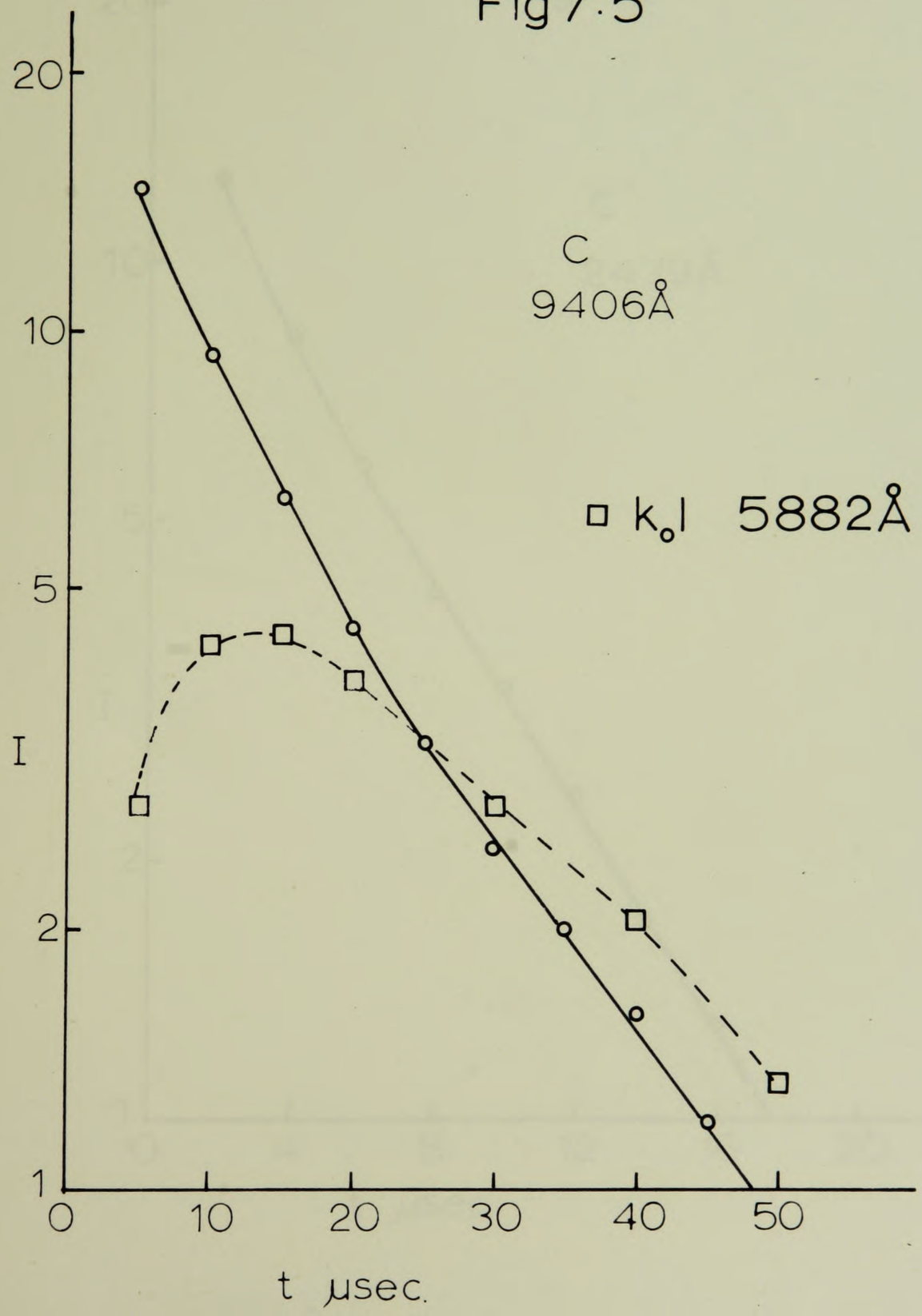

Fig7.6

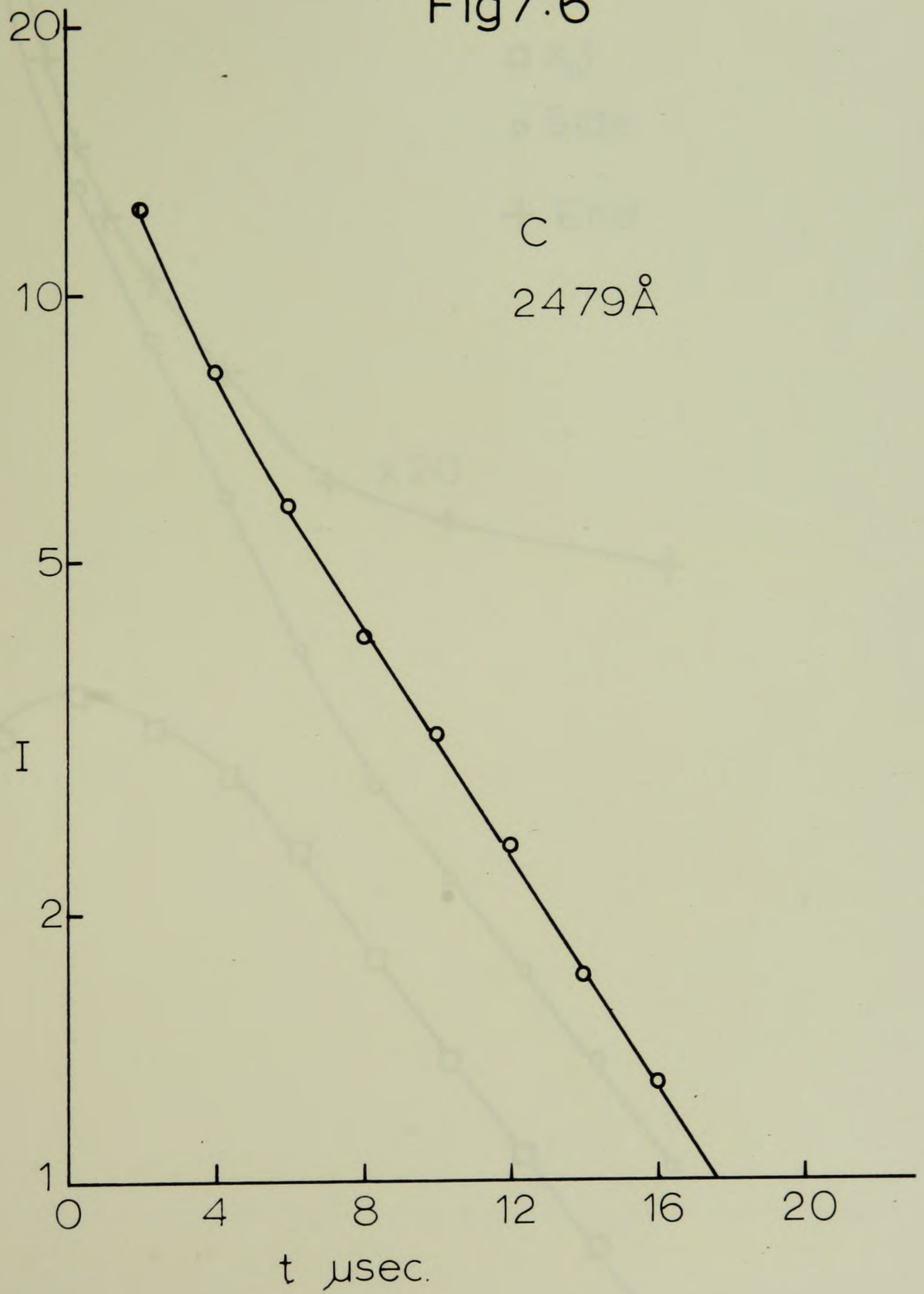

Fig 7.7

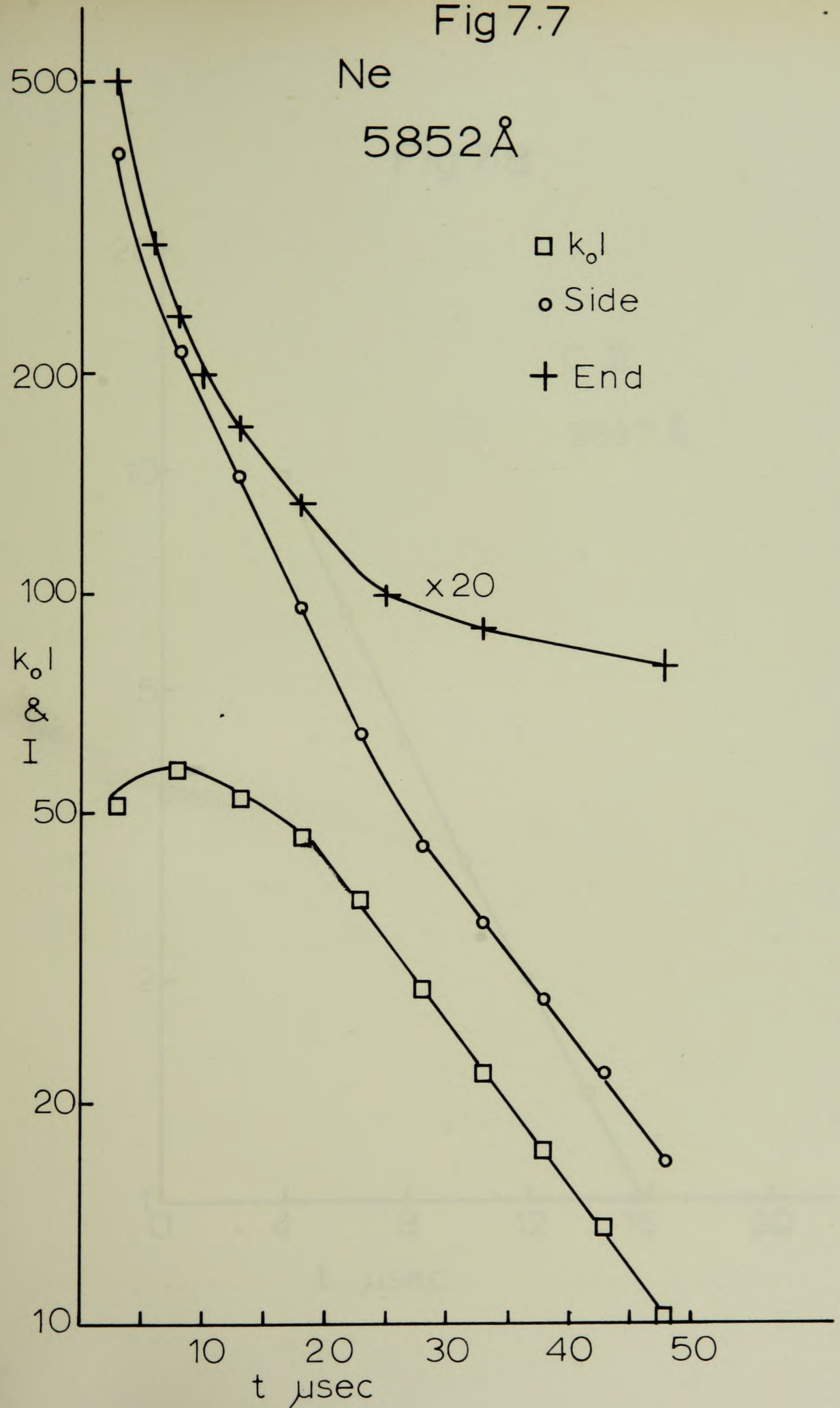
Ne
5852 Å
$k_o I$
Side
End
x 20
500
200
100
50
20
10
$k_o I$ & I
10
20
30
40
50
t μsec

Fig 7.8

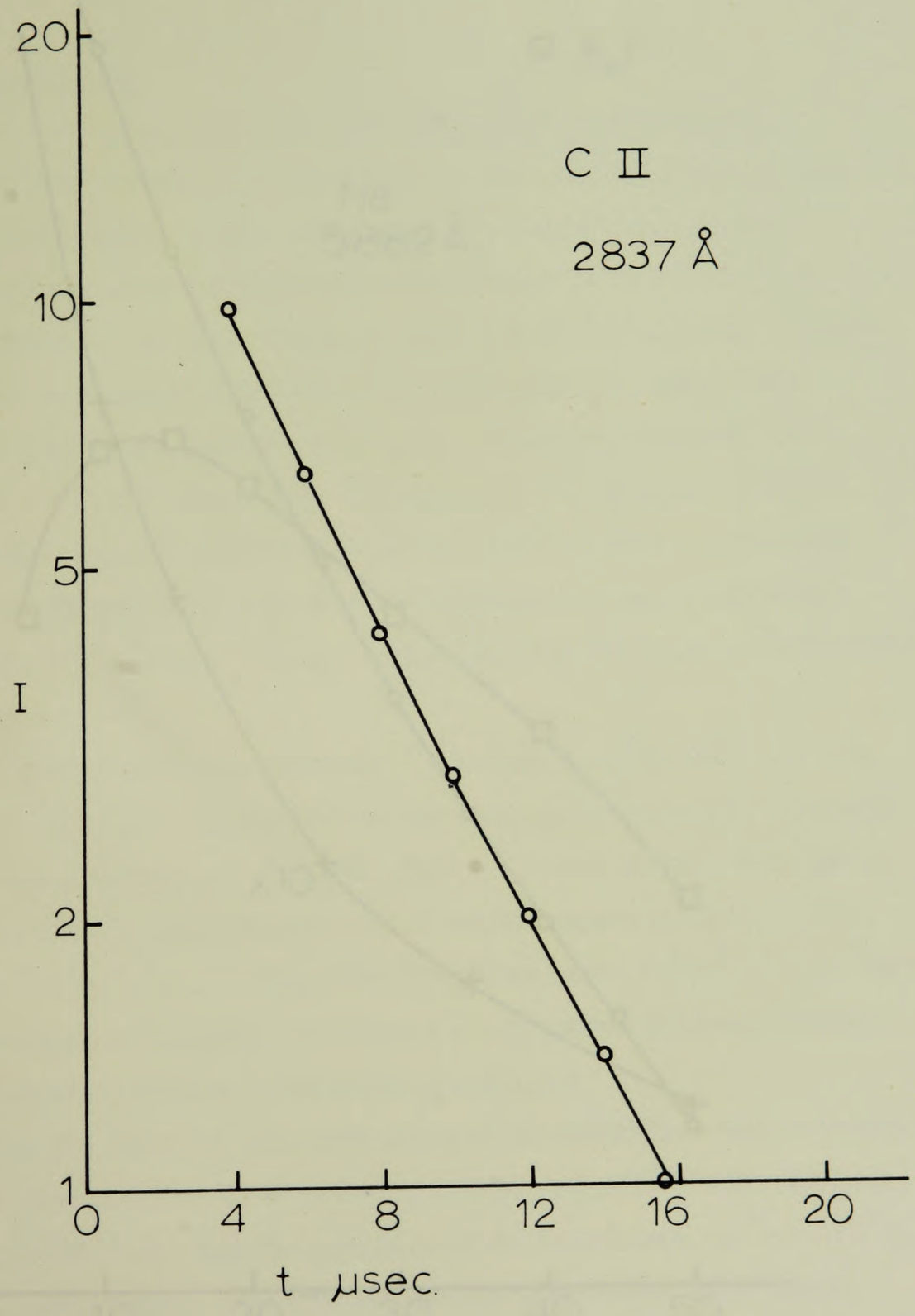

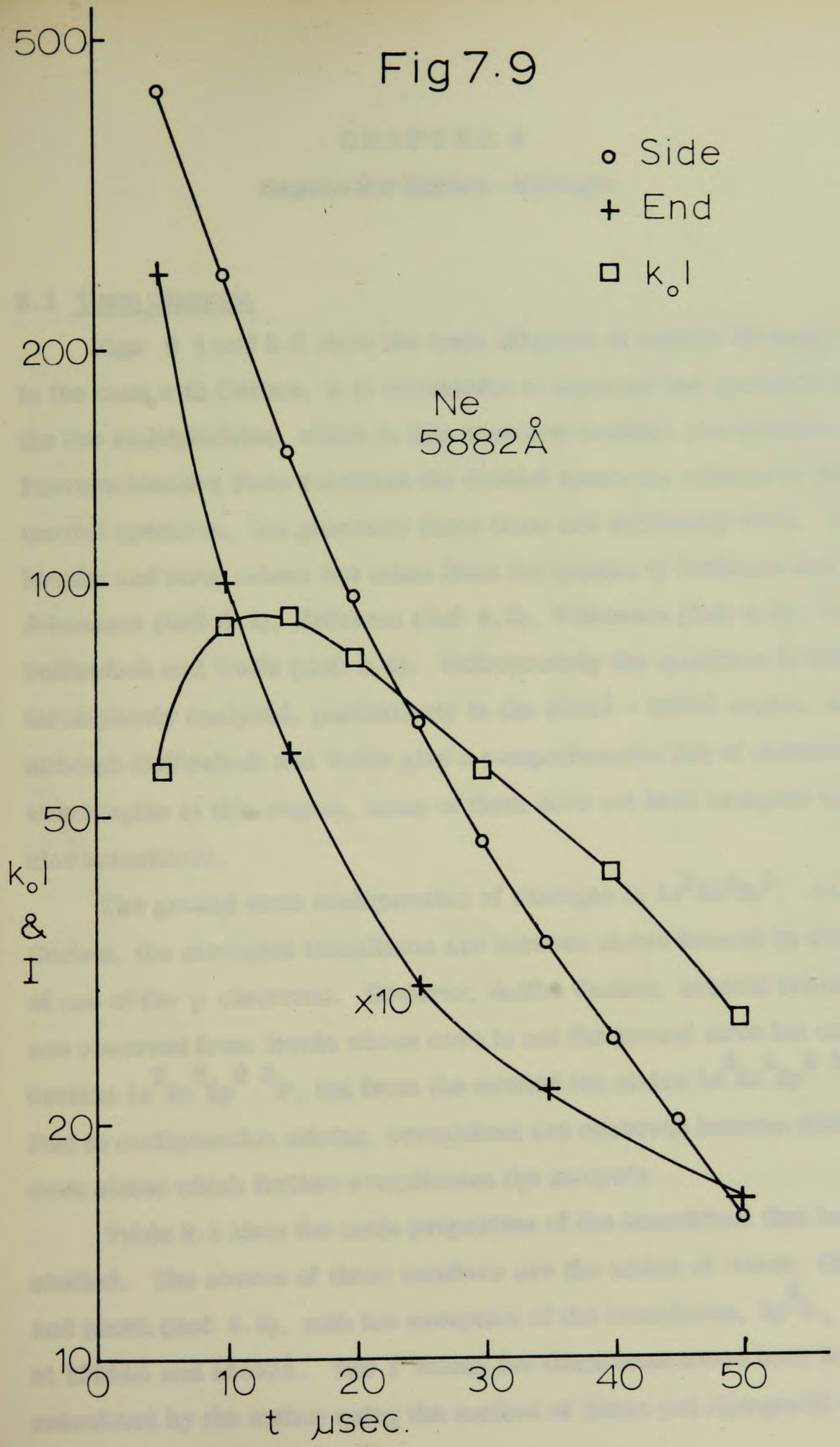
Fig 7.9
Side
End
$k_o l$
Ne
5882Å
500
200
100
50
20
10
$k_o l$
&
I
x10
0
10
20
30
40
50
t μsec.

CHAPTER 8

Results for Helium - Nitrogen

8.1 Term diagram

Figs 8.1 and 8.2 show the term diagram of neutral Nitrogen. As is the case with Carbon, it is convenient to separate the spectrum into the two multiplicities, which in this case are doublets and quartets. Intercombination lines establish the doublet spectrum relative to the quartet spectrum, but generally these lines are extremely weak. Wavelengths and term values are taken from the papers of Eriksson and Johansson (Ref. 8.1), Eriksson (Ref. 8.2), Wilkinson (Ref. 8.3), and Duffendack and Wolfe (Ref. 8.4). Unfortunately the spectrum is very incompletely analysed, particularly in the 4000Å - 5500Å region, and although Duffendack and Wolfe give a comprehensive list of observed wavelengths in this region, many of them have not been assigned to particular transitions.

The ground state configuration of Nitrogen is $1s^2 2s^2 2p^3$. As with Carbon, the strongest transitions are between states formed by excitation of one of the p electrons. However, unlike Carbon, several transitions are observed from levels whose core is not the ground state ion configuration $1s^2 2s^2 2p^2\ ^3P$, but from the excited ion states $1s^2 2s^2 2p^2\ ^1D$, ^1S. Due to configuration mixing, transitions are observed between different core states which further complicates the analysis.

Table 8.1 lists the main properties of the transitions that have been studied. The source of these numbers are the tables of Wiese, Glennon and Smith (Ref. 6.5), with the exception of the transitions, $3p^2S_{1/2} - 3s^2P_{3/2,1/2}$ at 13581Å and 13430Å. The f values for these transitions have been calculated by the author using the method of Bates and Damgaard (Ref. 6.6).

Table 8.1

λ Å	Upper Level	Lower Level	$\Delta\nu_D$ Mc/s	$\Delta\nu_N$ Mc/s	A x 10^8 sec^{-1}	f
1492.6	$3s^2P_{3/2}$	$2p^2D_{5/2}$	6660	128	5.3	0.12
1494.7	$3s^2P_{1/2}$	$2p^2D_{3/2}$	"	112	5.0	0.084
1742.7	$3s^2P_{3/2}$	$2p^2P_{3/2}$	5710	128	1.8	0.082
1745.2	$3s^2P_{1/2}$	$2p^2P_{1/2}$	"	112	1.3	0.059
9392.8	$3p^2D_{5/2}$	$3s^2P_{3/2}$	1060	131	0.218	0.432
9386.8	$3p^2D_{3/2}$	$3s^2P_{1/2}$	"	115	0.183	0.482
9460.7	$3p^2D_{3/2}$	$3s^2P_{3/2}$	1050	131	0.0334	0.0449
8629.2	$3p^2P_{3/2}$	$3s^2P_{3/2}$	1150	132	0.238	0.266
8590.0	$3p^2P_{1/2}$	$3s^2P_{1/2}$	1160	117	0.19	0.210
13581.3	$3p^2S_{1/2}$	$3s^2P_{3/2}$	733	129	0.0486	0.0671
13429.6	$3p^2S_{1/2}$	$3s^2P_{1/2}$	740	112	0.0251	0.0678
4935.0	$4p^2S_{1/2}$	$3s^2P_{3/2}$	2020	128	0.0158	0.0029
1199.5	$3s^4P_{5/2}$	$2p^4S_{3/2}$	8280	87	5.5	0.18
8680.3	$3p^4D_{7/2}$	$3s^4P_{5/2}$	1145	90	0.191	0.287

The natural width of all the 3p - 3s transitions is dominated by the lifetime of the 3s levels. The Doppler width of all these transitions is larger than the natural width, and the latter has been neglected in the calculations of gain and absorption from the populations of the levels.

8.2 Laser Lines - Results

Oscillation has been observed on the transitions listed in Table 8.2.

Table 8.2

λ Å	Upper Level	Lower Level	Comments
13581.33	$3p^2S_{1/2}$	$3s^2P_{3/2}$	Strong
9392.79	$3p^2D_{5/2}$	$3s^2P_{3/2}$	Strong
9386.81	$3p^2D_{3/2}$	$3s^2P_{1/2}$	Strong
8629.24	$3p^2P_{3/2}$	$3s^2P_{3/2}$	Moderate

C.W. oscillation at 13581Å has been reported by Patel, McFarlane and Faust (Refs: 6.7 and 6.8). C.W. oscillation at 9393Å and 9387Å has been reported by Shimazu and Suzaki (Ref: 6.10). Pulsed oscillation at all these wavelengths was reported by McFarlane (Ref: 8.5).

The behaviour of all these lines was similar in that they would oscillate only in the afterglow of the current pulse. The Nitrogen partial pressure was between 1mtorr and 0.5torr, with Helium at a partial pressure of up to 20torr. The measurement of the Nitrogen partial pressure was again complicated by Nitrogen being driven into the walls of the discharge tube, but the problem was not so severe as it was with Carbon Monoxide.

Figs. 8.3(a) and (b) show typical oscilloscope traces of the laser outputs at the different wavelengths. All were taken at the same current and pressures. The 9387Å line starts to oscillate before the 9393Å line, even though the latter has the larger gain. This will be discussed later. The laser output at 9393Å and 9387Å is shown in Figs. 8.3(c) and (d) at different currents. The similarity between these traces and the traces for

the Carbon transitions in Chapters 6 and 7 is immediately apparent.

Fig. 8.5 is a graph of the delay of the 9393Å laser output relative to the end of the current pulse as a function of current for different values of Helium pressure. The Nitrogen partial pressure was kept constant at 50mtorr. The 9387Å laser output delay is shown for only one Helium pressure for clarity, but the behaviour is fairly typical. Fig. 8.6 is a plot of the delay of the start of the 9393Å laser output as a function of Helium pressure for different values of current, the Nitrogen pressure again being 50mtorr. Fig. 8.7 shows the peak gain of both the 9393Å and 9387Å lines as a function of Helium pressure, the Nitrogen pressure again being 50mtorr. At each pressure, the current was adjusted to produce the maximum gain, the gain being measured in the usual way by inserting filters into the cavity until oscillation ceased.

Fig. 8.8 is a plot of the gain and output of the 9393Å laser transition as a function of time. The gain was once more measured by inserting filters into the cavity and noting the time at which the laser output commenced and terminated. The circles are the experimental points and the full line is a theoretical curve from the equation

$$k_o l(t) \propto g_1 N_2 (t=0) \exp(-t/\tau_2) - g_2 N_1 (t=0) \exp(-t/\tau_1)$$

with $g_1 N_2 (t=0) = g_2 N_1 (t=0)$. τ_2 was measured from the spontaneous emission of the upper level and found to be 10μsec. The transitions from the lower level cannot be observed so the lifetime for decay (τ_1) was obtained in the following way. From the expression above, the time at which $k_o l$ has its peak value is given by

$$t_m = \tau_1 \tau_2 / (\tau_2 - \tau_1) \log_e (\tau_2/\tau_1)$$

Experimentally, t_m = 8μsec and together with the value for τ_2 gives τ_1 = 6.67μsec. The theoretical curve has therefore been fitted to the experimental points at t = 0 and t = t_m. The agreement is good except at very late times. This is to be expected since the theoretical gain does not take into account stimulated emission. This will depopulate the upper level thus reducing the gain.

During the period when the gain is increasing, the experimental points should agree with the theory, since the method by which they are measured prevents stimulated emission until a later time. This follows from the method used, as each point refers to the commencement of laser action with a known loss in the cavity. This not the case when the gain is decreasing, and it is clear that stimulated emission has a larger effect on the gain at later times. Thus the measured curve lies between the curves that would be obtained in the complete absence of stimulated emission and when stimulated emission is not prevented.

It must be noted that the peak of the gain curve occurs at a later time than the peak of the laser output. Successive insertion of filters moved the peak of the laser output to later times. The largest effect was obtained with the first filter, the following filters shifting the peak far less, even though the absorption of all the filters was identical. The reason for this is that because of stimulated emission and the resulting reduction of gain described above, the gain when the transition is lasing will peak earlier than the gain when the transition is not lasing. This phenomenon is known as gain saturation. The effect of stimulated emission on the upper level population can in theory be observed by changes in the spontaneous side-light from the 9393Å transition. However, because the population difference is much less than the populations of the upper and lower levels, no change in the spontaneous side-light could be seen when laser action was interrupted.

Attempts to explain the different starting times for the 9393Å and 9387Å laser outputs were made more difficult by the inability of the Czerny-Turner spectrograph to resolve the side-light from these transitions. By noting when laser action commenced, it was possible to measure the relative spontaneous emission of the two transitions using the Ebert spectrograph, which could be used only for observing the end-light. At the time when laser action at 9387Å commences, the small gain on it and the small self-absorption at 9393Å will contribute a negligible correction factor to the relative spontaneous emission. Whereas the ratio of intensities should be 1.8 on the basis of L-S coupling, the measured ratio appeared to be approximately 1.6. Hence, the population of the $3p^2D_{3/2}$ level, relative to the $3p^2D_{5/2}$ level, is larger than the statistical weight factor. However, neither the relative intensities nor the time constants of decay of the lower levels could be measured. With the population difference being much less than the populations, the populations of the lower levels also cannot follow the statistical weights, and it seems more probable that a small difference in the decay rates of the lower levels causes the 9393Å laser to start later.

The other two laser transitions were not studied in great detail. The 8629Å line lased only under optimum pressure conditions for the 9393Å laser transition. Even then, the gain was less than 0.06 per metre. The 13581Å line would also lase only over a smaller range of pressures and currents than the 9393Å line, but this was due to the use of dielectric mirrors with a reflectivity of only 42% at this wavelength. Use of a gold-coated stainless steel mirror enabled measurements to be made over a wider range of pressures. Unfortunately, the response of the S-1 photocathode in the RCA 7102 photomultiplier is very small at this wavelength, so that spontaneous emission measurements could not be made. The InSb

photoconductive cell also proved to be too insensitive to observe the spontaneous emission. However, the following general properties of the laser output at 13581Å were noted.

First, the output power as a function of time was similar to that at 9393Å and 9387Å. Secondly, the delay after the current pulse before the laser action commenced was less than for the 9387Å output. Finally, the gain of this transition when it could be observed was always greater than the gain at 9393Å. Since the threshold gain for laser action is 0.13/ metre, with the one low reflectivity mirror, the range over which it would oscillate is obviously seriously restricted.

Even though the f value for the transition is lower than that for the 9393Å, 9387Å, and 8629Å transitions, a calculation shows that the population of the upper level is of the same order as the upper levels of the other transitions. Since the population difference is much less than the populations, a very small increase in relative populations of the upper levels will lead to large differences in gain. This also explains the small gain of the 8629Å, and the fact that the delay of the laser output is larger than any of the other lines.

Figs. 8.1(d) and (e), and 8.2 show typical oscilloscope pictures of the spontaneous emission of the 9393Å and 9387Å lines (unresolved) and the 8680Å line of Nitrogen, and the 3888Å and 5876Å lines of Helium. On all these photos, both the end-light and side-light are shown and the time-varying self-absorption can be clearly seen. The intensity scales for the side and end light are the same for a line which is not absorbed.

As has been mentioned previously, the transitions from the Nitrogen 3s levels to the ground state configuration could not be observed, since the longest wavelength from these levels is 1745Å, requiring the use of a vacuum spectrometer and special windows for the laser tube. Despite the inability to resolve many of the lines in the 3p - 3s transitions with

the Czerny-Turner spectrograph, the populations of the 3s levels can be inferred from the ratio of side-light to end-light from the 3p - 3s transitions.

Comparison of Figs. 8.3 to 8.8 with the equivalent ones in Chapters 6 and 7 show that the 9393Å and 9387Å laser output as a function of current and pressure is generally similar to the 9406Å laser output in Carbon. In addition, the spontaneous emission of the upper laser level is similar for the C and N transitions, and a comparison of the end light of the laser transition shows that the lower laser levels also behave in the same general way. The time constants of the lines are of course not exactly the same for Carbon and Nitrogen, but this is only to be expected. The theory derived for the delay of the start of laser action as a function of current in Chapter 6 is applicable here with similar limitations. The discharge was clearly not homogeneous at high currents with the Helium migrating to the live electrode which is negative, due to the higher mobility of the Helium ions. The effects were not so severe as with the He-CO mixture, and provided the discharge was run only for a short time when the data was being taken and then switched off for a period to allow the gases to interdiffuse again, the effects could be considerably reduced.

8.3 Excitation Mechanisms

Chapters 5, 6, and 7 have discussed excitation mechanisms both in general and in particular. The similarities in the laser behaviour and spontaneous emission between the He - CO and He - N mixtures suggests strongly that the mechanisms may be the same. The populations of the excited Helium levels in the afterglow are therefore due to recombination of He^+, the process being

$$He^+ + e + e \rightarrow He^* + e \rightarrow He + e + h\nu$$

The changes in the time constant of decay of the Helium lines with Nitrogen pressure and also the changes in the peak intensities of the lines are largely due to the effects of the Nitrogen during the current pulse. In particular, the lower ionisation potential of Nitrogen will tend to lower the electron temperature and the relative numbers of N_2^+, N^+ and He^+ ions, all of which determine the recombination rates. Figs 8.9 - 8.12 show the spontaneous emission of the 9393Å and 9387Å lines (unresolved) of Nitrogen, and the 3888Å, 5876Å and 5015Å lines of Helium. These were all taken with 5torr He and 50mtorr of N_2. The end light emission and calculated values of $k_o l$ are also shown for the Helium lines. These values are proportional to the populations of the 2^3S metastable level, the 2^3P level and the 2^1S metastable level of Helium. It can be seen that the population of the singlet metastable is much smaller than the other two levels since the factors converting $k_o l$ into populations are of the same order of magnitude. These values of $k_o l$ do not take into account the line shape of the absorbing transition. As was noted in Chapter 6, this will change the values of $k_o l$ and hence the population of the lower level by a constant factor.

It is very obvious from these figures that the decay rate for the Carbon $3p^2D$ levels is much less than the decay rate for the Helium levels. However, the decay rates for the $3p^2D$ Carbon levels and the Helium 2^3S metastable are identical to within the accuracy of the measurement. This is strong evidence that, as in the case of Carbon, the upper level for the laser transition is pumped by Helium metastables. Further evidence in favour of this comes from the fact that $k_o l$ and the upper laser level population are almost constant with respect to current, whereas the radiating Helium Level populations increase approximately linearly with current. However, from the term diagram for Nitrogen, it can be seen that the Helium 2^3S metastable does not have sufficient energy to dissociate and excite the

resulting Nitrogen atom in one collision. The dissociation energy of the Nitrogen molecule is known to be 9.76eV. (Ref: 6.15), and this was subtracted from the energy of the Helium levels. Only the 2^3P Helium level is shown in Figs. 8.1 and 8.2, the two metastable levels being at 81,126cm.$^{-1}$ (2^3S) and 87,547cm.$^{-1}$ (2^1S). The energy discrepancy can be overcome if the collision process is between a vibrationally excited ground electronic state Nitrogen molecule and a Helium 2^3S metastable. The lifetime for these vibrationally excited states is governed by collision processes, and is typically of the order of milliseconds. Hence, as far as the afterglow time constants observed for the atomic transitions are concerned, these populations are effectively constant.

If the Nitrogen molecule can be dissociated by collision with a metastable atom, it should also be dissociated by electron collision. Massey and Burhop (Ref: 4.1) quote an experiment by Hughes in which no dissociation was observed. The method used was to observe increases in pressure in a chamber containing Nitrogen when a monoenergetic electron beam was passed through the chamber. The sensitivity of the method was, however, rather low. In contradiction to this experiment, there are two experiments in favour of dissociation by electrons. In the first one, Turner and Samson (Ref: 8.6) observed atomic transitions from the 3p levels of atomic Nitrogen when a monoenergetic electron beam was passed through Nitrogen. They measured a minimum electron energy of 23±1 eV, for the excitation of the $3p^4P$ level. This is to be compared with 21.6eV which is the sum of the dissociation energy for Nitrogen and the excitation energy for the $3p^4P$ level. They also noted that a higher electron energy was needed to excite the $4p^2S$ level, although the threshold for this was more difficult to measure.

A more recent experiment in favour of electron dissociation has been performed by Winters (Ref: 8.7). This was also an indirect experiment, as it consisted of measurement of adsorption of Nitrogen excited by a monoenergetic electron beam. Evidence is produced to show that this adsorption is caused by formation of Nitrogen atoms by dissociation, and cross-sections for dissociation as a function of electron energy are given. At 20eV, the cross section is 5×10^{-17}cm.^{2} rising to a peak value of 2×10^{-16}cm.^{2} at 90eV.

Spontaneous emission measurements showed that all the 3p levels of Nitrogen had the same time dependence, indicating a common excitation mechanism. All these levels will therefore be excited by a collision between a Helium 2^3S metastable and a vibrationally excited Nitrogen molecule producing a ground state Nitrogen atom and a Nitrogen atom in a 3p level, and a ground state Helium atom. The fact that vibrationally excited Nitrogen molecules are needed to produce any excited 3p levels also explains the failure to observe laser action during the current pulse risetime.

Examination of Figs. 8.2(a) and (b) which are typical of the quartet transitions, also explains the absence of laser action on these transitions. From the comparison of end-light to side-light, it can be seen that the lower level of the transition ($3s^4P$) decays more slowly than the corresponding doublet levels ($3s^2P$). This is almost certainly due to resonance trapping on the 1200Å transition between the $3s^4P$ level and the Nitrogen atom ground state ($2p^4S$). This phenomenon is the same as was observed for the 3s triplet levels in Carbon.

Failure to observe laser action on the 4935Å ($4p^2S - 3s^2P$) transition is due to two causes. First, the f number for the transition

is 20 times smaller than the equivalent 3p - 3s transition, as can be seen from Table 8.1. Secondly, the population of the 4p levels is found experimentally to be considerably smaller than the 3p levels. On energy considerations, a more highly excited molecule is needed for the collision process, and the populations of the vibrational levels will follow a Maxwell-Boltzmann distribution with a temperature given by the excitation temperature during the current pulse.

The calculation of the cross-section of the dissociation and excitation process not only requires a knowledge of the metastable Helium population and the excitation rate of the upper levels, but also the temperature of the vibrational levels of the Nitrogen molecule ground state. On the basis of the same value for the cross-section, the temperature of the vibrational levels is equivalent to 2eV.

The CO and Nitrogen molecules are very similar in their properties, since the constituent atoms have almost the same atomic weights. The assumption of the same cross-section for collisional dissociation and excitation is therefore not unreasonable, while the vibrational temperature of 25,000 ^{o}K ($\approx$ 2eV) is a typical electron temperature in a gas discharge.

References

8.1	K. B. S. Eriksson & I. Johansson	Arkiv för Fysik 19, 235 (1961)
8.2	K. B. S. Eriksson	Arkiv för Fysik 13, 429 (1958)
8.3	P. G. Wilkinson	J. Opt. Soc. Am. 45, 862 (1955)
8.4	O. S. Duffendack & R. A. Wolfe	Phys. Rev. 34, 409 (1929)
8.5	R. A. McFarlane	Physics of Quantum Electronics Ed. Kelley, Lax & Tannenwald p 655 (1966)
8.6	L. A. Turner & E. W. Samson	Phys. Rev. 34, 743 (1929)
8.7	H. F. Winters	J. Chem. Phys. 44, 1472 (1966)

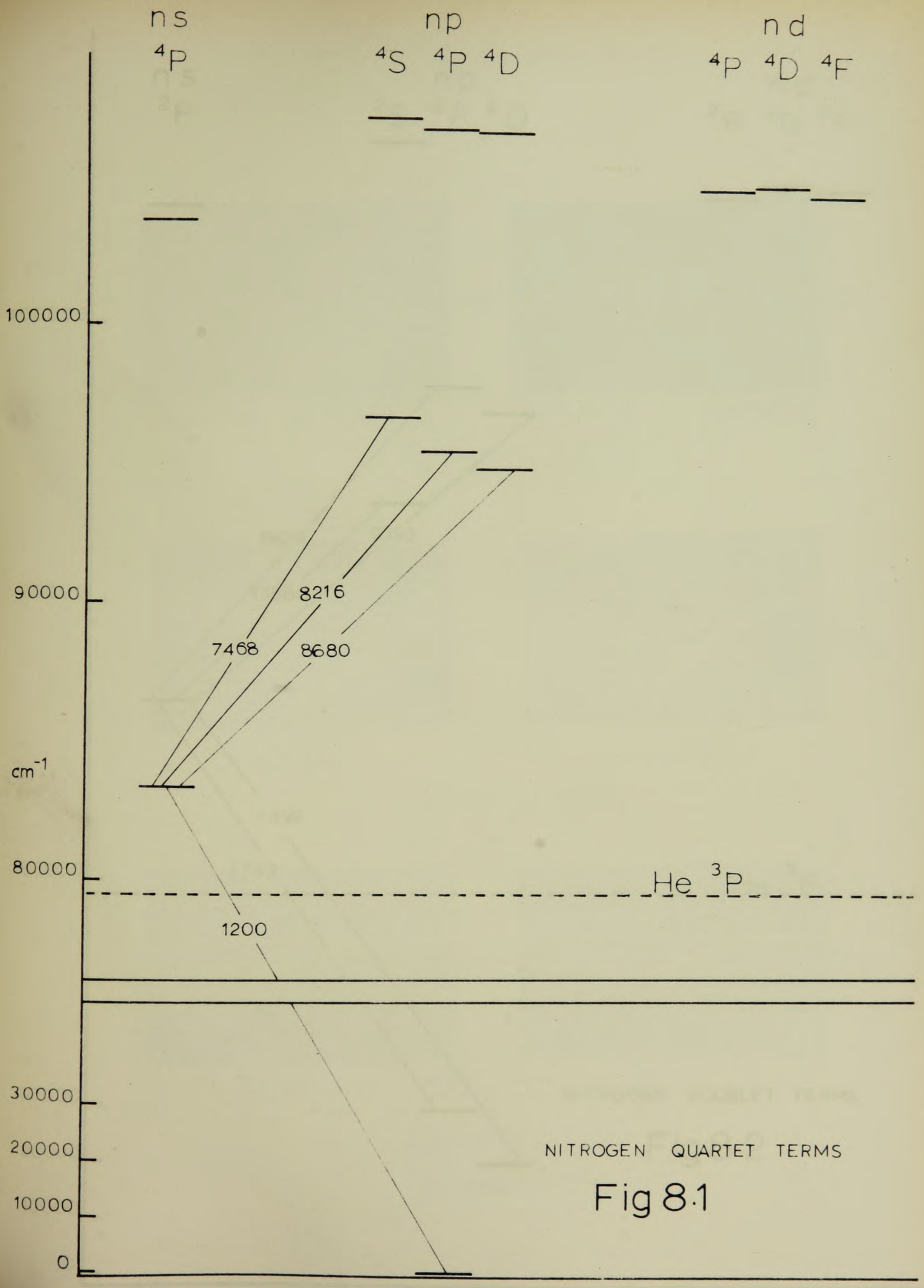

NITROGEN QUARTET TERMS

Fig 8.1

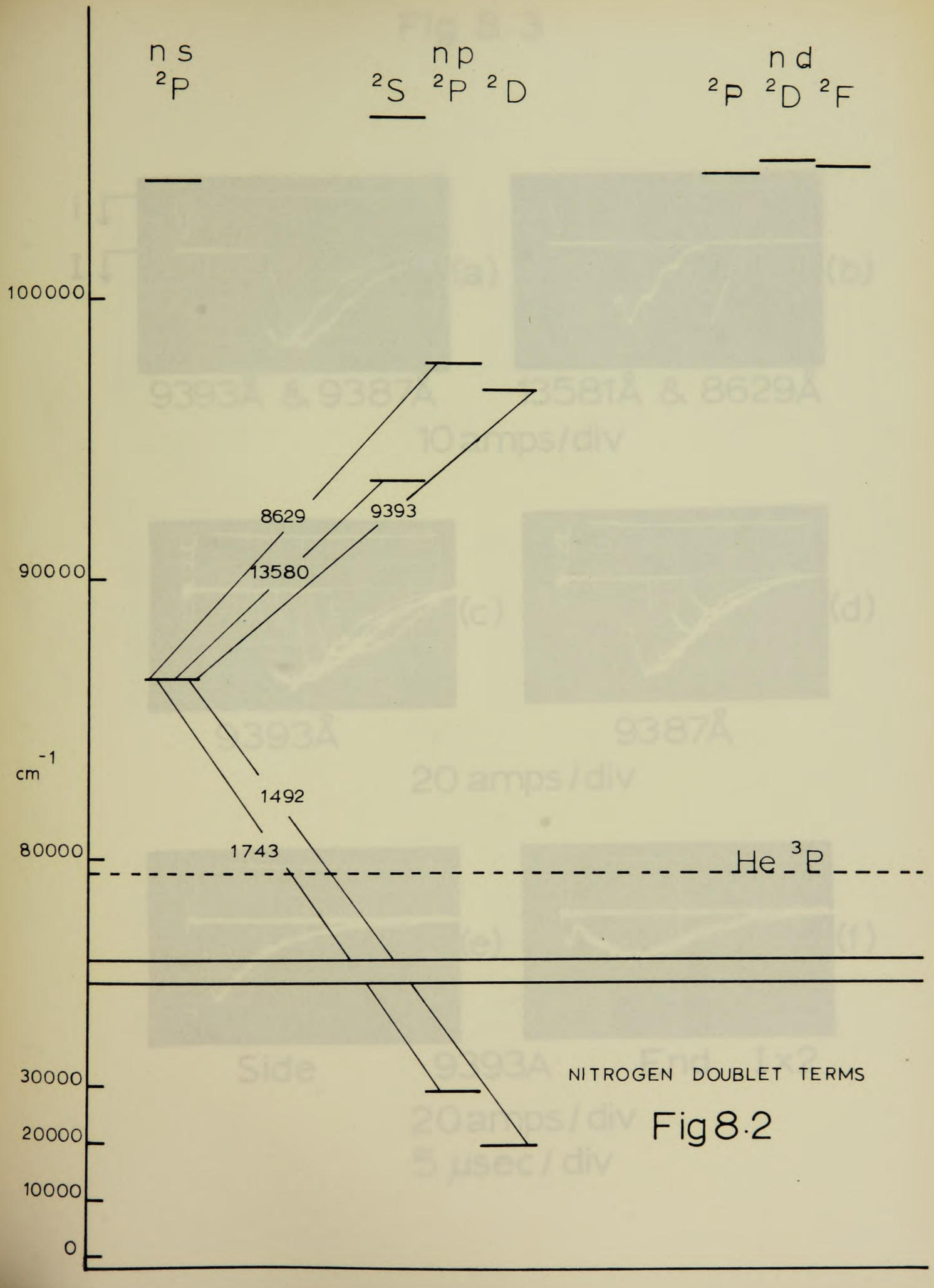

NITROGEN DOUBLET TERMS

Fig 8.2

Fig 8.3

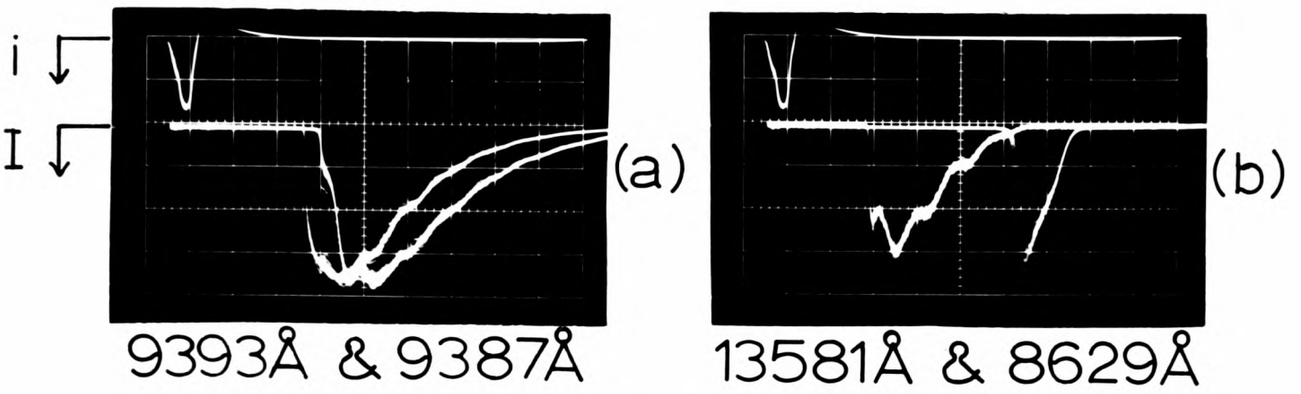

9393Å & 9387Å 13581Å & 8629Å

10 amps/div

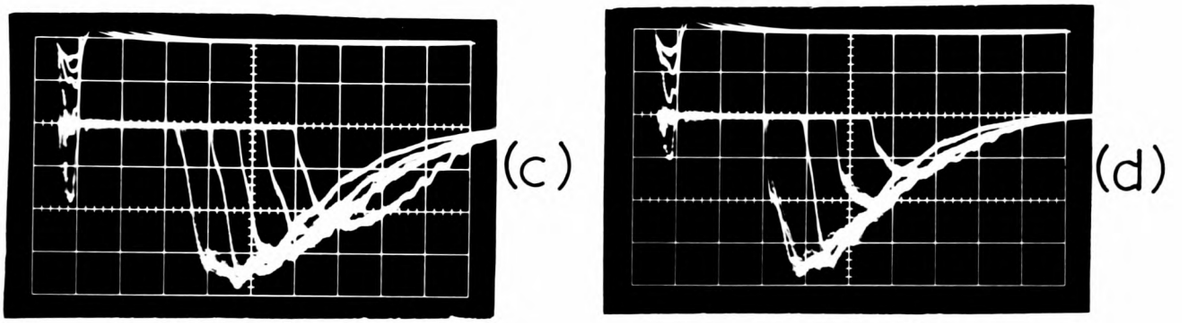

9393Å 9387Å

20 amps/div

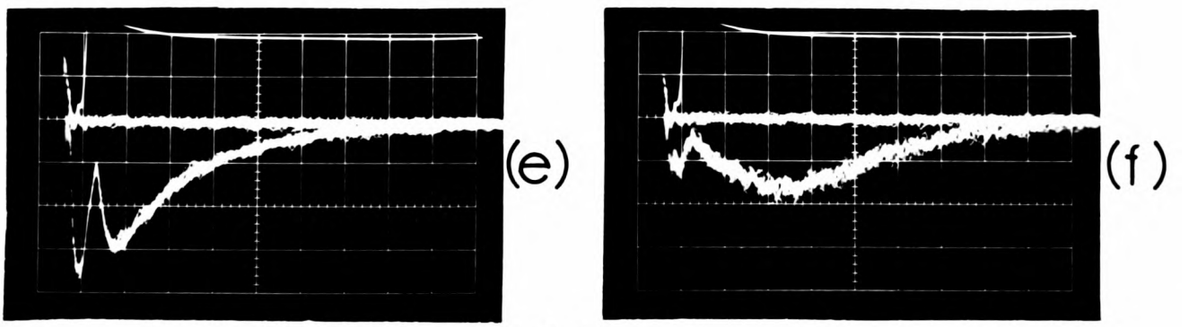

Side 9393A End Ix2

20 amps/div

5 μsec/div

Fig 8.4

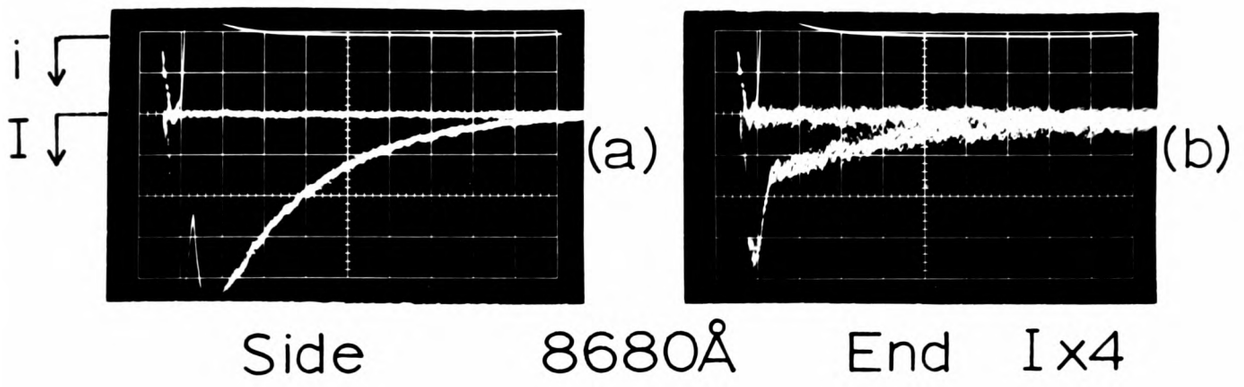

Side 8680Å End I x4

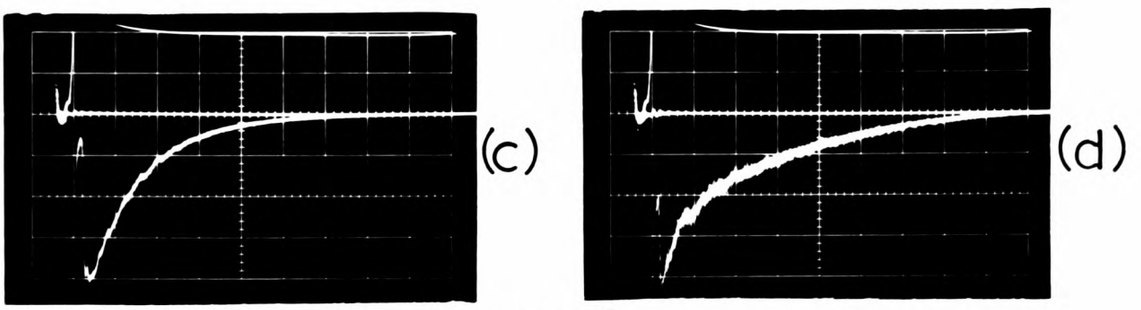

Side 3888Å End I x5

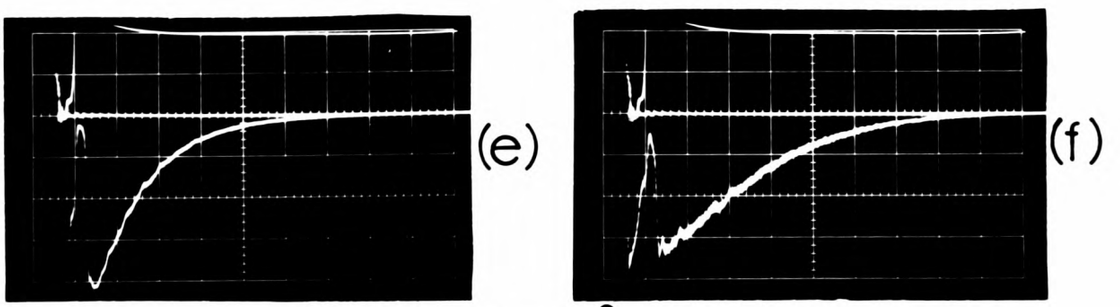

Side 5876Å End I x4

20 amps/div 5 μsec / div

Fig 8.5

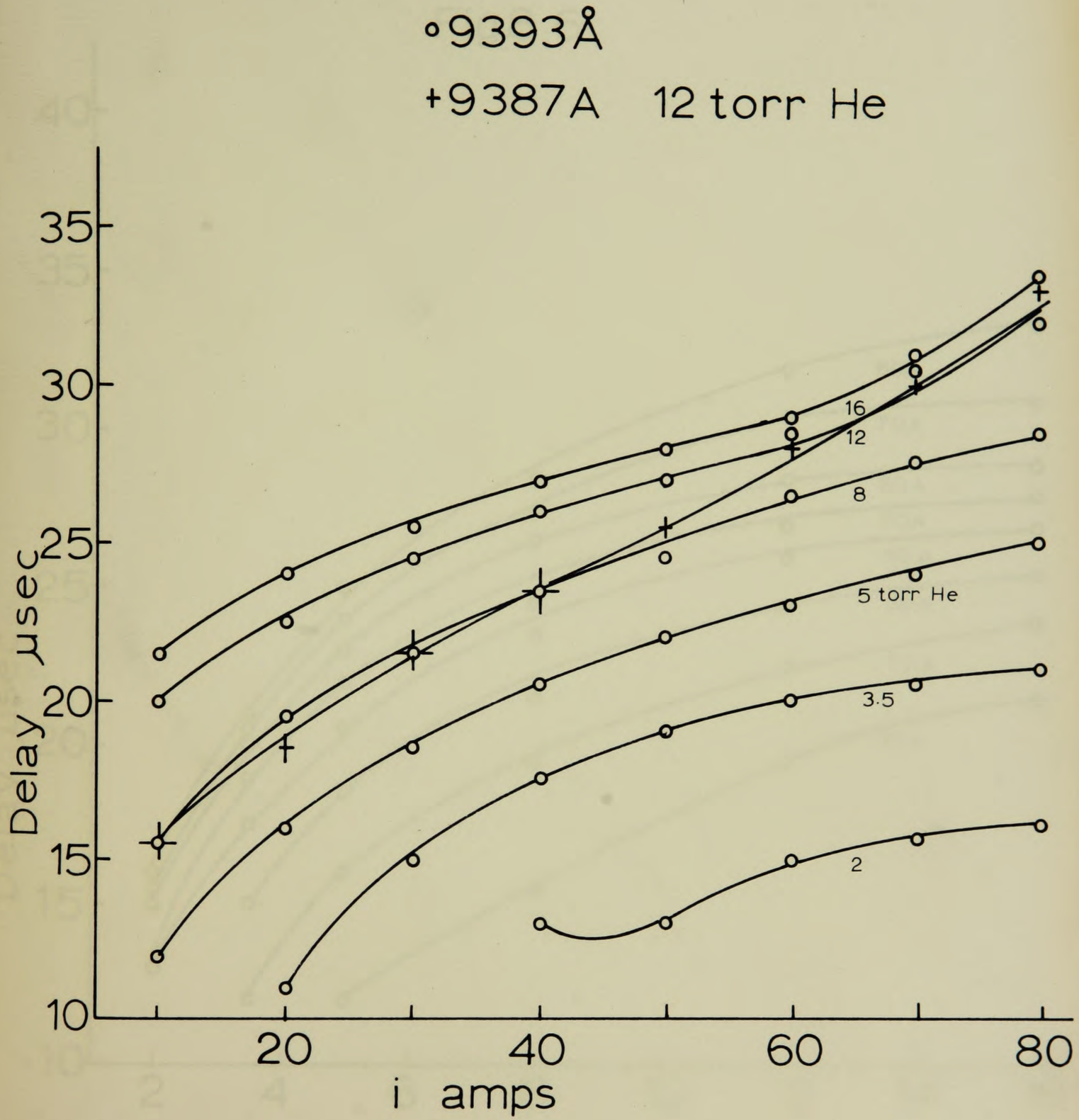
∘9393Å
+9387A 12 torr He
35
30
25
20
15
10
Delay μsec
16
12
8
5 torr He
3.5
2
20
40
60
80
i amps

Fig 8.6

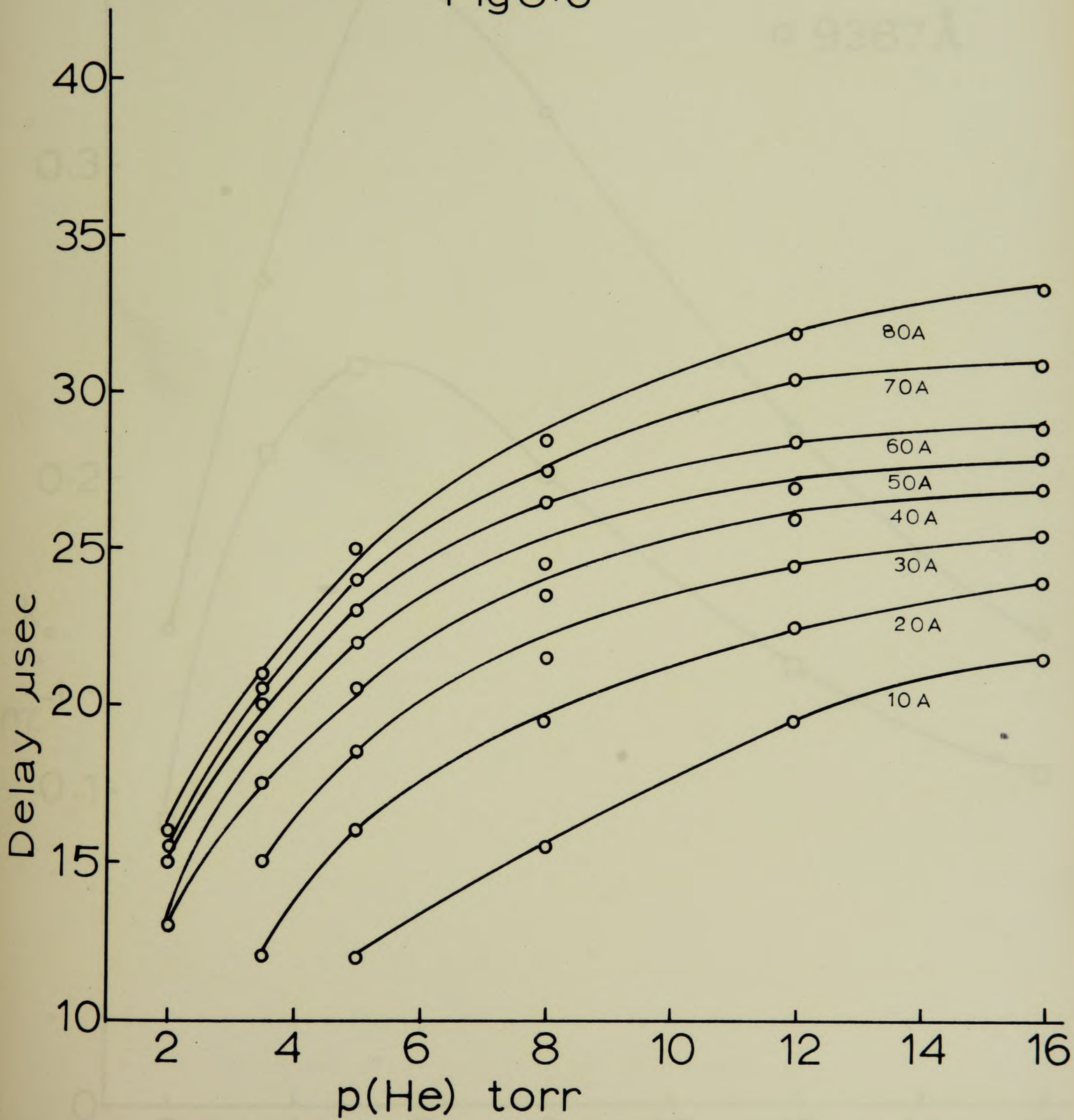
40
35
30
25
20
15
10
Delay μsec
2
4
6
8
10
12
14
16
p(He) torr
80A
70A
60A
50A
40A
30A
20A
10A

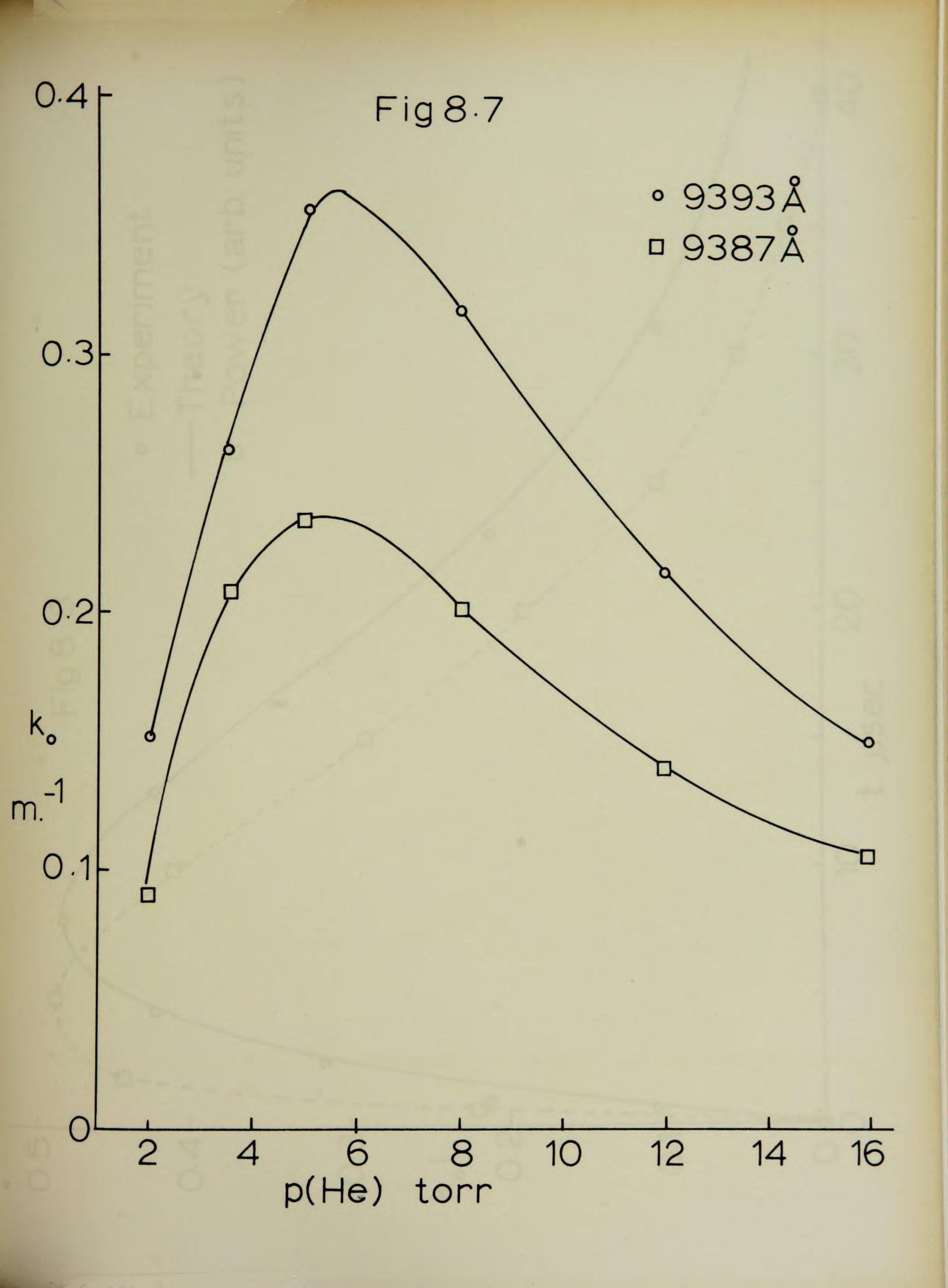
Fig 8.7
9393 Å
9387 Å
0.4
0.3
0.2
0.1
0
k_o
$m.^{-1}$
2
4
6
8
10
12
14
16
p(He) torr

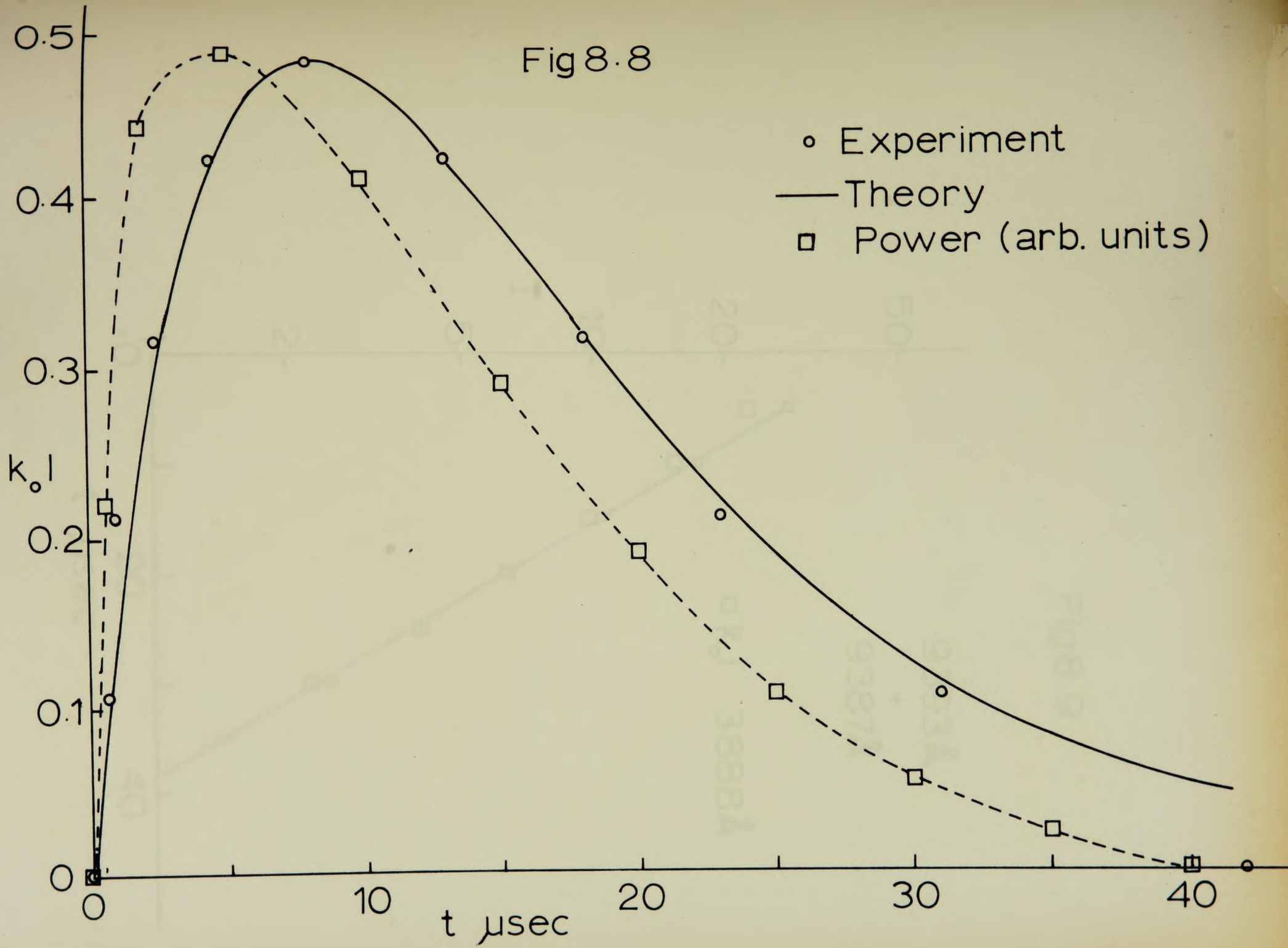
Fig 8.8
Experiment
Theory
Power (arb. units)
0.5
0.4
0.3
0.2
0.1
0
$k_o l$
0
10
20
30
40
t μsec

Fig8·9

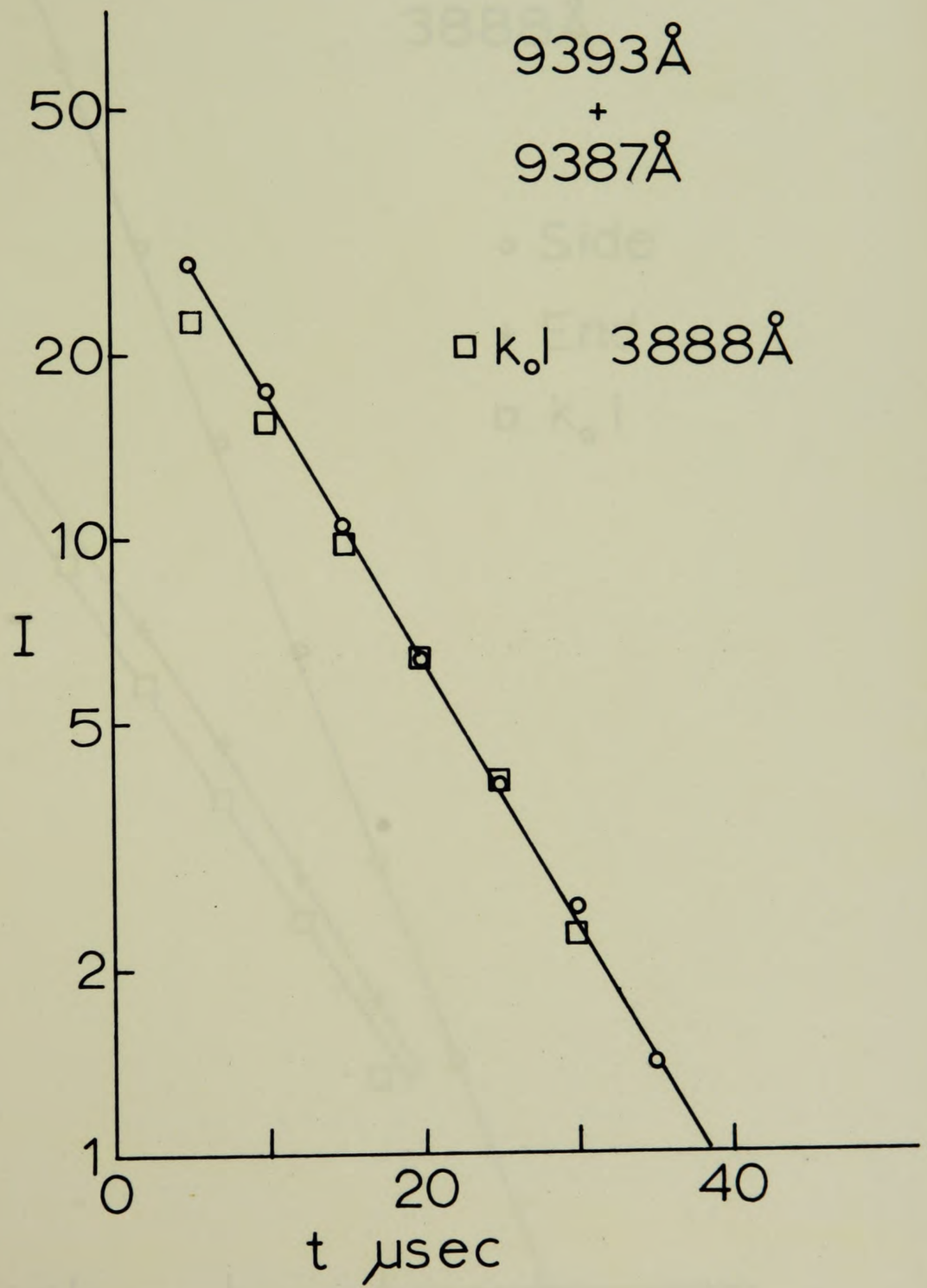

Fig 8.10

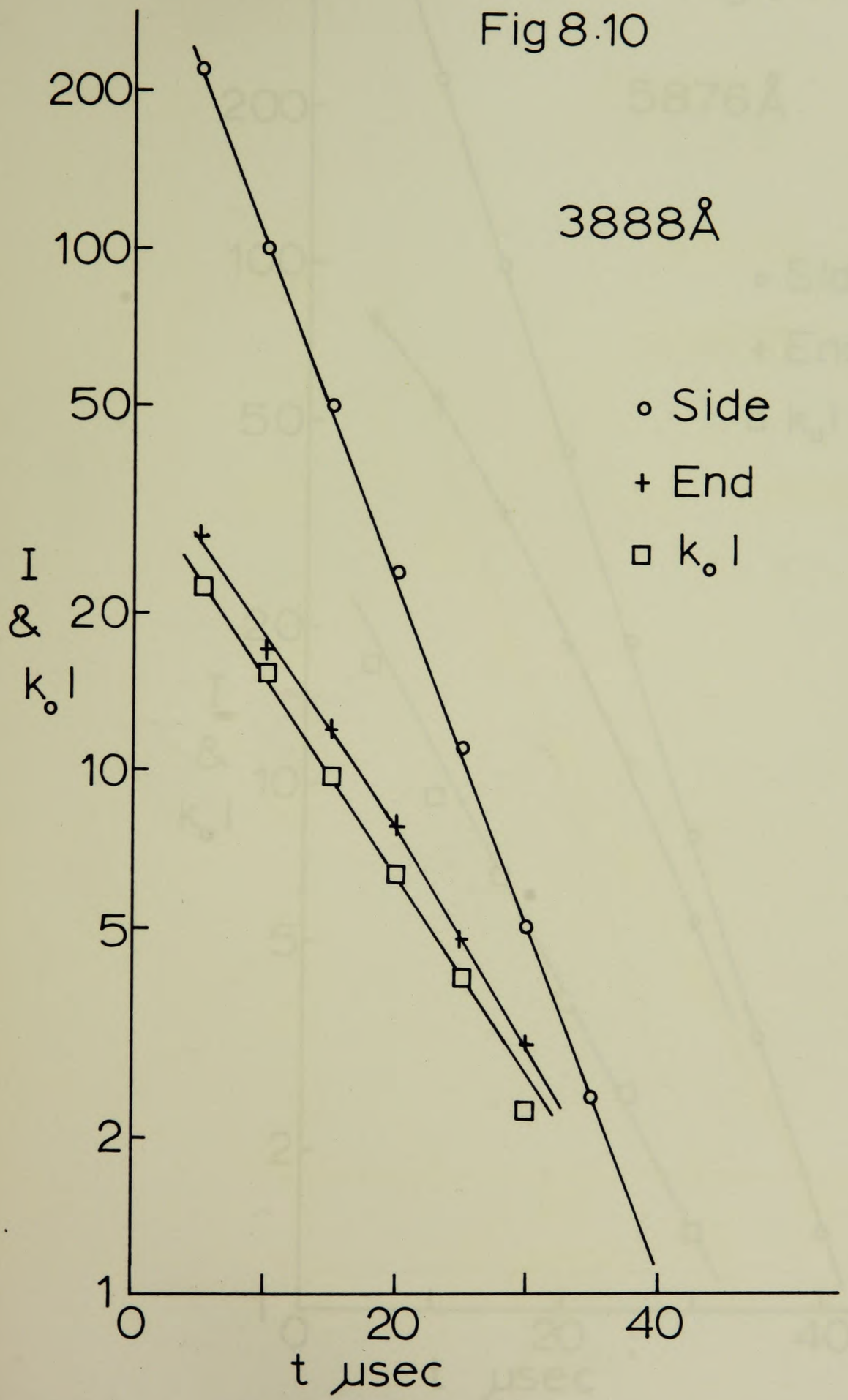

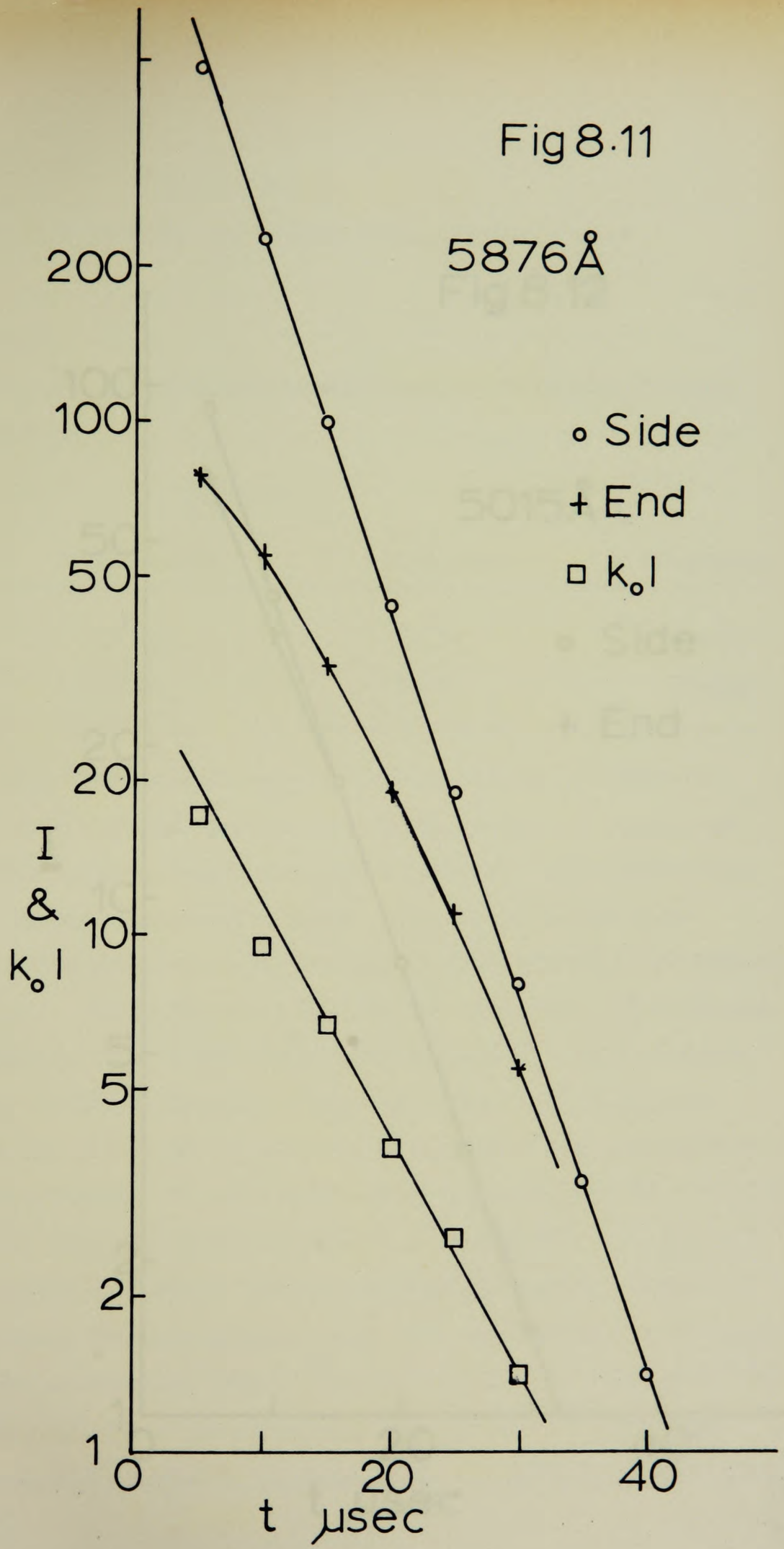
Fig 8·11
5876 Å
200
100
50
20
10
5
2
1
I & $k_o l$
0
20
40
t μsec
∘ Side
+ End
□ $k_o l$

Fig 8.12

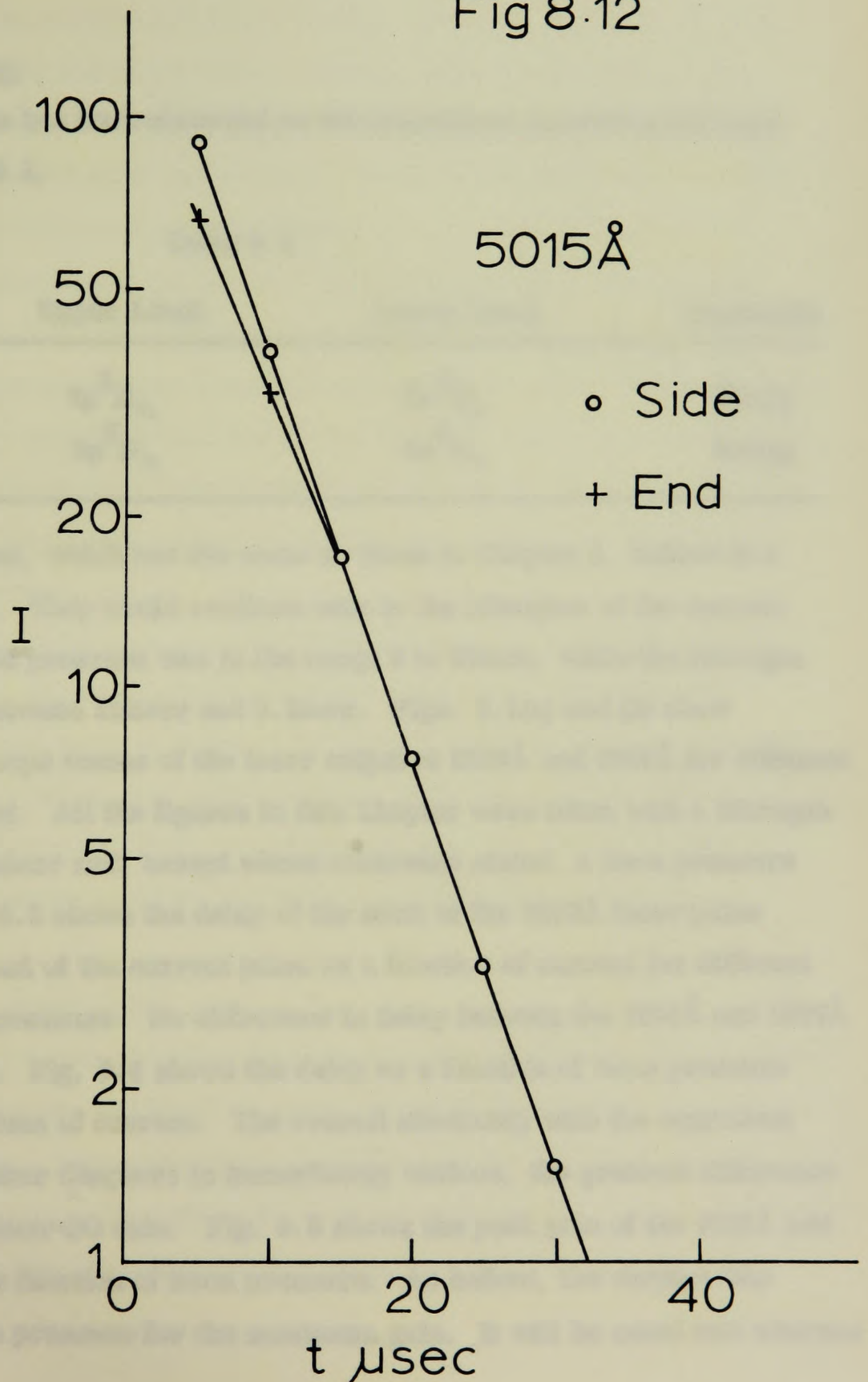

CHAPTER 9

Results for Neon-Nitrogen and Helium-Neon, and Conclusions

9.1 Laser Lines

Oscillation has been observed on the transitions in neutral Nitrogen listed in Table 9.1.

Table 9.1

λ Å	Upper Level	Lower Level	Comments
9392.79	$3p\,^2D_{5/2}$	$3s\,^2P_{3/2}$	Strong
9386.81	$3p\,^2D_{3/2}$	$3s\,^2P_{1/2}$	Strong

These lines, which are the same as those in Chapter 8, behave in a similar fashion. They would oscillate only in the afterglow of the current pulse. The Neon pressure was in the range 0 to 20torr, while the Nitrogen pressure was between 1mtorr and 0.2torr. Figs. 9.1(a) and (b) show typical oscilloscope traces of the laser output at 9393Å and 9387Å for different values of current. All the figures in this Chapter were taken with a Nitrogen pressure of 50mtorr and, except where otherwise stated, a Neon pressure of 5torr. Fig. 9.3 shows the delay of the start of the 9393Å laser pulse relative to the end of the current pulse as a function of current for different values of Neon pressure. No difference in delay between the 9393Å and 9387Å lines was found. Fig. 9.4 shows the delay as a function of Neon pressure for different values of current. The overall similarity with the equivalent figures in the other Chapters is immediately obvious, the greatest difference being with the Neon-CO data. Fig. 9.5 shows the peak gain of the 9393Å and 9387Å lines as a function of Neon pressure. As before, the current was adjusted at each pressure for the maximum gain. It will be noted that whereas

there is a gain measurement at 16torr of Neon, there is no delay measurement. The reason for this is shown in Figs. 9.1(c) and (d) which are oscilloscope photos of the 9393Å laser output at 16torr. The two pictures are taken with the same excitation conditions, but with one of the laser mirrors slightly rotated. A full explanation of the effect would be difficult without a number of further experiments, but it seems likely that it is due to some form of mode interaction, which may be caused by a particular spatial distribution of excited atoms. Further discussion of this will be made later. Figs. 9.1(e) and (f) and 9.2 are oscilloscope photos of the side-light and end-light of the 9393Å and 9387Å lines (unresolved) the 8680Å line, both of Nitrogen, and the 5852Å and 5882Å lines of Neon. Once again, the effect of the time varying self-absorption can be clearly seen, and the different decay rates of the upper and lower laser levels can be inferred from the 9393Å photo.

Neither the 8629Å nor the 13581Å were observed to oscillate, even under conditions when the 9393Å gain was a maximum. On the basis of observations of the relative gains of the lines in Helium-Nitrogen mixtures, oscillation would not be expected at 8629Å. With suitable high reflectivity mirrors, oscillation at 13581Å would be expected, but with the available mirrors, the peak gain will be insufficient to overcome the losses.

9.2 Excitation Mechanisms

In Chapter 7, the afterglow in pure Neon was discussed and the relevant excitation mechanism for the Neon levels shown to be a combination of atomic ion recombination, both radiative and collisional, and dissociative recombination of the molecular ion. The effect of small amounts of Nitrogen are to decrease the intensities of the Neon lines in the afterglow and to increase the decay

rates of the levels. With pressures of Nitrogen as low as 0.3torr and with 20torr of Neon, afterglow emission could only just be observed at the highest currents and the time constant of decay was of the order of 4 or 5μsec. The explanation is the change in excitation conditions during the current pulse. Since observations could not be made on the relative numbers of Ne^+, N^+ and N_2^+ ions, a comprehensive explanation cannot be made, but it seems probable that the higher density of Nitrogen molecules with a lower ionisation potential will decrease the electron temperature, and considerably decrease the number of Neon ions. Furthermore, it seems likely that the number of Nitrogen atomic ions will decrease relative to the molecular ions which are also formed Since it has been found experimentally that the recombination of the molecular Nitrogen ions is extremely rapid, (Ref: 9.1), the resulting overall effect will be a more rapid decay of the ions and electrons, and therefore of the excited atomic levels.

At pressures of 100mtorr or less of Nitrogen, it was found that the intensities of the Neon lines and the upper laser levels was constant at a fixed time in the afterglow when the current was varied. The only effect of increasing the current was to make the afterglow intensity increase more rapidly immediately after the end of the current pulse. This caused the peak intensity to increase, the time at which the peak occurs to be earlier and the delay between the end of the current pulse and the peak of the afterglow to decrease.

Fig. 9.6 is a graph of the side-light and end-light intensities and the resulting value of $k_o l$ as a function of time for the 5852Å Neon transition ($2p_1 - 1s_2$). Fig. 9.7 is a similar graph for the 5882Å Neon transition ($2p_2 - 1s_5$). Fig. 9.8 are graphs of the 9393Å and 9387Å Nitrogen lines (unresolved) and the 8680Å Nitrogen line.

The differences in the decay rates for the different lines are not so large as they were for Helium-Nitrogen mixtures, but nevertheless, there is significantly better agreement between the $1s_5$ Neon level population ($k_o l$ on the 5882Å line) and the 9393Å and 8680Å lines than there is between the other levels. These figures were taken with pressures of 50mtorr Nitrogen and 5torr Neon. Measurements were also made with the same Neon pressure but with 0.1torr Nitrogen. The decay rates of the 9393A and the $1s_5$ metastable again were the same in the late afterglow to within experimental error. Furthermore, the ratio of the 9393Å intensity to the product of metastable density and Nitrogen pressure was the same.

The evidence given above points strongly to the excited levels in Nitrogen atom being populated by a collision between a Nitrogen molecule and the Neon $1s_5$ and $1s_3$ metastables, the molecule being dissociated and one of the resulting atoms excited. By considering the energy required for this process, it can be seen that the molecule will have to be in a vibrationally excited state with an energy of 41,500cm.$^{-1}$ which corresponds to the v = 20 state.

The cross-section for the dissociation and excitation process can be estimated as in the previous Chapters if the vibrational temperature is known. The metastable populations in Neon are higher than in Helium, but much higher vibrational states of the molecule are needed. If the cross-section is of the same order as in Helium, the vibrational temperature will have to be of the order of 25,000°K. Since it should reflect the excitation temperature during the current pulse, it is not unreasonable.

A little more insight into the mode interaction effect noted earlier can now be made. The upper laser level population is governed by the Neon metastable population. Depopulation of the metastables is by collision processes and by diffusion to the walls. Thus, particular diffusion "modes"

will be set up causing a non-uniform distribution across the tube bore. The most direct way of verifying this would be to measure the gain on the laser line as a function of radial position in the tube, but with a tube bore of only 7mm. and tube length of 2m. this proved impractical.

9.3 Helium-Neon Laser

Fig. 9.9 shows oscilloscope traces of the laser output at 9393Å and 11523Å under identical conditions of excitation and pressure. The gas mixture consisted of 2torr of Helium with 0.1torr of Neon and traces of Nitrogen given off by the walls of the discharge tube. The 9393Å transition is the one discussed earlier, while the 11523Å transition was one of the first to be observed in a gas laser and is the $2s_2 - 2p_4$ transition in Neon It has been clearly established that one of the dominant mechanisms for exciting the Neon laser upper level is a collision of the second kind involving a Helium 2^3S metastable and a ground state Neon atom (Ref 9.2). The only other important mechanism for exciting the laser upper level in an r.f. discharge is electron impact from the ground state, since these two states are optically connected This is relatively unimportant in the afterglow of the pulsed discharge used in this experiment because of the low electron temperature, as discussed in Chapter 6.

Fig. 9.10 shows the delay of the start of laser action on the 11523Å transition relative to the end of the current pulse as a function of current for different values of Helium pressure. The Neon pressure was 50mtorr. There is a notable similarity between this figure and the preceding figure and the results for the Carbon and Nitrogen lines. The main difference is that the range of Helium pressures over which laser action could be obtained on the Neon transition was less than for the Carbon and Nitrogen transitions.

Although not shown here, the peak gain as a function of Helium pressure and the change in laser output as a function of current is also similar to the results for the Carbon and Nitrogen lines. The relevance of the Helium-Neon results will be discussed in the final section.

9.4 Conclusions

In Chapter 5, the methods by which populations could be measured were discussed, and techniques developed for use with pulsed discharges. These methods were then used to analyse the results in the following Chapters. By means of the theory of Chapter 4, possible excitation processes, such as electron impact, were shown to be relatively unimportant in the afterglow. The conclusions reached was that the excited p states of Carbon and Nitrogen were produced by a collision between a Helium 2^3S or Neon $1s_5$ or $1s_3$ metastable atom and a Carbon Monoxide or Nitrogen molecule in an excited vibrational level of the ground electronic state.

The evidence by which this conclusion was reached can be summarised as follows :-

a) The decay rates of the excited p states are similar to the decay rates of the metastables.

b) The populations of the excited p states in the afterglow are constant with current as are the metastable populations.

c) The explanation for the prompt laser action at only 10691Å, 10683Å and 14542Å is consistent with the above theory as discussed in Chapter 6.

d) The line width for the 9406Å transition in the afterglow is the Doppler width at room temperature (see Chapter 6).

e) The similarity between the laser parameters in the four

different mixtures and the Helium-Neon mixture point to a common mechanism, namely a collision of the second kind involving a metastable atom.

f) The decay rate for the C^+ 3p level, the only C^+ level observed to have a significant afterglow lasting more than 2μsec., is consistent with the collision process

$$Ne(1s_5) + C^+ = C^+(3p) + Ne$$

when the C^+ and Ne ($1s_5$) decay rates are taken to be the same as the 2479Å and the 9406Å Carbon transition decay rates (see Chapter 7).

Finally, using the measured populations, a cross-section for the dissociation and excitation process was estimated to be $7 \times 10^{-16} cm.^2$, and the vibrational temperature of the molecules to be 25,000°K.

References

9.1 W.H.Kasner, W.A.Rogers & M.A.Biondi — Phys. Rev. Letts. 7, 321 (1961)

9.2 W.R.Bennett, Jr. — App. Optics Supplement on Optical Masers p 40, (1962)

Fig 9.1

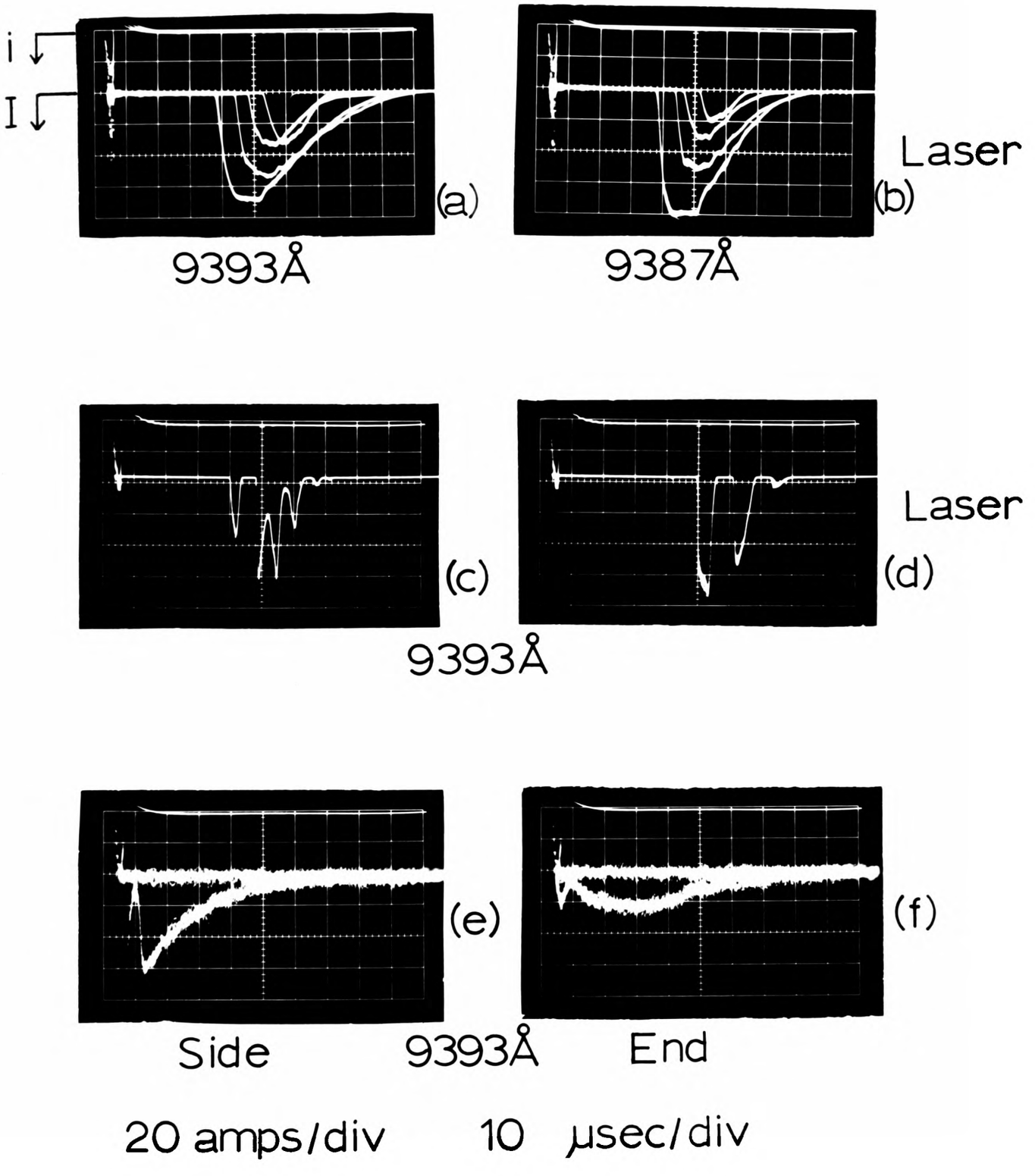
i
I
(a)
9393Å
(b)
9387Å
Laser
(c)
(d)
Laser
9393Å
(e)
(f)
Side
9393Å
End
20 amps/div
10 μsec/div

Fig 9.2

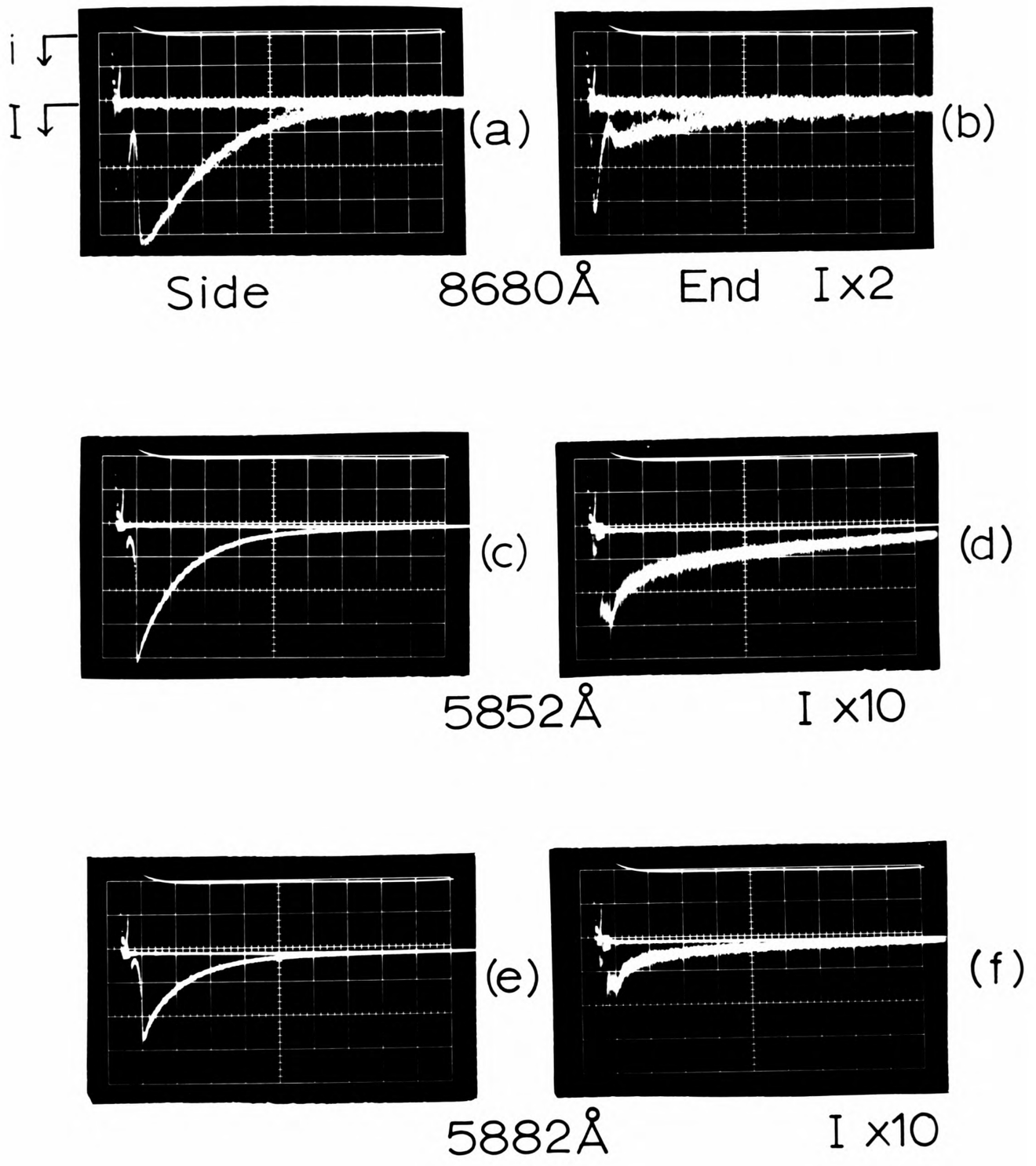
i
I
(a)
(b)
Side
8680Å
End I x2
(c)
(d)
5852Å
I x10
(e)
(f)
5882Å
I x10
20 amps/div
10 μsec/div

Fig 9.3

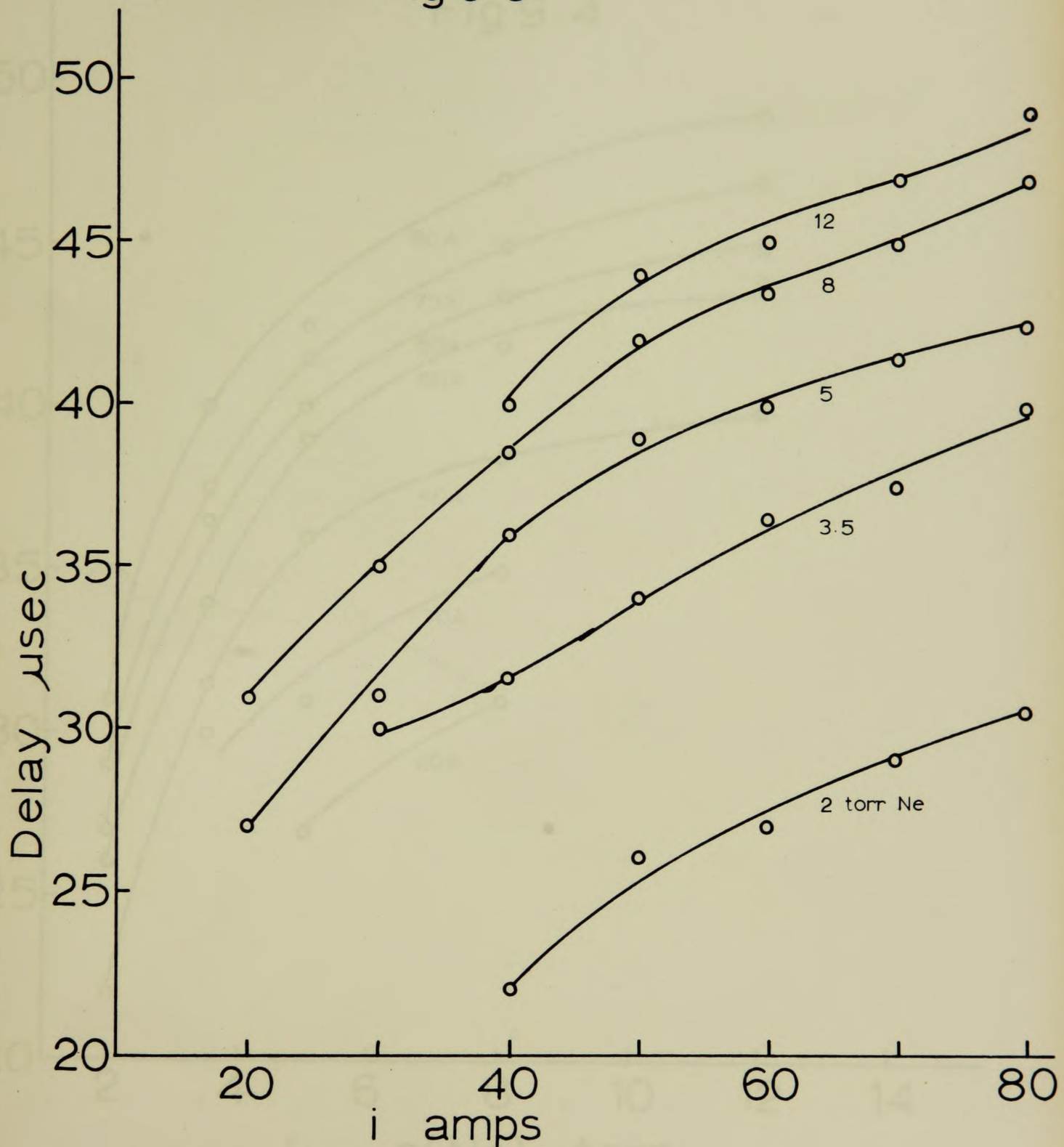

Fig 9.4

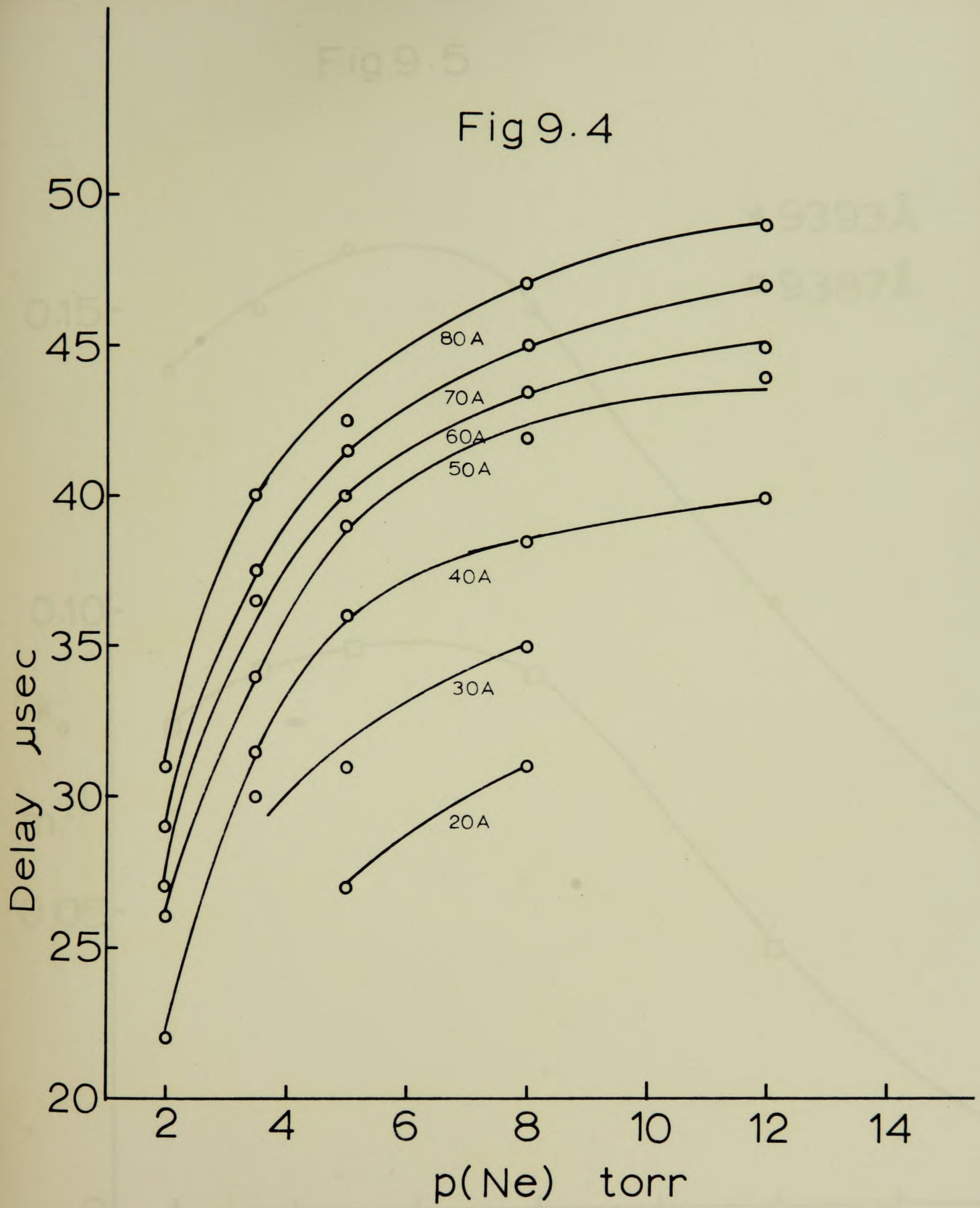
50
45
40
35
30
25
20
Delay μsec
80A
70A
60A
50A
40A
30A
20A
2
4
6
8
10
12
14
p(Ne) torr

Fig 9.5

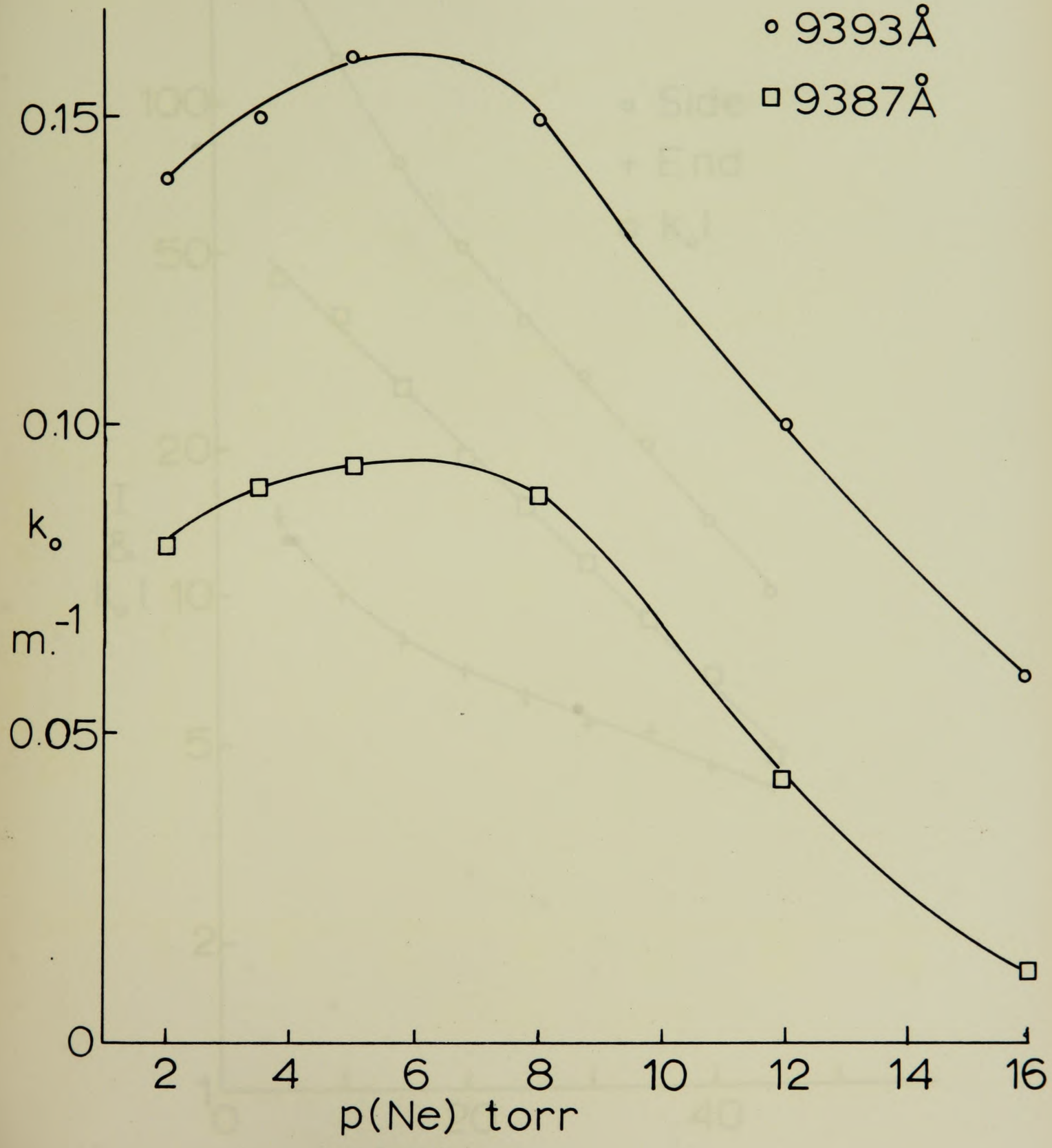

Fig 9.6

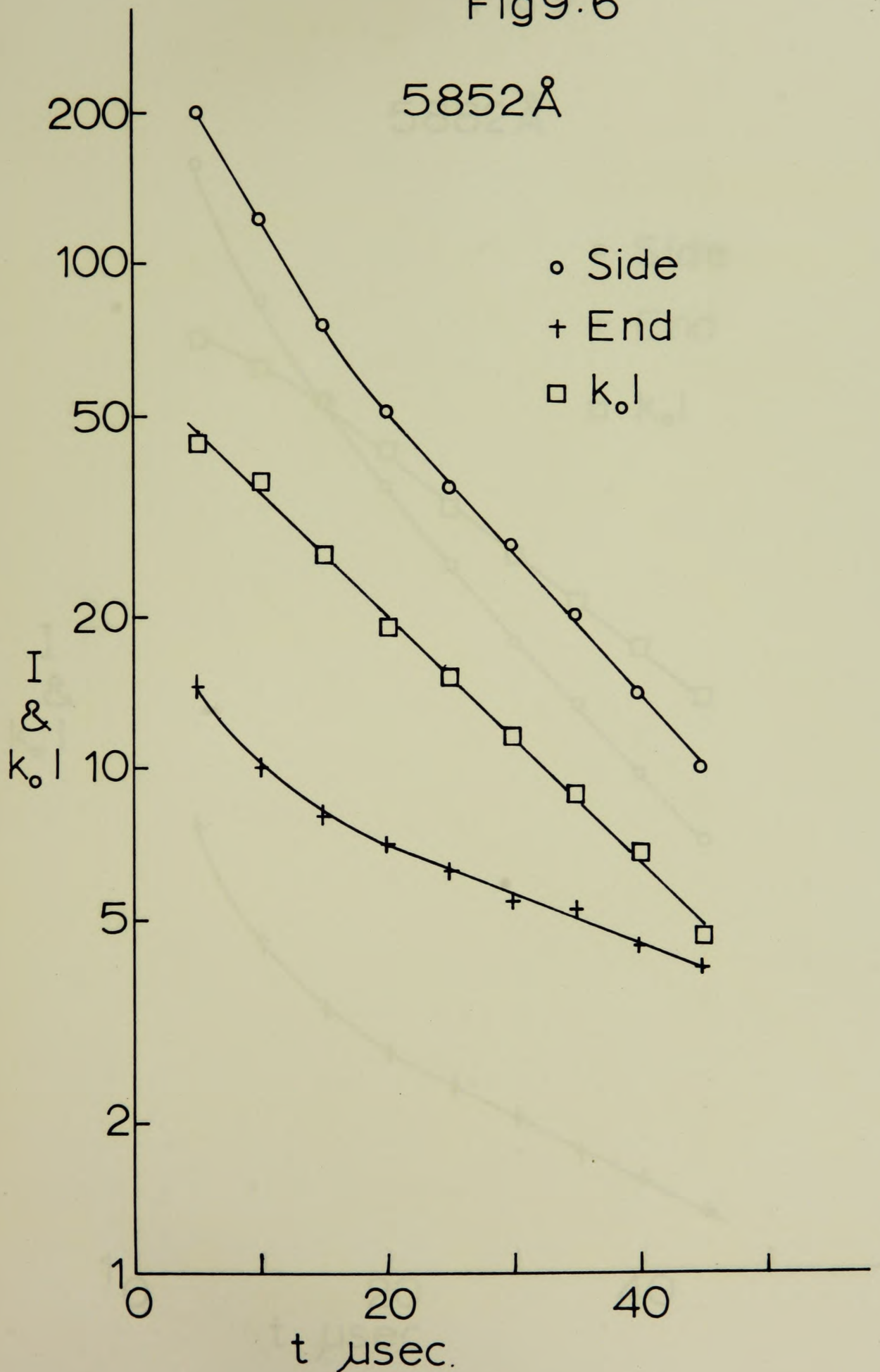

Fig 9.7

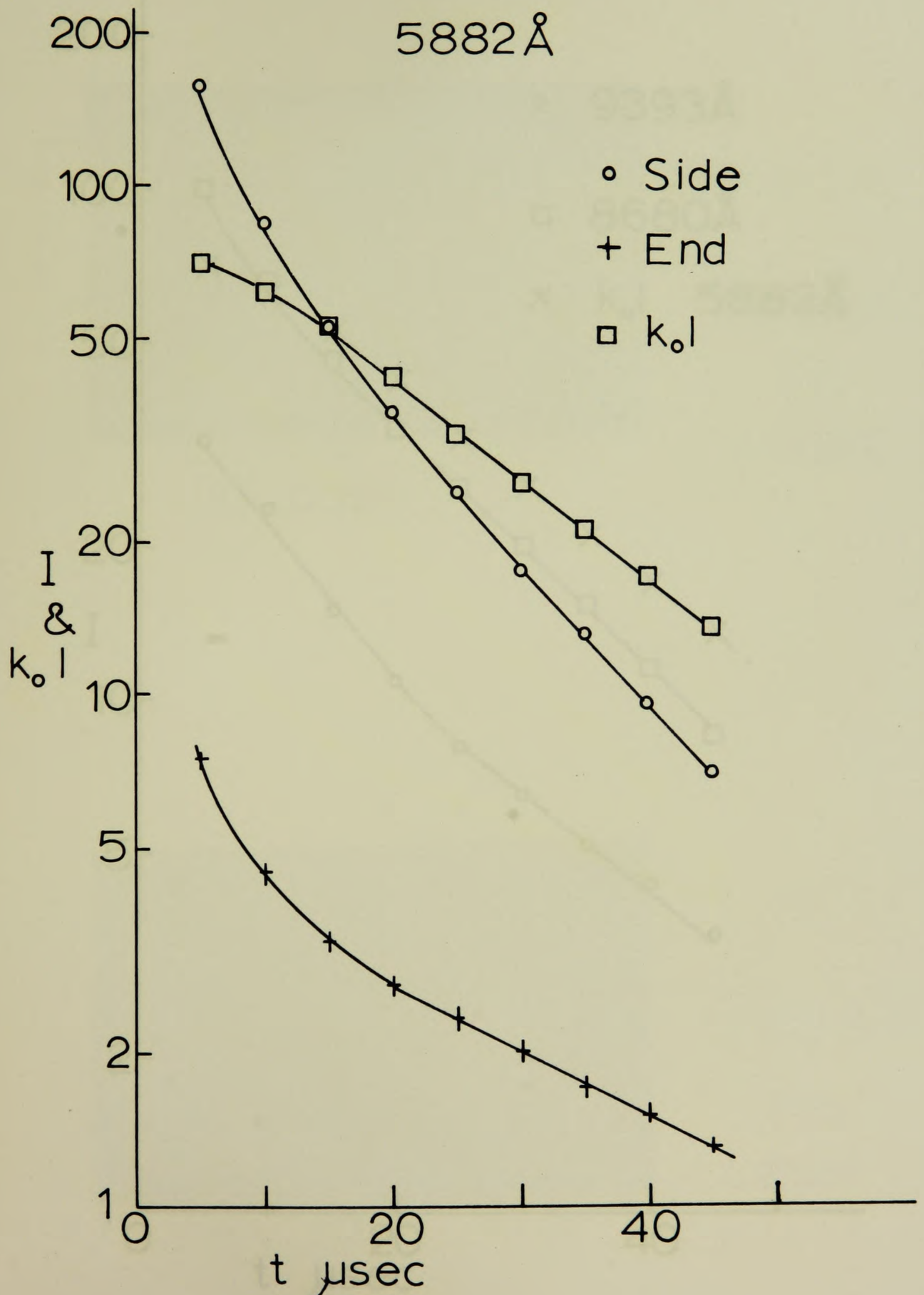

Fig 9.8

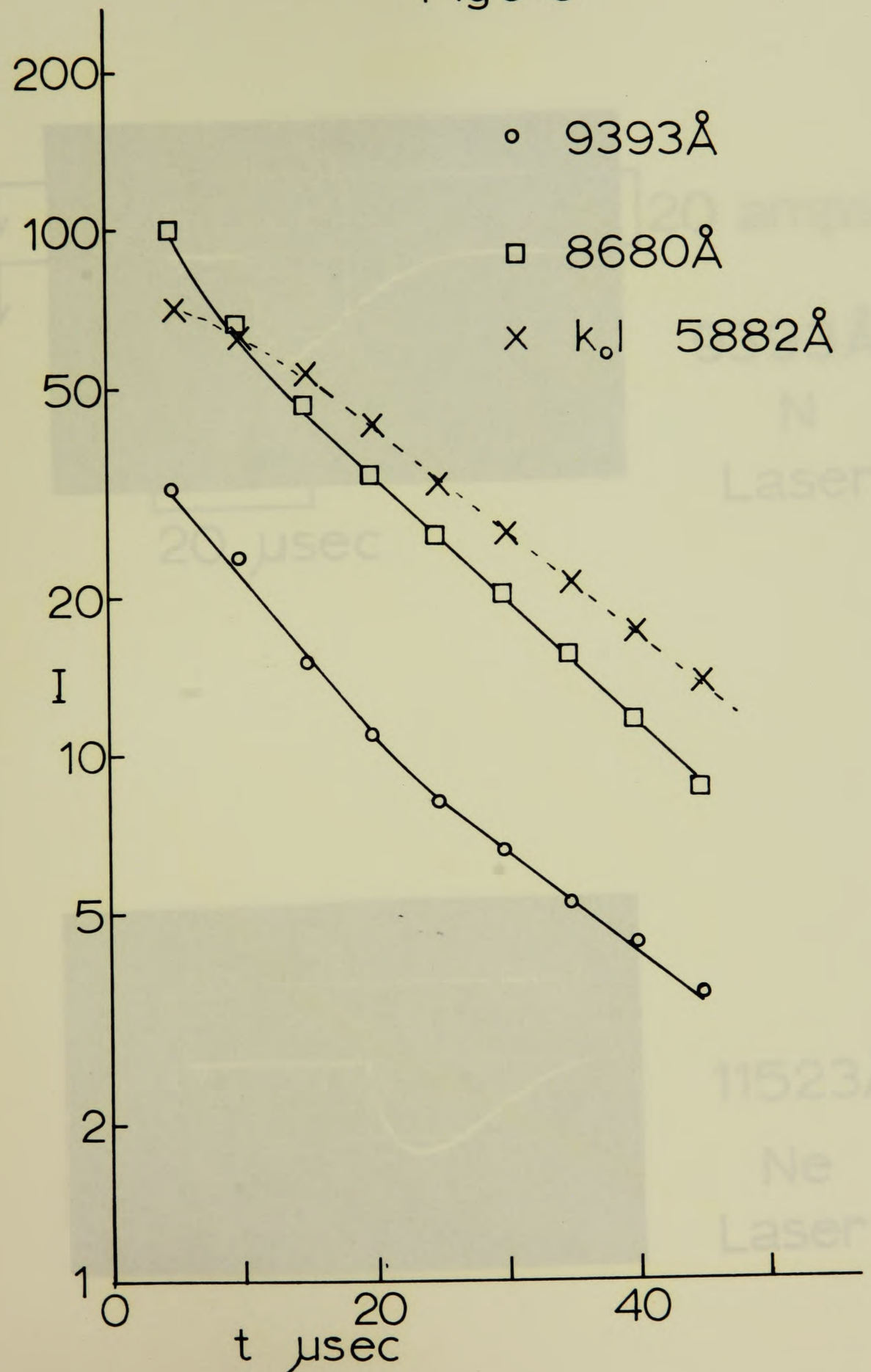

Fig 9.9

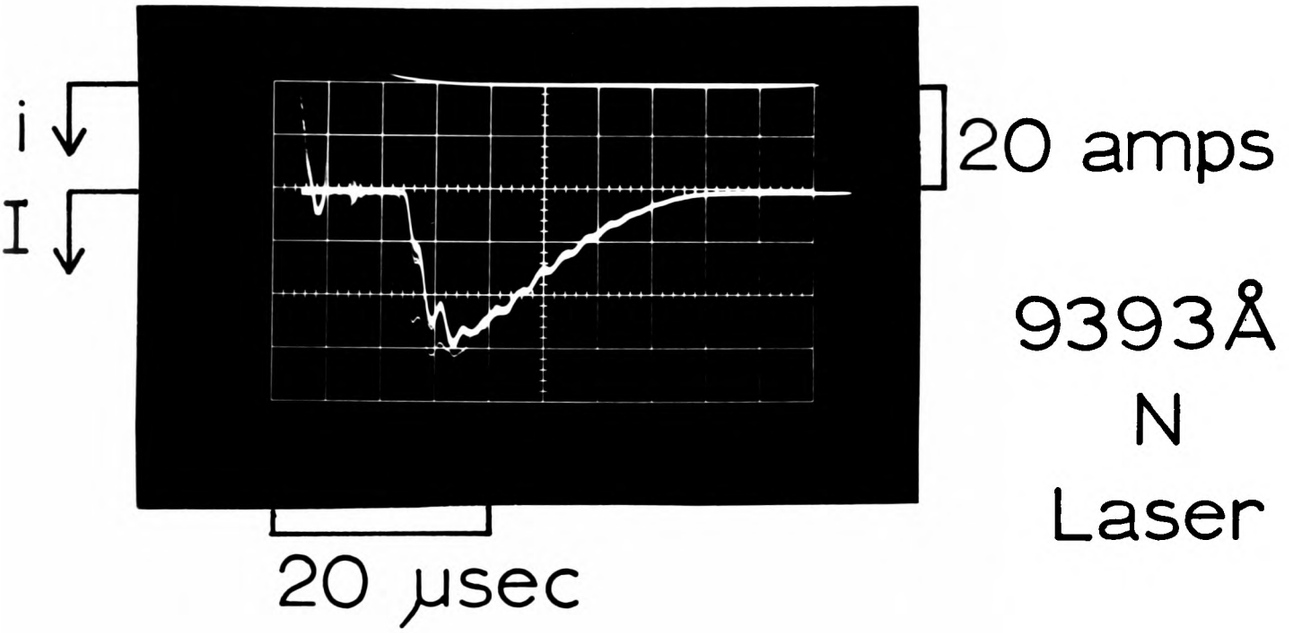

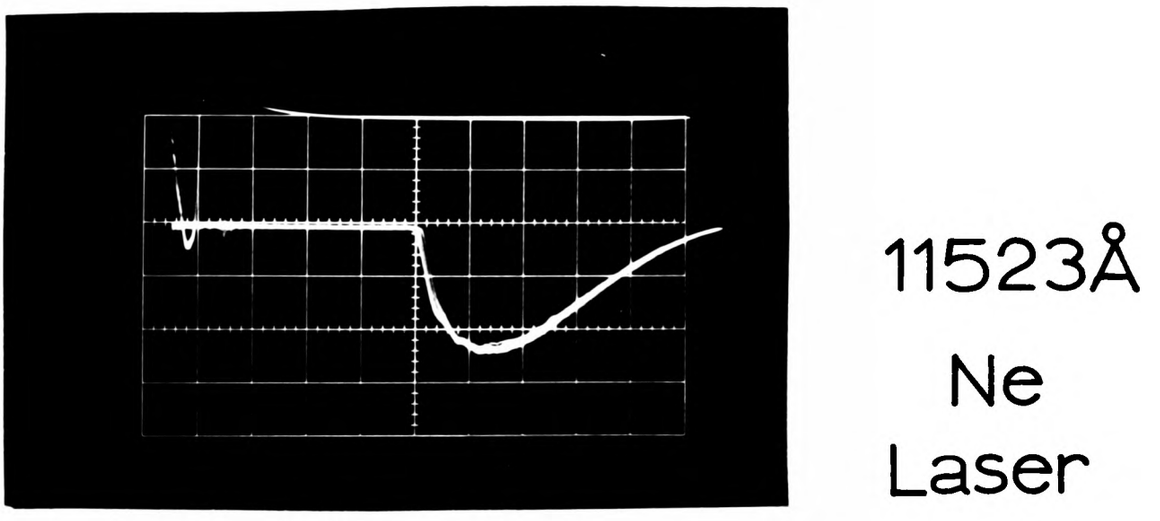

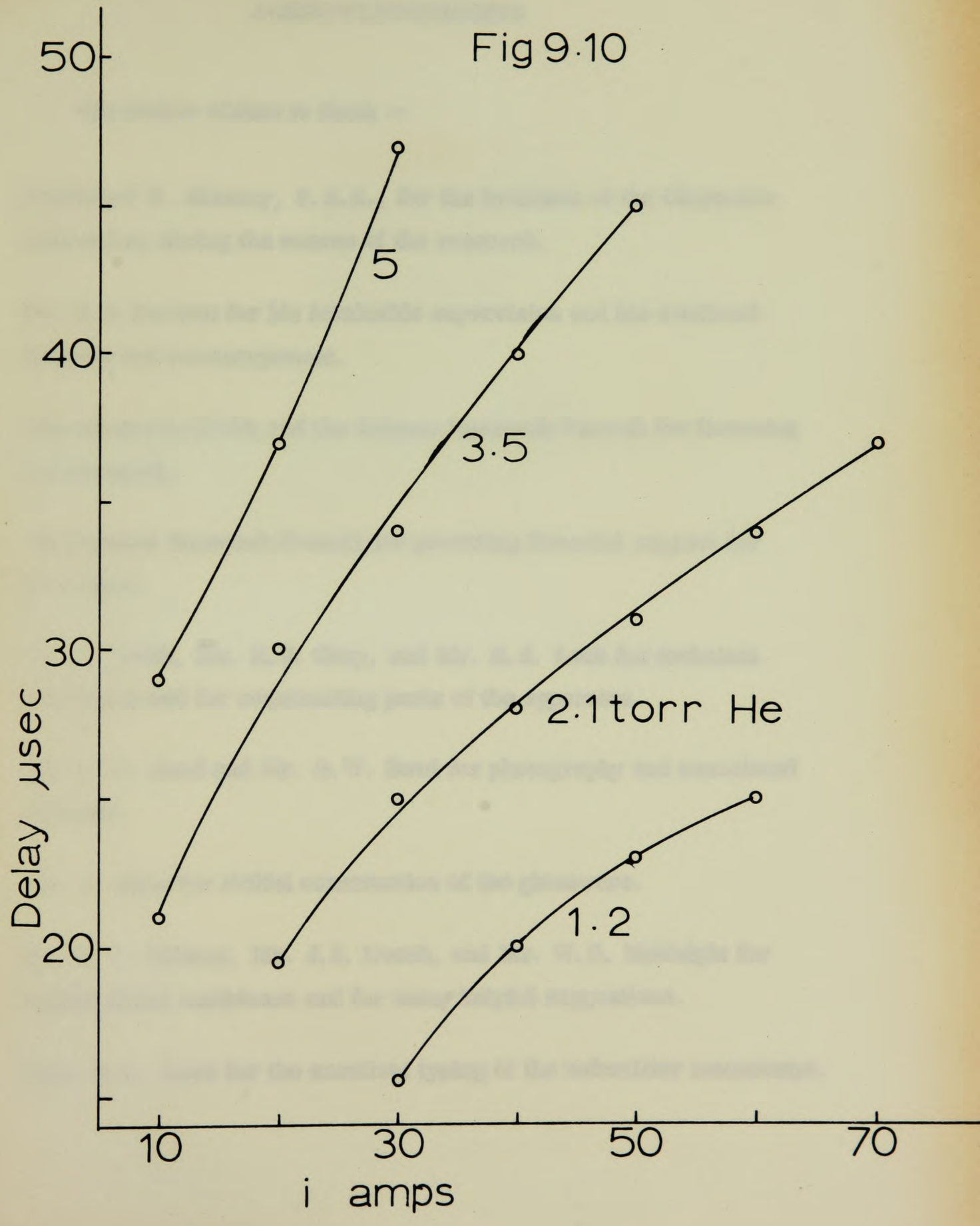
Fig 9.10
50
40
30
20
Delay μsec
5
3.5
2.1torr He
1.2
10
30
50
70
i amps

ACKNOWLEDGEMENTS

The author wishes to thank :-

Professor B. Bleaney, F.R.S., for the facilities of the Clarendon Laboratory during the course of the research.

Dr. J.H. Sanders for his invaluable supervision and his continual interest and encouragement.

The Admiralty (CVD) and the Science Research Council for financing the research.

The Science Research Council for providing financial support for the author.

Mr. D. Meek, Mr. H.J. Grey, and Mr. H.S. Lock for technical assistance and for constructing parts of the apparatus.

Mr. C.W. Band and Mr. R.W. Bowl for photography and associated services.

Mr. S. Giles for skilful construction of the glassware.

Dr. W.T. Silfvast, Mr. J.S. Deech, and Mr. W.B. McKnight for experimental assistance and for many helpful suggestions.

Mrs. E.A. Lowe for the excellent typing of the unfamiliar manuscript.